CHALMERS
UNIVERSITY OF TECHNOLOGY

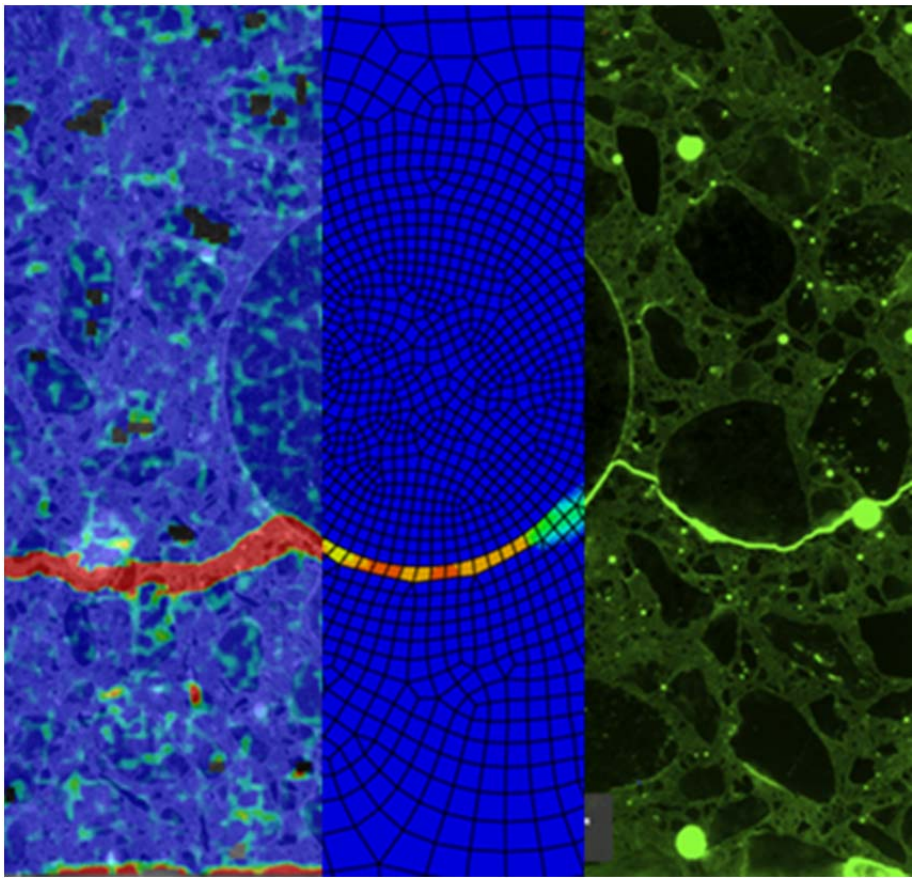

Meso mechanical study of concrete

Numerical modelling with experimental verification

Master's Thesis in the Master's Programme Structural Engineering and Building Technology

ELIN ALEXANDERSSON
BIRGIT AMBLIE SOLERØD

Department of Civil and Environmental Engineering
Division of Structural Engineering
Concrete Structures
CHALMERS UNIVERSITY OF TECHNOLOGY
Gothenburg, Sweden 2015
Master's Thesis 2015:111

MASTER'S THESIS 2015:111

Meso mechanical study of concrete

Numerical modelling with experimental verification

Master's Thesis in the Master's Programme Structural Engineering and Building Technology

ELIN ALEXANDERSSON

BIRGIT AMBLIE SOLERØD

Department of Civil and Environmental Engineering

Division of Structural Engineering

Concrete Structures

CHALMERS UNIVERSITY OF TECHNOLOGY

Göteborg, Sweden 2015

Meso mechanical study of concrete
Numerical modelling with experimental verification

Master's Thesis in the Master's Programme Structural Engineering and Building Technology

ELIN ALEXANDERSSON

BIRGIT AMBLIE SOLERØD

Examensarbete 2015:111/ Institutionen för bygg- och miljöteknik,
Chalmers tekniska högskola 2015

Department of Civil and Environmental Engineering
Division of Structural Engineering
Concrete Structures
Chalmers University of Technology
SE-412 96 Göteborg
Sweden
Telephone: + 46 (0)31-772 1000

Cover:
Image of the simple concrete specimen treated in this Master's Thesis project, seen with parts from a DIC-image, the FE-model and a fluorescence image respectively.

Chalmers Reproservice
Göteborg, Sweden, 2015

Meso mechanical study of concrete
Numerical modelling with experimental verification

Master's Thesis in the Master's Programme Structural Engineering and Building Technology

ELIN ALEXANDERSSON
BIRGIT AMBLIE SOLERØD
Department of Civil and Environmental Engineering
Division of Structural Engineering
Concrete Structures
Chalmers University of Technology

ABSTRACT

Concrete is one of the most important and commonly used materials in today's building industry. The impact on the environment due to the manufacturing of building materials is of great importance in modern society. In order to develop concrete into a more environmental friendly building material, a better understanding of concrete's behaviour at meso level is needed.

The purpose of this Master's thesis project was to establish a 2D finite element model that can simulate crack initiation and propagation of concrete at meso level. This was approached by combining finite element modelling with tensile testing of small-scale samples. A finite element model consisting of a simple fictitious concrete specimen with one single aggregate was first established in the finite element program Abaqus. To improve this model, tensile tests were carried out on real small-scale concrete specimens similar to the modelled one. A tensile stage was used during the tests and results were monitored with the Digital Image Correlation system Aramis. By using the Digital Image Correlation results in form of images and stress-displacement curves, different material properties could be updated in the finite element model.

With results in form of modelling techniques and stress-displacement curves, an experimentally verified finite element model of concrete crack initiation and propagation was achieved. The shape of the improved finite element model's stress-displacement curve was very similar to the one for the tensile tested specimen. Results showed that both the tensile tested specimen and the modelled specimen had crack initiation in the interface at the same stress level and also gave similar cracks in the final stage. The finite element model and the tensile test specimen had the same behaviour, crack initiation and propagation and also the same crack appearance.

It can be concluded that the finite element model can be used for simulating concrete cracking and evaluate material properties at meso level. The model can also be used to give a better understanding of how the meso structure influences cracking propagation and the behaviour of concrete.

Key words: Abaqus, Aramis, Concrete, Concrete cracking, Digital Image Correlation, Finite element modelling, Fracture mechanics, Meso level, Numerical modelling, Tensile stage testing.

Mesomekanisk studie av betong
Numerisk modellering med experimentell verifiering

Examensarbete inom masterprogrammet Structural Engineering and Building Technology

ELIN ALEXANDERSSON
BIRGIT AMBLIE SOLERØD
Institutionen för bygg- och miljöteknik
Avdelningen för konstruktionsteknik
Betongbyggnad
Chalmers tekniska högskola

SAMMANFATTNING

Betong är idag ett av de viktigaste och mest använda materialen inom byggindustrin. Miljöpåverkan från tillverkning av byggmaterial är av stor betydelse i det moderna samhället. För att utveckla betong till ett mer miljövänlig byggmaterial behövs en bättre förståelse för dess beteende på mesonivå.

Syftet med detta examensarbete var att skapa en finit elementmodell i 2D som visade sprickinitiering och propagering i betong på mesonivå. Detta utfördes genom att kombinera finit elementmodellering med dragprovning av småskaliga betongprover. Först skapades en finit elementmodell bestående av ett enkelt och fiktivt betongprov med endast ett ballastkorn i det finita elementprogrammet Abaqus. Dragprover av verkliga småskaliga betongprover likt det modellerade utfördes därefter för att kunna förbättra den finita elementmodellen. Testerna gjordes i ett dragsteg och resultaten registrerades med det optiska deformationsmätningssystemet Aramis. Genom att använda resultat i form av bilder och spännings-förskjutningsdiagram från deformationsmätningssystemet kunde olika materialegenskaper uppdateras i den finita elementmodellen.

Med resultat i form av modelleringstekniker och spännings-förskjutningsdiagram kunde en experimentellt verifierad finit elementmodell av sprickinitiering och propagering i betong skapas. Formen på den förbättrade finita elementmodellens spännings-förskjutningkurva liknade formen på kurvan för det dragtestade provet. Resultaten visade att både det dragtestade provet och det modellerade provet hade sprickinitiering i vidhäftningszonen vid samma spänningsnivå och de gav även liknande sprickor i slutskedet. Den finita elementmodellen och det dragtestade provet hade samma beteende, sprickutveckling och utseende på sprickan.

Slutsatsen från projektet är att den finita elementmodellen kan användas för att simulera betongs sprickbildning och utvärdera materialegenskaper på mesonivå. Modellen kan dessutom användas för att ge en bättre förståelse för hur mesostrukturen påverkar sprickpropagering och betongs beteende.

Nyckelord: Abaqus, Aramis, Betong, Brottmekanik, Finit elementmodellering, Mesonivå, Numerisk modellering, Optisk deformationsmätning (DIC), Provning med Dragsteg, Sprickor i Betong.

Contents

Preface

This Master's thesis project has been carried out from December 2014 to June 2015 at the Division of Structural Engineering at Chalmers University of Technology, Göteborg, Sweden. This has been done with great support and guidance from Professor Rasmus Rempling.

The tensile testing have been performed at headquarter of SP Technical Research Institute of Sweden. This part of the project was carried out with the help of Adjunct Professor Mathias Flansbjer, whom is very appreciated for his help and guidance during the test period and also during the whole project. This Master's thesis project is a part of an on-going study at SP regarding the cracking process of concrete.

We would also like to thank Erika Abrahamsson and Josefin Petersson for cooperation and exchange of good advice during the writing process of the thesis and during the presentation.

Göteborg, May 2015

Elin Alexandersson and Birgit Amblie Solerød

1 Introduction

Concrete is one of the most important and commonly used materials in today's building industry (Domone & Illston 2010). Due to on-going climate changes, the impact on the environment from production of building materials is of great importance in modern society. There is thus a need to develop concrete into a more environmental friendly building material, and one way into achieving this goal is to decrease the carbon dioxide emissions from the manufacturing of concrete (European Commission 2014; PBL Netherlands Environmental Assessment Agency 2014). Also infinite resources should be more widely used in concrete manufacturing in order to develop it into a more environmental friendly building material. Crushed rock material, which is an infinite resource, should therefore in long term not only be used for the larger aggregate particles but also replace natural rock material as finer aggregate particles in the concrete mix (CBI Betonginstitutet 2008).

If concrete is to be developed in order to match the requirements from modern society, a better understanding of its behaviour at meso level is needed. A better understanding of the physical appearances at meso level will improve the knowledge of concrete's mechanical behaviour at macro level (van Mier 2013). Proper experimental methods and equipment for studies at meso level are needed in order to achieve this.

Due to an absence of methods for performing experimental studies at meso level of concrete, (Lindgren & Östergren 2010) developed a tensile testing machine especially for small-scale specimens - a tensile stage. This experimental method was further developed by (Nilsson & Pagrotsky 2012) where the tensile stage was combined with the Digital Image Correlation (DIC) system Aramis. This development resulted in a reliable and effective method to observe crack initiation and propagation of small-scale concrete specimens tested in tension.

SP Technical Research Institute of Sweden together with The Swedish Cement and Concrete Research Institute (CBI) are in an on-going project using the developed tensile stage to study the cracking process in concrete. This is done together with acoustic emissions and microscopy analysis. The aim of their study is to understand how cracking is influenced by the concrete structure at meso and micro level, and the effect from aggregate shape on the cracking process is of great focus in the study (Flansbjer & Lindqvist 2013).

Further steps into gaining more knowledge about how the meso structure influences the concrete cracking process is to combine results from tensile stage tests of small-scale concrete specimens with finite element modelling. Results from the tensile stage tests could thus be used as more realistic input data in the FE-models and also act as verification of the models.

1.1 Purpose

The purpose of this Master's thesis project was to, with the combination of finite element modelling and tensile testing; establish a 2D finite element model of concrete at meso level. The model should be based on real concrete behaviour and reflect crack initiation and propagation.

In order to accomplish a realistic model, different objectives were to be achieved:

1. Establish a FE-model of a simple fictitious concrete specimen with one single aggregate.
2. Carry out tensile stage tests on real small-scale concrete specimens similar to the modelled specimen.
3. Create improved simple FE-model after comparison with results from the tensile stage tests of the real concrete specimens.
4. Develop the FE-model in order to reflect actual concrete structure with more aggregate particles.

Such a model can be used to give a better understanding of how the meso structure influences crack propagation and the behaviour of concrete. The model can also be used to show the cracking behaviour at meso level of a specific concrete. It will therefore contribute to the research of developing and designing new environmental friendly types of concrete mixes, including optimization of the concrete and better utilization of the material components.

To simulate real concrete in the FE-model and to get proper results, the following was considered in the modelling:

- Material properties of the concrete components
- Which material models should be used
- How to put up boundary conditions of the model
- How to model the interface zone between cement paste and aggregate
- Where cracking was likely to start and how it would propagate

1.2 Limitations

The study was limited to small-scale concrete specimens with one aggregate and with the same geometry for both the tensile tested specimens and the modelled specimen. When studying the different tests and models, regarding crack initiation and propagation, it was only executed at meso level. The FE-modelling was performed in the FE-program Abaqus and was executed in 2D. Aramis was the DIC-program which was used for the measurements and evaluations of the tensile testing.

1.3 Method

In order to establish a FE-model which realistically represents concrete crack initiation and propagation at meso level, the methodology used can be summarized into the following parts:

- Literature study
- Modelling in the finite element program Abaqus
- Tensile testing of small-scale concrete specimens
- Improvement of the finite element model

Modelling of concrete at meso level with finite element method has been done before, which can be read about in Section 3.1. But in order to develop the modelling of concrete at meso level and take it one step further, the FE-modelling has in this project been combined with tensile testing of small-scale concrete specimens. The methodology of this combination is illustrated in Figure 1.1.

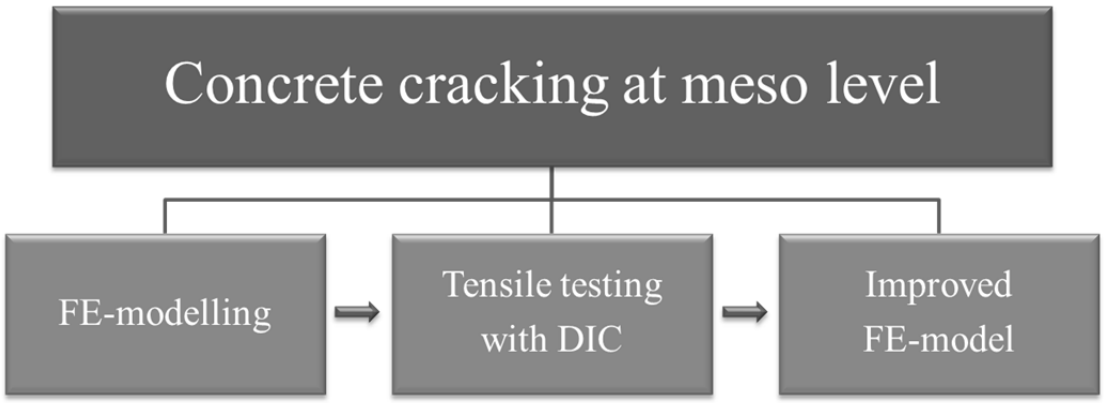

Figure 1.1 Methodology of the combination of FE-modelling and tensile testing.

FE-modelling
At first, a simple concrete specimen consisting of cement paste, interface zone and one aggregate particle was modelled in the finite element program Abaqus. In order to establish a reasonable FE-model of a simple concrete specimen at meso level, different modelling techniques and settings were tested in order to investigate how they influenced the results. The established simple FE-model should show expected crack initiation and propagation for the modelled simple specimen.

Tensile testing with DIC
Secondly, specimens of idealized concrete were made by SP based on the modelled simple specimen in Abaqus. The real small-scale concrete specimens were tested in tension at SP Technical Research Institute of Sweden in Borås. The results of the tests were thereafter evaluated with the DIC-system Aramis in order to get images and stress-displacement curves which showed crack initiation and propagation for the tested specimens due to the applied tensile load.

Improvement of FE-model
The last step was to improve the simple FE-model after comparison with results from the tensile stage tests. This step was the main objective of the project and was made in order to obtain a FE-model which would, based on the tests, show the real concrete cracking behaviour. The stress-displacement curves together with images of the crack initiation and propagation from the tests were used to adjust the input data in the simple FE-model. Especially stresses for when cracking initiated in the interface and cement paste respectively were used to adjust the material properties of these components in the FE-model.

In order to reflect actual concrete surface structure, the specimen in the improved simple FE-model was developed to have a more accurate appearance. Two new

complex models with larger amount of aggregate particles and larger dimensions were modelled. The complex models were assigned the same material properties as the components in the single aggregate specimen in order to verify if the improved simple FE-model could be used also for more realistic concrete specimens.

2 Concrete

Concrete is, with its production of two tonnes per capita every year, one of the most commonly used building materials today and the most used counted in volume. It has been used for many years, and will probably be used for many more to come due to its accessibility and its ability to be produced with different material properties (Domone & Illston 2010).

Concrete is a material that consists mainly of cement, water and aggregates and the amount of each component is decisive for the properties of the concrete. It is therefore of great importance to choose right amount of each component in the mix proportions to get the desired properties of the concrete. Besides the main components, also admixtures and additions can be used to get the desired behaviour of the concrete (Burström 2010).

2.1 Concrete at meso level

The structure of concrete is normally studied at one of the following levels; macro, meso or micro level. At macro level, concrete is studied as a homogeneous material, but concrete is in fact a heterogeneous material. Therefore, concrete is in some aspects seen as a two-phase material consisting of aggregates and hardened cement paste. When concrete is studied at meso level, it consists of three different components instead of two components. Besides hardened cement paste and aggregates, it also consists of an interface zone, i.e. transition zone. At meso level, each component with its own properties and behaviours together with how the components react with each other are studied. Micro is the smallest level of the three presented, where the details of each component are studied (van Mier 1995). The different levels can be seen in Figure 2.1.

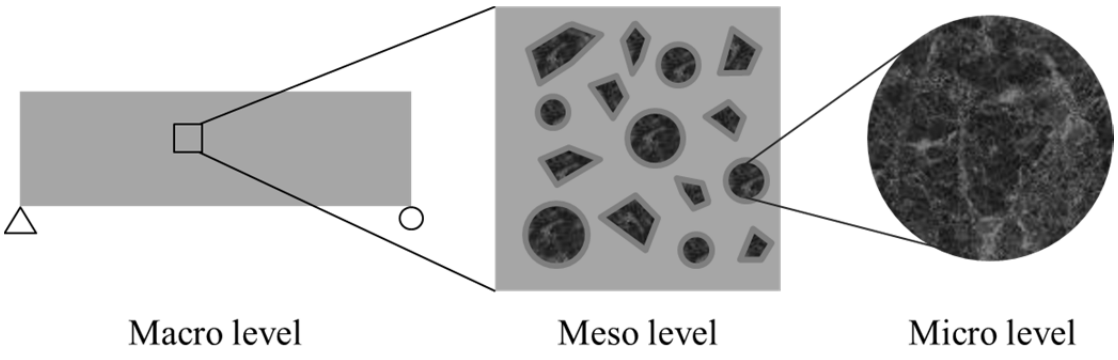

Figure 2.1 Concrete seen at macro, meso and micro level.

When studying cracking and strength of concrete, it is necessary to observe the material at meso level where it is seen as a three-phase material consisting of hardened cement paste, aggregates and the interface zone, see Figure 2.2 (Domone & Illston 2010).

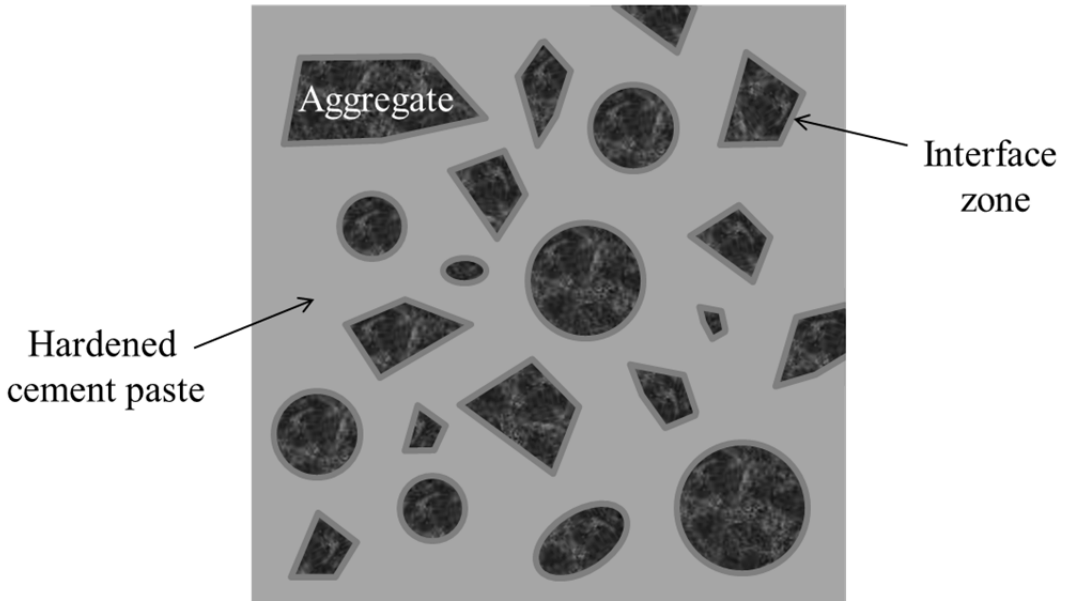

Figure 2.2 Concrete seen at meso level with aggregates, hardened cement paste and interface zones visable.

2.1.1 Cement paste

Cement is the most important component in concrete, but has the smallest proportion counted in volume. It is a hydraulic material which reacts chemically in contact with water and becomes a hardened cement paste, able to withstand water. The most commonly used cement is Portland cement (CEM I) with a usage of 95 % in the world (Domone & Illston 2010). Byggcement, which is a CEM II Portland-limestone cement, is however used more frequently in Sweden due to its better effects on the environment during manufacturing than ordinary Portland cement (Cementa n.d.; Burström 2010).

Cement together with water creates the cement paste, also called binder, which binds the aggregates together and form the homogeneous material concrete. The properties of the cement paste is determined by the water:cement ratio. A lower water:cement ratio gives a higher strength for the cement paste and therefore also for the concrete, compared to concrete with higher water:cement ratio (Burström 2010). The strength of the cement paste is also closely connected to the degree of hydration, i.e. how far the chemical reaction between the cement and water has developed. The strength increases gradually with the degree of hydration and thus the age of the cement paste. About 90 % of the hydration is completed after 28 days but the hydration and therefore also the strength can continue to increase for many years (Domone & Illston 2010).

2.1.2 Aggregates

The hardened cement paste could work as a construction material on its own. It has however high changes in dimensions due to low elastic modulus, high creep and shrinkage, and this together with the high cost makes it inappropriate to use

individually. Aggregates are therefore used together with the cement paste to get a material with properties suitable for construction use (Domone & Illston 2010).

To decrease the disadvantages from the cement paste when creating concrete, the amount of aggregates should be as high as possible. The amount of aggregates, counted in volume, in ordinary concrete is therefore approximately 65-80 % (Domone & Illston 2010). As large aggregate size as possible is also desired since this as well limits the amount of cement paste needed. There are though limitations for the amount and maximum size of aggregates; too high amount will make the fresh concrete difficult to handle (Burström 2010), and the maximum size is depending on the handling, mixing and placing requirements of the fresh concrete (Domone & Illston 2010).

Different sizes of the aggregate particles, from fine sand to coarse stones, are used to minimize the voids between the aggregates and thus the amount of cement paste needed (Domone & Illston 2010). Sufficient amount of cement paste is though needed to enclose each aggregate particle and thus achieve the bond between all aggregates and the cement paste (Burström 2010).

Both natural and crushed rock materials are used as aggregates in concrete mixes (Burström 2010). Natural rock material is nowadays used as the finer aggregate particles (0-8 mm), and crushed rock material as coarse aggregate particles (> 8 mm) (CBI Betonginstitutet 2008). The natural particles are originally from natural gravel deposits, such as hill sides, and are therefore uncrushed with a rounded or irregular shape. The crushed particles have instead a sharp and angular shape since they are extracted from bulk sources (Domone & Illston 2010). The different shapes of the aggregates are illustrated in Figure 2.3. Natural rock material is, as mentioned, the major aggregate resource for finer particles, but is today a limited resource. It is also, due to environmental reasons, of importance to preserve the hill sides where natural rock material is extracted from. Crushed rock material should therefore, as stated in the introduction, in long term replace the natural rock material as finer aggregate particles in the concrete mix (CBI Betonginstitutet 2008).

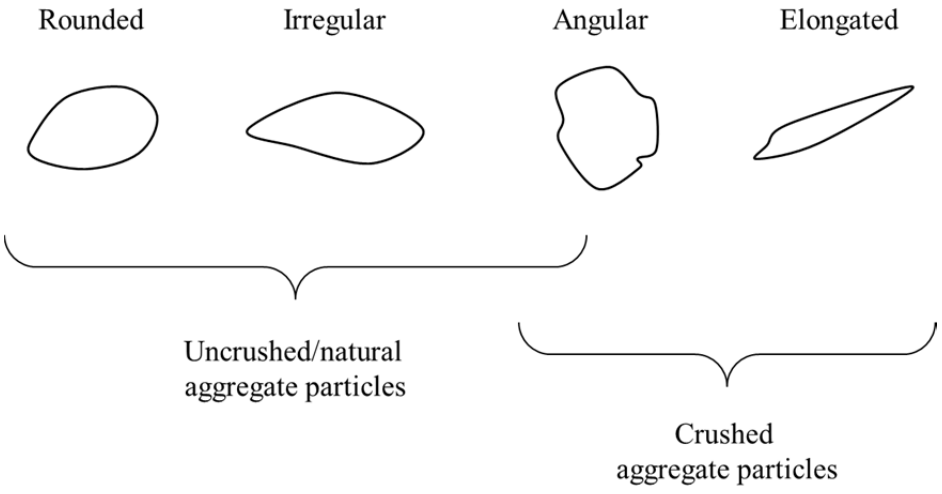

Figure 2.3 Different shapes of the aggregate particles, redrawn from (Domone & Illston 2010).

Aggregates are divided in the range of filler ≤ 0,125 mm, sand ≤ 4 mm, fine gravel ≤ 8 mm and stone > 8 mm, and as mentioned earlier different sizes are used in the same concrete mix. Aggregates could also be separated into fine and coarse aggregates where 8 mm is the separation size of the two definitions (Burström 2010; Domone & Illston 2010).

The type of particles used and their shapes have a great impact on the properties of fresh and hardened concrete (Domone & Illston 2010). As concluded by (Flansbjer & Lindqvist 2013), concrete with crushed aggregates have more secondary fractures branching out from the primary fracture, while concrete with natural aggregates instead have more diagonal fractures. More crushed particles are wanted, as mentioned earlier, in the concrete mix due to environmental reasons in term of infinite resources. Despite this, natural particles are better to use in order to decrease the need for cement paste, which also is desirable due to environmental reasons. Rounded particles pack more efficiently and therefore give as low void content as possible and hence decrease the need for cement paste (Domone & Illston 2010).

2.1.3 Interface zone

Between the aggregate surface and the hardened cement paste is the interface zone, also called the transition zone. It is a part of the cement paste which is weaker than the rest of the bulk paste due to its more porous structure. Since the interface zone also is weaker than the aggregates it is a component with large effects on the concrete properties and especially the concrete strength (Domone & Illston 2010).

The size of the interface zone is about 30-50 μm and consists of two parts. The part closest to the aggregate surface is a very thin layer of calcium silicate hydrate fibres with some small calcium hydroxide (portlandite) crystals. The other part contains more and larger calcium hydroxide crystals and fine ettringite needles (calcium sulphoaluminate) than in the bulk cement paste. This gives the interface zone its more porous structure (Domone & Illston 2010). An illustration of the interface zone can be seen in Figure 2.4.

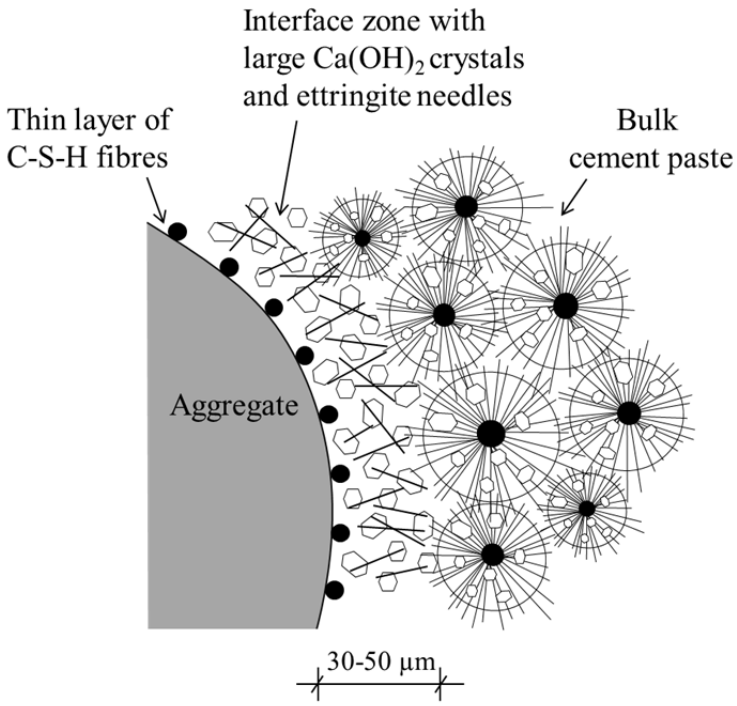

Figure 2.4 An illustration of the interface zone, redrawn from (Domone & Illston 2010).

The formation of the interface zone is probably a result of increased water:cement ratio in the interface between the paste and the aggregate surface. This is due to two reasons; the wall effect and mix water separation. The wall effect is about how the cement grains pack together. The grains do not pack as proper against the aggregates as in the bulk paste, which leads to higher water:cement ratio in the interface zone. Mix water separation also leads to a higher local water:cement ratio at the interface zone, and appears when the aggregate particles and the cement paste moves during mixing of the concrete (Domone & Illston 2010).

2.1.4 Strength of concrete at meso level

When normal concrete is seen as a two-phase material, aggregates are generally the stronger component and cement paste the weaker one. The strength of the cement paste is therefore decisive for the strength of the concrete. However, when examining the concrete strength, it is almost always less than the strength of the cement paste. This is due to the interface zone which is a weaker part of the cement paste, and like said earlier, has a major effect on the concrete properties such as strength. The aggregate strength is of more interest in very high strength concrete (compressive strengths over 80 MPa) and also when using lightweight aggregates, because the strength of the cement paste and the aggregates are more equal in both cases (Domone & Illston 2010).

The aggregates in normal concrete often have a lot higher strength than the actual strength of the concrete. This is in fact required to avoid cracks in the aggregates before cracks in the cement paste, since local stresses at the aggregate edges appear due to stress concentration effects in the concrete. These local stresses for normal-

density aggregates are approximately around three times higher than the average stress in the concrete. This leads to a need of a compressive strength of the aggregates about three times higher than the required concrete strength. Consideration of this is more important for high-strength concrete when the strength of aggregates and cement paste are more similar than in normal concrete (Domone & Illston 2010).

The elastic modulus for aggregates is a lot higher than for the cement paste and the interface zone. The elastic modulus for the interface is around the same value as for the cement paste, or a bit lower since it has a more porous structure (Domone & Illston 2010).

Not only the increasing water:cement ratio near the aggregate surface affects the structure and chemistry of the interface zone, but also the aggregate mineralogy and surface texture have an impact. Which type of aggregates used in the concrete mix therefore affects the concrete strength. Aggregates of crushed rock material have a rougher surface and also a better mechanical interlocking of the cement particles than natural rock material. This is due to the angular shape of the crushed rock material, which gives a better adhesion between the aggregates and the cement paste. Concrete with aggregates of crushed rock material therefore have a strength which is about 15-20 % higher than concrete with natural rock material. To get a good adhesion, it is also of importance that the aggregate surface is not contaminated by materials such as mud or clay (Domone & Illston 2010).

A change of the volumetric proportions in the concrete mix, such as increasing the amount of aggregates when keeping the water:cement ratio constant, does not affect the concrete strength considerably. An aggregate increase of 50 % will only lead to an increase of 10 % in concrete strength. As mentioned in Section 2.1.2, as large size as possible should be chosen for the aggregates. If though larger size for the aggregates than the maximum appropriate is used, the concrete strength will be reduced instead of achieving positive effects (Domone & Illston 2010).

2.2 Cracks in concrete

Concrete is a material that has defects and microcracks even before the material has been stressed. These defects enter the material during the making of the material, when the concrete goes through changes corresponding to volume and temperature changes. The microcracks and the defects will grow when the material is loaded with an external load (Engström 2014).

There are many different types of cracks when it comes to concrete. Cracks can be created not only because of external loads, but also because of loads caused by the material itself or by accidents. Normally, cracks occur in concrete structures during the construction stage or during service life. Disregarding external loads, the most common reasons for cracks in concrete are:

- Temperature stresses due to contraction of the cooling concrete
- Drying shrinkage
- Shrinkage caused by the cement hydration

External loads are the main reason to why cracks occur in concrete, and the loads can affect structures in different directions and sizes. Figure 2.5 below shows different types of cracks caused by external loading such as shear, tension, torsion, concentrated load and bending (Engström 2014).

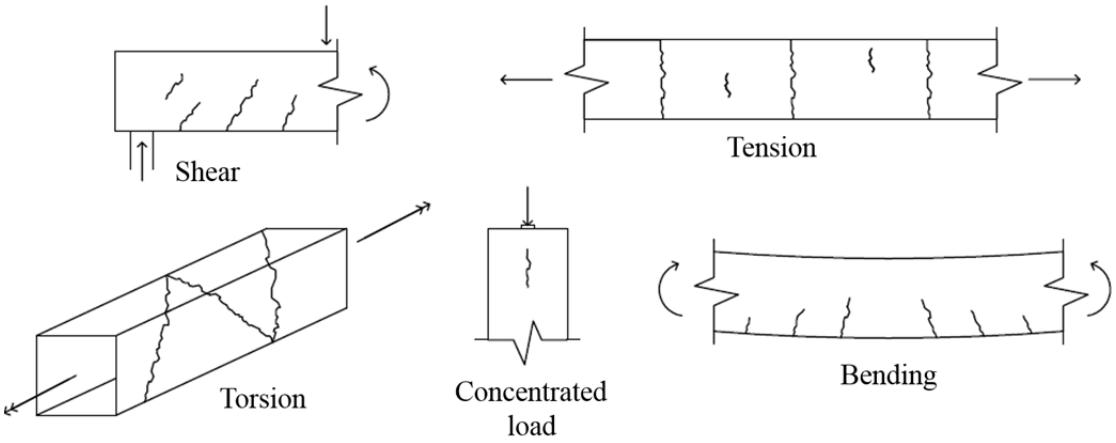

Figure 2.5 Different types of cracks due to external load, redrawn from (Engström 2014).

2.2.1 Consequences of cracks

Cracks are natural for all concrete structures, but the fact that cracks appear in concrete also has a lot of consequences, some more serious than others. It weakens or in worst case takes away the load-bearing capacity of the concrete. If the concrete is accurately reinforced, the cracking has less significance since the reinforcement will take care of the acting tensile stresses. Due to this, the structure can remain load-bearing. On the other hand, a lighter reinforced concrete structure could have a brittle fracture due to the lack of resistance in tension. When cracks occur in the cross-section, it leads to a reduction of the stiffness as well as the stability of the concrete. The lack of stiffness can lead to greater deflection, which again affects the stability as well as shortens the possible span of the concrete. Water and other natural substances can leak into the cracks and lead to serious consequences, such as reinforcement corrosion, frost damage and chemical attacks. In total, the durability of the concrete will weaken. The cracking does not only influence the strength of the concrete but also the aesthetics as the cracking will lead to a less attractive appearance (Engström 2014).

2.2.2 Fracture mechanics

A uniaxial concrete tensile test is used for describing the non-linear fracture mechanics models of concrete. During a tensile test, the concrete goes through different processes. In the beginning, when the specimen is loaded with a tensile force, microcracks start to grow through the concrete specimen (Figure 2.6 II)). These cracks can also be described as weak points in the concrete and they will grow as the tensile force increases. With increasing load, the cracks will grow bigger and start to connect with each other, which again creates even bigger cracks and a bigger area of microcracks. Simultaneously with the crack growth, a deformation begins to form in

this weaker part, i.e. the fracture zone, of the concrete specimen (Figure 2.6 III)). After the concrete has reached its maximum load, the deformation will continue to increase in the fracture zone and slowly opens the cracks. At the same time the material on both sides of the fracture zone will be elastically unloaded. After the maximum load is reached, less load is needed for increasing the deformation within the fracture zone (Figure 2.6 IV)). Figure 2.6 V) shows the last step of the cracking process, when the tensile force separates the concrete into two separated parts and no more load can be added (Plos 2000).

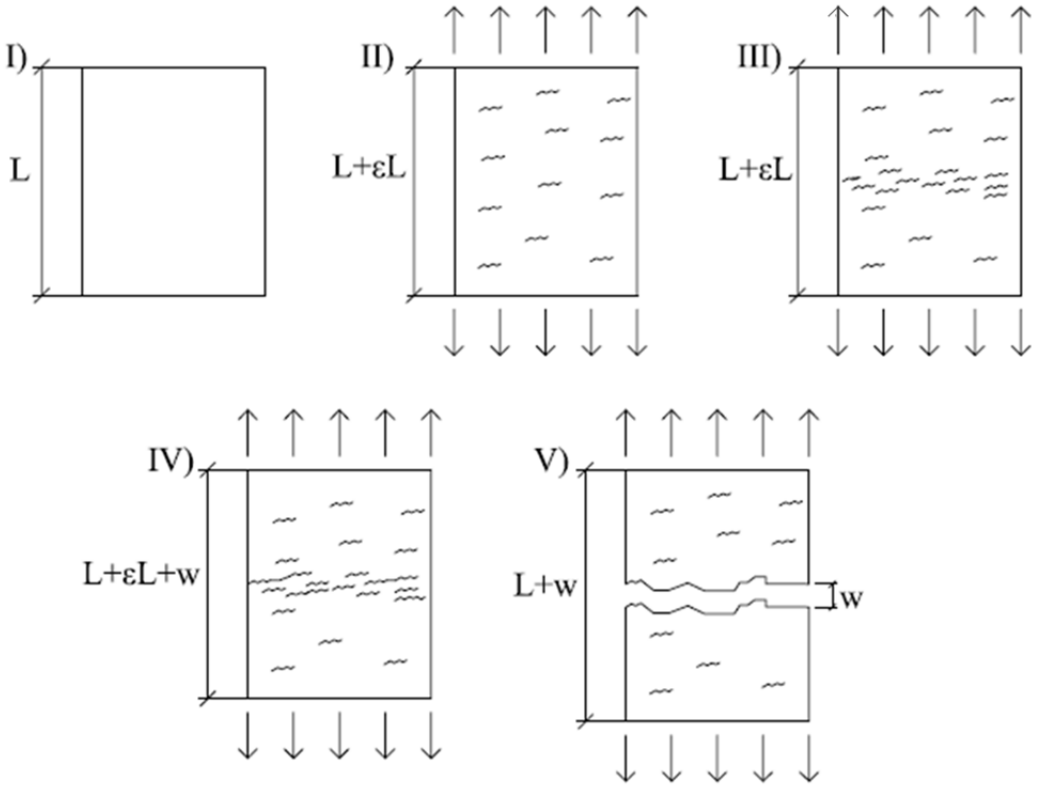

Figure 2.6 *The different stages of cracking in a concrete specimen subjected to tensile loading. Redrawn from (Plos 2000).*

The different stages of cracking have different stress levels as well as displacements. Figure 2.7 shows the values of the stresses and displacements for each stage which are represented in Figure 2.6. Each of these stages can be seen in the stress-displacement curve, which is illustrated in Figure 2.7.

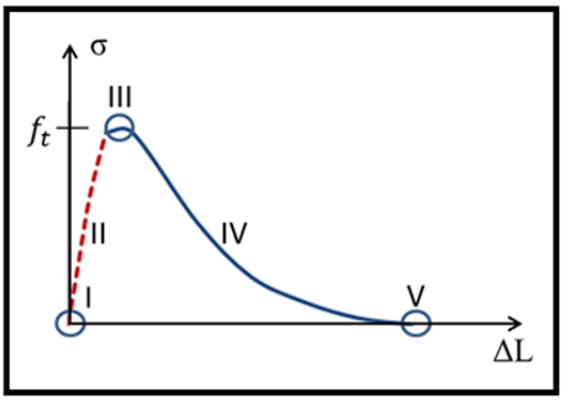

Stage	Stress	Displacement
I	0	0
II	$\sigma < f_t$	εL
III	$\sigma = f_t$ *(w = 0)*	εL
IV	$\sigma = f(w)$ *(0 < w < w_u)*	εL + w
V	$\sigma = 0$ *(w ≥ w_u)*	w

Figure 2.7 *Stress-displacement curve to the left and the corresponding values for each stage to the right of a concrete specimen subjected to tensile load.*

The fracture mechanism of a concrete specimen can be shown in a stress-displacement diagram (Figure 2.7) as mentioned previously. This diagram shows the typical stress-displacement shape for a concrete specimen as the one described above. In the tensile testing used to describe the concrete, the material has been seen as a homogenous material. Measurements during testing give a stress-displacement relation which again can be recalculated to a stress-strain relation. Since the concrete acts differently throughout the specimen due to localization of the deformation, the recalculations get more complicated. Figure 2.8 shows how the final graph consists of two different graphs. The left image in this figure represents the material outside the cracking zone, where the material can be described by an elastic stress-strain relation. In the fracture zone, the material is described with a stress-crack opening displacement relation, which represents the additional deformation due to cracking in the concrete (Plos 2000). The middle image in Figure 2.8 illustrates this.

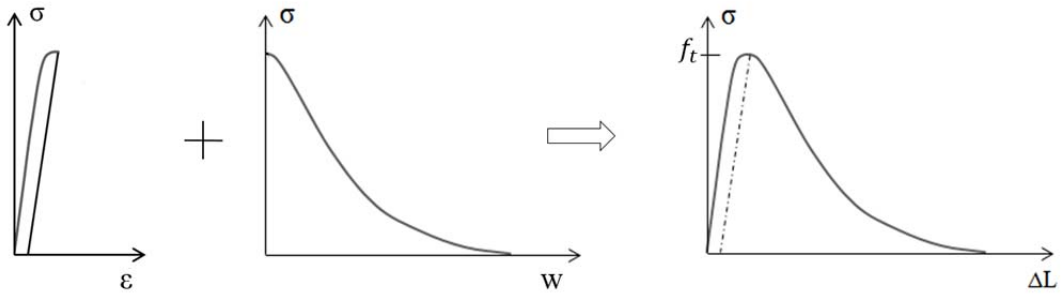

Figure 2.8 *The stress-displacement curve divided into a stress-strain curve and a stress-crack opening curve.*

The area under the graph in the stress-crack opening curve in Figure 2.8 represents the fracture energy, G_f. This area describes how much energy that is used in the fracture process and is also described as the amount of strain energy transformed to heat. In the stress-displacement graph, in Figure 2.8, the tensile strength, f_t, represents the maximum stress that can be applied to the concrete specimen before it cracks (Plos 2000).

The stress-displacement graph is linear in the first part of the curve up to a value just before the maximum tensile strength. After this point, the curve is non-linear all the way down to zero-level. If the descending part of the graph is very steep, the fracture in the concrete is brittle and if it is slowly decreasing, the fracture instead takes time to separate the concrete specimen.

2.2.3 Cracks at meso level

Concrete has non-linear stress-strain behaviour while the components cement paste and aggregate show a linear behaviour until a point just before the maximum value, see Figure 2.9. It could in the figure also be seen that the behaviour of concrete in form of elastic modulus lies in between the ones for cement paste and aggregate (Domone & Illston 2010).

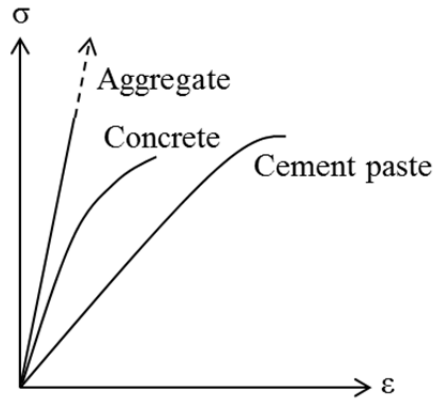

Figure 2.9 Stress-strain behaviour for aggregate, cement paste and concrete. Redrawn from (Domone & Illston 2010).

This non-linear behaviour is a result of existing microcracks in concrete before loading, explained in Section 2.2. Increased loading leads to further development of these cracks in length, width and number. The growing cracks will affect the overall strain with a gradually increasing contribution which gives the non-linear behaviour of concrete (Domone & Illston 2010).

The microcracks are present in the interface zone, and since this zone is the weakest component of concrete and has a different microstructure than the cement paste, it is where the development of cracks starts when load is applied. After the formation of cracks in the interface zones around the aggregates in normal concrete, the cracks will continue to propagate into the cement paste and finally form crack paths in the concrete (Domone & Illston 2010). See the left image in Figure 2.10 for an illustration of this. If crack propagation is studied in high-strength concrete where the aggregates and cement paste have similar properties, the crack paths can form in two ways. The cracks could either propagate in the cement paste and go around aggregate particles, like in normal concrete, or go through both the cement paste and aggregate particles to form much straighter cracks (Flansbjer & Lindqvist 2013). This is illustrated in the right image in Figure 2.10.

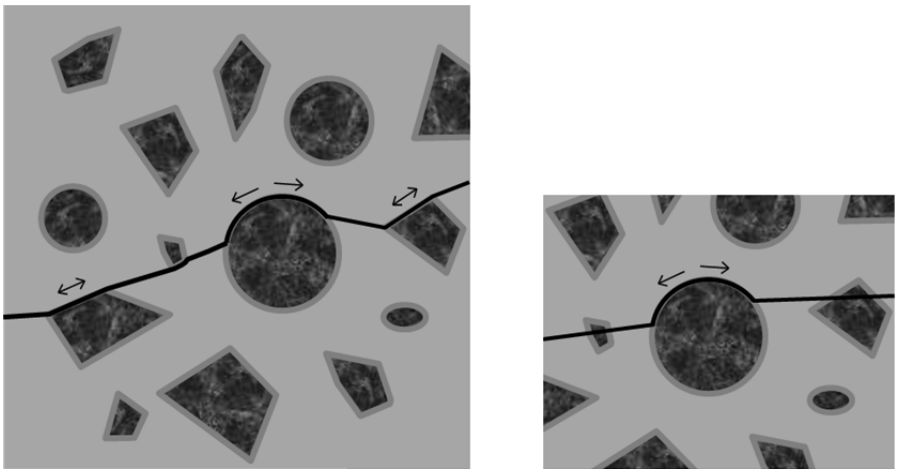

Figure 2.10 *Left image: formation of a crack, starting in the interfaces and propagating into the cement paste. Right image: possible crack path in high-strength concrete.*

Concrete when seen at meso level also shows a stress-displacement curve like the one explained in Section 2.2.2 when subjected to tensile loading. In stage II, see Figure 2.6, the existing microcracks in the interface start to grow and also new cracks in the interface develop. Crack initiation of concrete at meso level therefore starts in the interface around the aggregate particles. After this point the curve starts to have a non-linear behaviour and the microcracks also grow together and form larger cracks. Near stage III, where the curve has its maximum stress value, the cracks start to propagate into the cement paste as well. After stage III, the created macrocrack develops even further until it separates the concrete (Flansbjer & Lindqvist 2013).

3 Numerical Modelling at Meso Level

The numerical modelling in the finite element program Abaqus started with a mapping of the geometry, and also finding the most appropriate approach to model the different components. Next step was to find the right material models regarding linear and nonlinear behaviour for each component, as well as figuring out which restraints to take into account. All this was done with the help from previous models, Abaqus manuals and information retrieved when testing different approaches.

3.1 Previous modelling of concrete at meso level

Advanced modelling of concrete at meso level with finite element method has been done in various ways. As explained by (Skoček 2010), concrete as a heterogeneous material can be modelled for example by the continuum mechanics approach, with lattice models or with particle models. In the work by (Grassl & Jirásek 2010), they were using a discrete lattice approach in combination with a damage mechanics model. (Wang et al. 2015) were instead modelling concrete at meso level with zero-thickness cohesive interface elements and (López et al. 2008) were modelling with zero-thickness interface elements.

Modelling can be done with the help of various commercial software programs, and (Du et al. 2014) were using extended finite element modelling (XFEM) in the FE-program Abaqus to simulate the failure process of concrete at meso level. The different components were assigned different areas and material properties. Aggregate distribution, interface zone strength and aggregate shape and size were modelled and evaluated for a specimen with a lot of coarse aggregates.

Doctor Matthew Pais, employed by Dassault Systèmes Simulia Corp., has done some research about XFEM; the research can be found at (Pais 2015). XFEM is an approach that could have been used in this Master's thesis project. Although, the methodology is rather complicated and there are a lot of unknown parameters. Therefore, it was chosen not to be studied in this project, but an investigation in further studies could be of great interest.

(Kim & Al-Rub 2011) were also using Abaqus to investigate concrete at meso level. In their study, they investigated how the overall tensile strength and the crack initiation and propagation were affected by; aggregate shape, distribution and volume fraction, interface thickness and also interface and cement paste strength. The aggregates were modelled as linear elastic meanwhile the interface and the cement paste were modelled as a coupled plasticity-damage model. Also in this work, the different components at meso level were assigned different mechanical properties and the specimen contained a lot of aggregates.

In this Master's thesis project, the modelling was done with more simple specimens and modelling techniques than the ones described above. Besides XFEM, two different constitutive models for analysis of concrete; the *Smeared crack model* and the *Concrete damaged plasticity model*, were considered as material model to be used. More information about these models can be found in (Dassault Systèmes 2012b; Dassault Systèmes 2012c; Dassault Systèmes 2012e). Since the *Smeared crack model* is more complicated to use, the *Concrete damaged plasticity model* was chosen to use

in the FE-modelling. The *Concrete damaged plasticity model* used in Abaqus is based on the models by (Lubliner et al. 1989) and (Lee & Fenves 1998).

3.2 Representation of geometry

Continuum solid elements were chosen to represent the concrete specimen in the model. The size of the modelled concrete specimen was limited due to the size of a tensile stage device. This was because real concrete specimens similar to the modelled one were later on tested in the tensile stage. See Chapter 4 for more information about the tensile testing. This limitation was done in order to be able to compare the results from the numerical model and from the tensile test specimen with each other. The testing was to be done on thin small-scale concrete specimens. Therefore the numerical model was developed in 2D, since cracks have a similar appearance in the third direction for a thin specimen.

In Figure 3.1, the geometry of the numerical model as well as the dimensions can be seen. The whole model was a square with the dimensions of 65x65 mm^2 and with one coarse circular aggregate with a diameter of 25 mm located in the centre of the square. The size of the aggregate was chosen based on available cores of rock material which later on could be used for casting of small-scale concrete specimens. The model was also assigned a thickness of 10 mm and was modelled with plane stress state. This geometry was chosen since a simple model was preferable for the study. The interface zone between the cement paste and the aggregate was modelled with a thickness of 1 mm. At first a thickness of 40 µm, which was an average value of the thickness described in Section 2.1.3, was modelled for the interface zone. Since the analysis was time consuming for a model with this interface thickness and it also gave numerical problems, the thickness of the interface was increased.

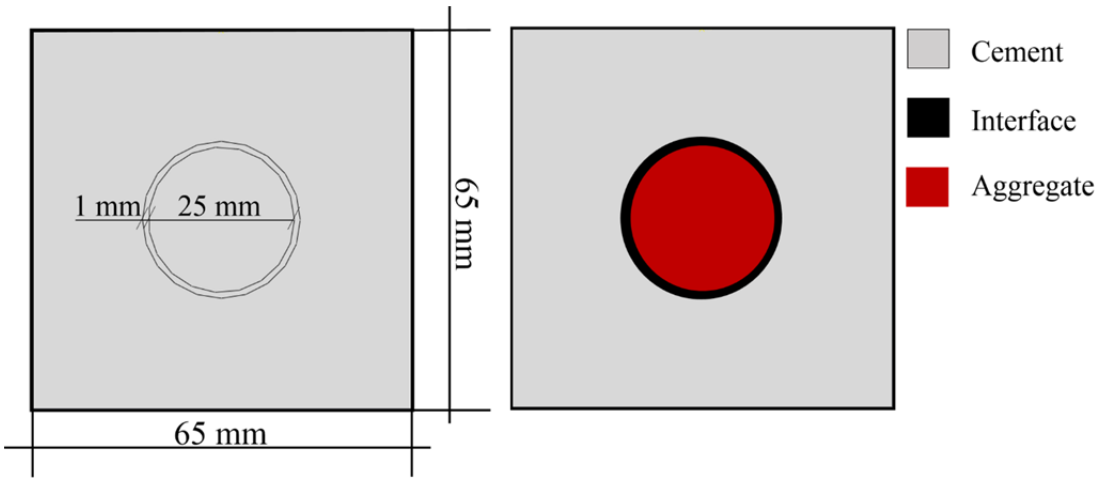

Figure 3.1 Geometry and dimensions of the specimen to the left and the different components to the right.

Figure 3.1 shows how the concrete model was separated into cement paste, interface zone and aggregate. There are various approaches that can be used when modelling the transition zone between the cement paste, aggregate and interface zone in the numerical model. In this Master's thesis project, the function *partition* was chosen to use for separation of the different components of the specimen. When the specimen

had been divided into different parts with this function, each component was assigned different material properties. Another way to model the different components could have been to use the function *constraint with tie*. With this method each component would have been modelled separately and then tied together. Also the mesh could have been modelled differently with these two functions. Since these two functions gave the same result, the *partition* method was chosen because it was easier as well as more efficient to use. The interface zone could also have been modelled as a cohesive zone since it is a small region, but this was not further investigated.

3.3 Material models and properties

The cement paste, interface zone and aggregates in concrete behave in different matters, and therefore they had to be modelled with different material properties. Also, both elastic and plastic behaviours for the different components had to be added in the numerical model in order to reflect the nonlinearity of concrete at macro scale.

Since the aggregate is much stronger than the cement paste and the interface, and therefore probably would not reach its tensile strength, it was modelled with only linear elastic behaviour as a simplification. Both the cement paste and the interface zone were instead modelled with both linear elastic and non-linear behaviour with elastic and plastic values for each component entered as material properties in the model.

The elastic material properties for the aggregate, cement paste and interface zone can be seen in Table 3.1 and were retrieved from (Grassl & Rempling 2008). The value for Poisson's ratio for the cement paste was obtained from (Domone & Illston 2010).

Table 3.1 Material properties – Elastic.

Material	Young's Modulus [GPa]	Poisson's Ratio
Aggregate	120	0.25
Cement	30	0.20
Interface	48	0.25

The *Concrete damaged plasticity model* was used to simulate the plastic behaviour of the cement paste and the interface zone. This model uses an assumption of isotropic damage for a concrete specimen subjected to arbitrary loading conditions. The fracture energy of the specimen is taken into account since the plastic part in tension is modelled. This gives a degradation of the elastic stiffness of the modelled specimen.

The input data for the components in this model can either be stress-strain, stress-displacement or fracture energy. When using stress-strain or stress-displacement for the interface and cement paste, both the obtained global stress-displacement curve for the concrete specimen and the crack propagation were similar for the two different ways of modelling. When using the fracture energy instead, the global stress-displacement curve differed from the one obtained when modelling based on displacement or strain input values. In this project, the concrete damaged plasticity

was therefore chosen to be modelled with displacement input values for the interface and the cement paste. Input data used when evaluating the different ways to model the plastic behaviour can be seen in Appendix A.

Three points for stress and displacement were added in the material model *Concrete damaged plasticity* in the numerical model. The three points can be seen in Figure 3.2 and the corresponding values are displayed in Table 3.2. The tensile strength value, point [1] in Table 3.2, for the cement paste was modelled according to the value in (Grassl & Rempling 2008), and the tensile strength for the interface zone was chosen to be 20 % lower. Point [2] was thereafter chosen in order to get a realistic bi-linear shape of the plastic model. The plastic behaviour was chosen to be modelled bi-linearly due to simplicity.

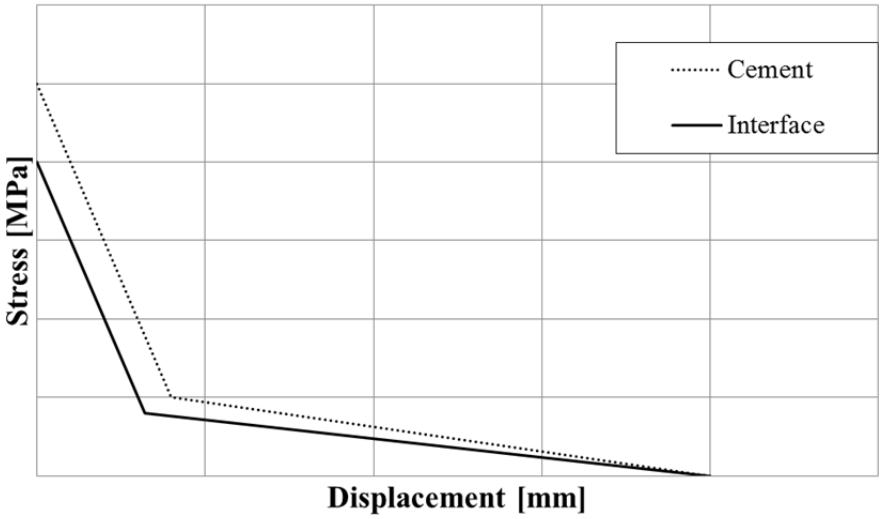

Figure 3.2 *Plastic material models for cement paste and interface - Concrete damaged plasticity.*

Table 3.2 *Material properties – Plastic.*

Cement			
	[1]	[2]	[3]
Stress [MPa]	5.0	1.0	0.0
Displacement [mm]	0.000	0.040	0.200
Interface			
	[1]	[2]	[3]
Stress [MPa]	4.0	0.8	0.0
Displacement [mm]	0.000	0.032	0.200

Besides the values for tensile behaviour in the *Concrete damaged plasticity model* seen in Table 3.2, the dilation angle was set to 30. Also, compressive behaviour had to be defined for the two components, and the compressive strength was set to a value much greater than the tensile strength since the compressive behaviour was irrelevant in this case.

Even though the components of concrete have a more linear behaviour, as explained in Section 2.2.3, the interface and the cement paste were modelled with plastic behaviour as well. This was due to the fact that the available damaged plasticity model in Abaqus was used at meso level instead of macro level, which it was designed for. When modelling the interface and the cement paste with non-linear behaviour at meso level, a non-linear behaviour for the whole concrete specimen was achieved.

3.4 Mesh

The mesh was modelled with 4-node, linear quadrilateral elements of type CPS4R in order to get a mesh as symmetrical as possible. A symmetric mesh was desired since the mesh structure influenced how the crack propagated in the modelled specimen.

A convergence study was done by using different mesh sizes to get a valid mesh, see Appendix B. In order to get the strains which represented the crack to fit in one element row, a finer mesh was chosen for the interface zone since it was the weakest component and the crack therefore was predicted to start there. A finer mesh was also modelled for area D of the cement paste since the crack was likely to propagate into this area. The final mesh with the different zones; A, B, C and D can be seen in Figure 3.3.

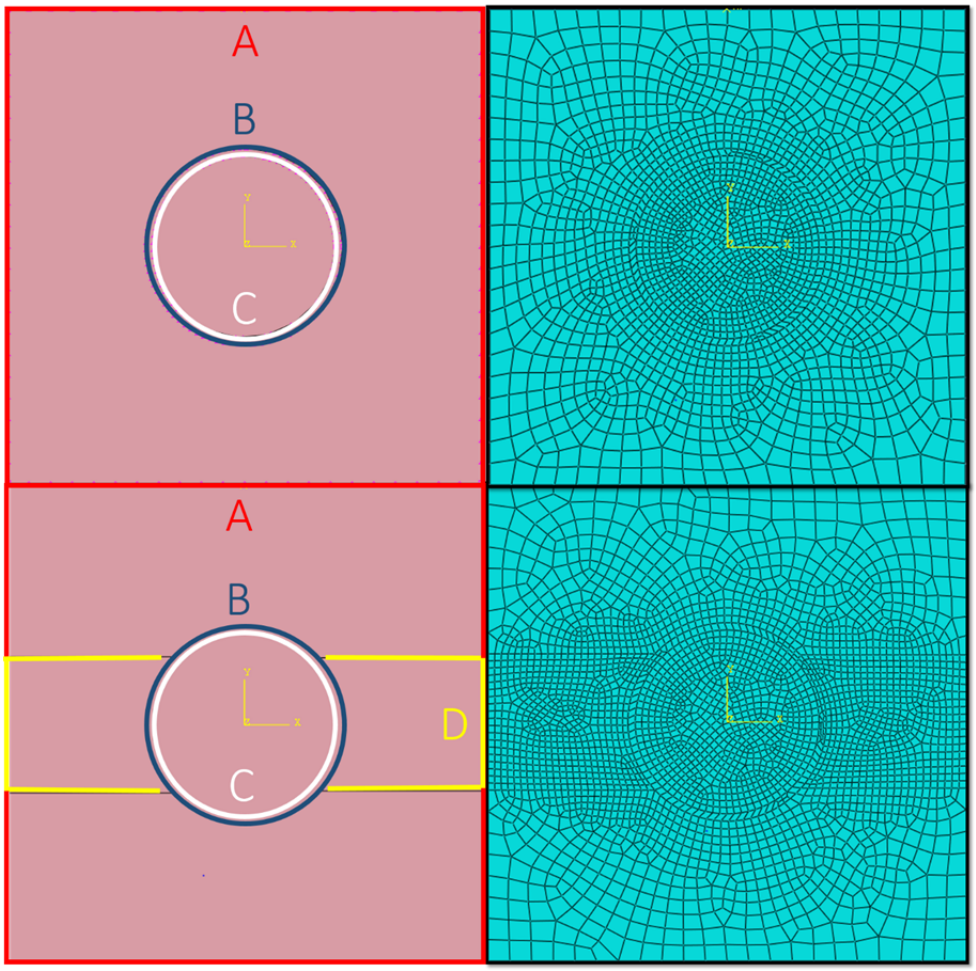

Figure 3.3 Mesh with different sizes and areas.

The final mesh, which can be seen in the lower part of Figure 3.3, was decided to be 3 mm at the edges (A) of the cement paste, 1 mm between the cement paste and the interface zone (B), 1 mm between the interface and the aggregate (C) and also 1 mm at the edges of the finer part of the cement paste (D).

3.5 Boundary conditions

To make the numerical model comparable to the tensile tested specimens, the boundary conditions had to have the same effect as the test specimens during the tensile testing. Since the test specimens were going to be glued to the loading platens and therefore be fixed, see Section 4.2.3, the lower part of the numerical model was restrained in x- and y-direction and it was also prevented to rotate.

The upper boundary was restrained in all directions except y-direction. A reference point was added in the middle of the upper boundary and connected to the whole boundary with the function *rigid body constraint*. To simulate a tension test, a displacement of 0.035 mm was added to the reference point, as shown in Figure 3.4.

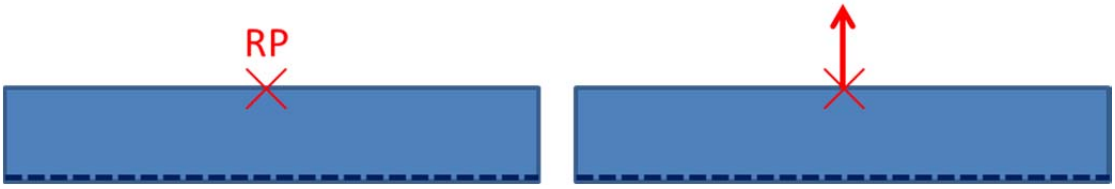

Figure 3.4 Boundary conditions for the upper part of the modelled specimen.

3.6 Results and effects of different parameters

In this section, the results from the simple FE-model is presented. This is done with the help of stress-displacement curves and contour plots of the crack initiation and propagation. In the FE-model a circular aggregate was placed exactly in the middle. In real life, aggregate position, size and shape most likely differ from how it was modelled in this project. Therefore, a parametric study was done to investigate how the following parameters affected the result:

- Aggregate position
- Aggregate size
- Aggregate shape

The impact on the results from interface strength was also investigated.

When performing the parametric study, the interface zone had a thickness of 3 mm since this decreased the computation time of the analysis. The conclusions drawn from these results were still valid on the original model with 1 mm interface zone.

3.6.1 Results from the numerical model

According to theory, see Section 2.2.3, the crack initiation should start in the interface and then propagate into the cement paste. As seen in Figure 3.5, the crack pattern for

the modelled specimen subjected to load actually started and propagated like predicted. When comparing the stress-displacement curve for the modelled specimen with the theoretical curve, also these where similar, see Figure 3.6. Plastic strains represented the crack initiation and propagation when looking at the results in the FE-model.

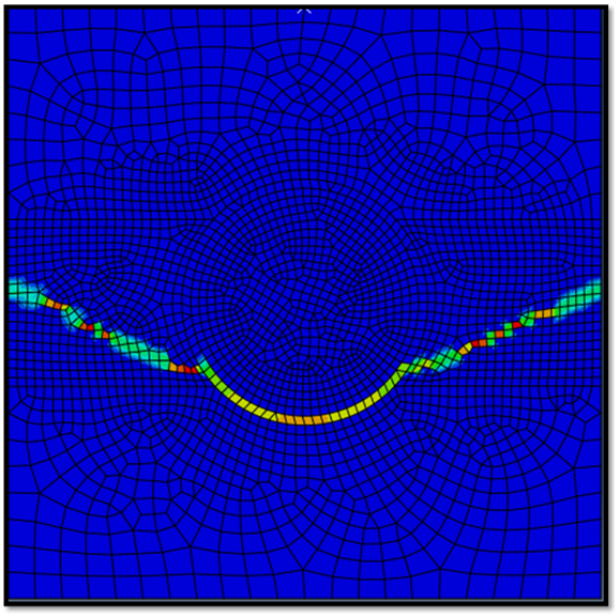

Figure 3.5 Crack pattern for the modelled concrete specimen.

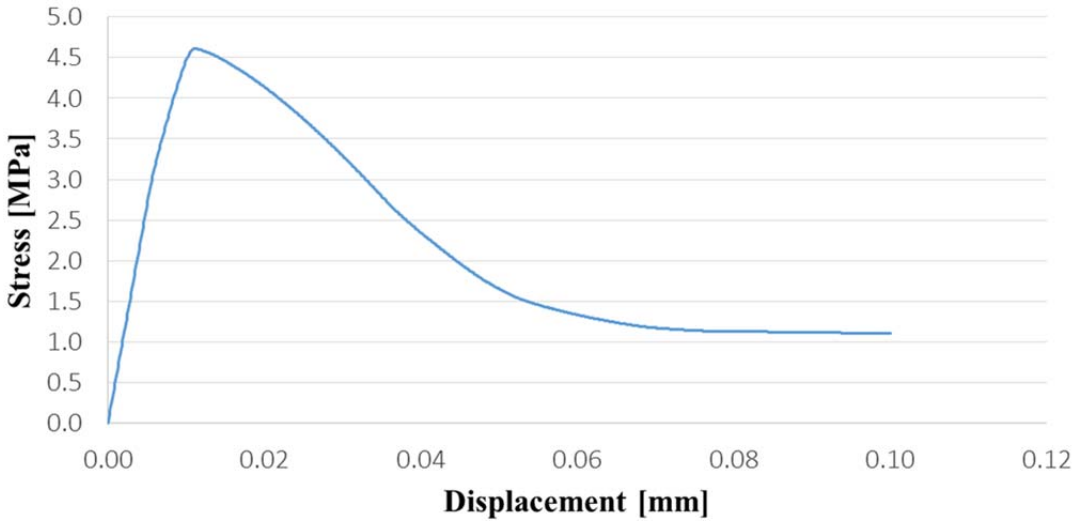

Figure 3.6 Stress-displacement curve for the modelled concrete specimen.

The specimen modelled like this in Abaqus hence showed crack initiation and propagation in a proper way. This FE-model was therefore used later on for improvement and verification with results from tensile stage tests of similar concrete specimens as the modelled.

3.6.2 Effect of aggregate position

The aggregate in the modelled specimen was, as explained earlier, placed in the centre of the specimen. It was though also investigated how other placement arrangements of the aggregate affected where crack initiation in the interface occurred.

Different models were tested by placing the aggregate 10 mm from the centre of the concrete. One model had the aggregate located downwards from the centre and one model had the aggregate located to the right side of the centre. A model with a combination of these two models was also done. The images in Figure 3.7 show where the crack appeared for the different positions of the aggregate. In Figure 3.8 it is illustrated with the help of stress-displacement curves how the different crack propagations affected the global response. Models with the aggregate located upwards and also to the right and upwards were also made but are not visualised with figures.

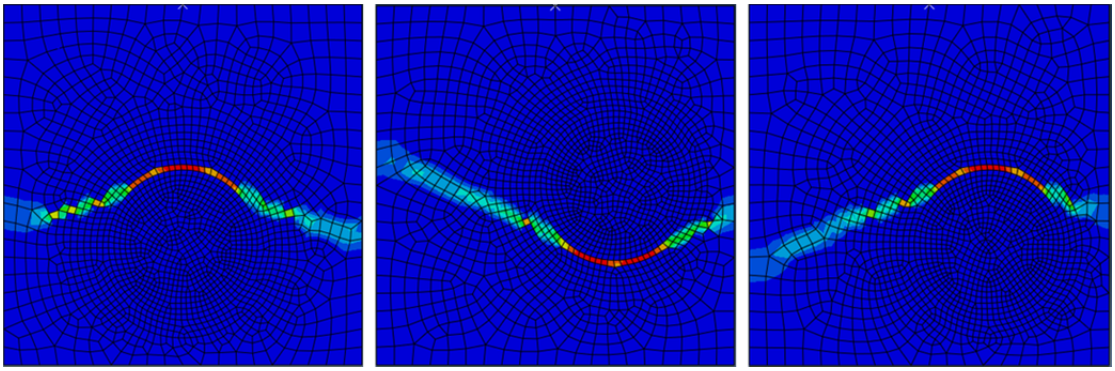

Figure 3.7 *Visualisation of crack location for models with the aggregate placed down, aggregate placed to the right and aggregate placed to the right and down instead of centred.*

When the aggregate was placed 10 mm downwards from the centre, the crack was located above the aggregate. The crack instead initiated below the aggregate when located upwards, which can be expected because of the symmetry of the test. For the model with the aggregate located down and to the right, the crack was located above the aggregate similar to the model with the aggregate placed downwards. Due to symmetry, the model with the aggregate located upwards and to the right showed a similar result, but with the crack located below the aggregate instead.

It can in the stress-displacement curves for the different models in Figure 3.8 be seen that the placement of the aggregate does not affect the fracture energy considerably, but it does effect the location of the crack, seen in Figure 3.7.

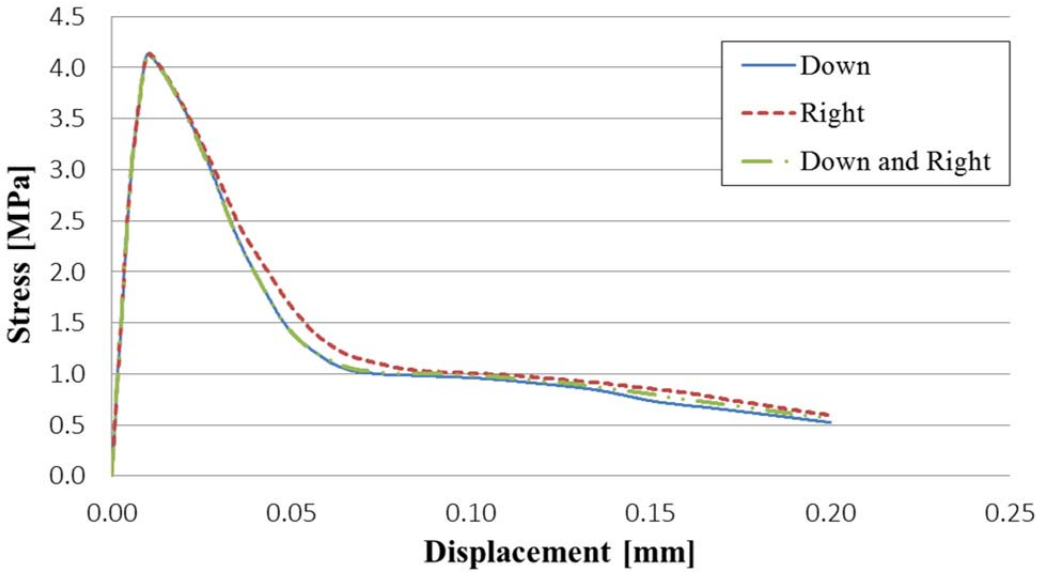

Figure 3.8 *Stress-displacement curves for the models with different placement of the aggregate.*

3.6.3 Effect of aggregate size

A study on how much the size of the aggregate matters was also done. Two models are presented below; one with a 25 mm aggregate and one with a 10 mm aggregate. The crack propagation looked primarily the same when comparing the two different images to the right in Figure 3.9. The stress-displacement curves, shown to the left in the same figure, were almost identical, so the fracture energy was not affected that much of the aggregate size. The model with an aggregate of 10 mm had only slightly higher fracture energy. There was also not a big difference regarding the maximum stress, but the model with a 10 mm aggregate had a slightly higher maximum stress. These results are reasonable, since the length of the interface was shorter for the model with a 10 mm aggregate. The model with a 25 mm aggregate was therefore somewhat weaker due to the interface length than the model with a 10 mm aggregate. The difference in maximum stress and fracture energy would probably have been larger if specimens with more aggregates were modelled.

The fact that the crack was located below the aggregate for the model with an aggregate of 10 mm and above for the aggregate with a size of 25 mm is probably not an effect of the aggregate size. It could be an effect of the element distribution in the meshes for the different models.

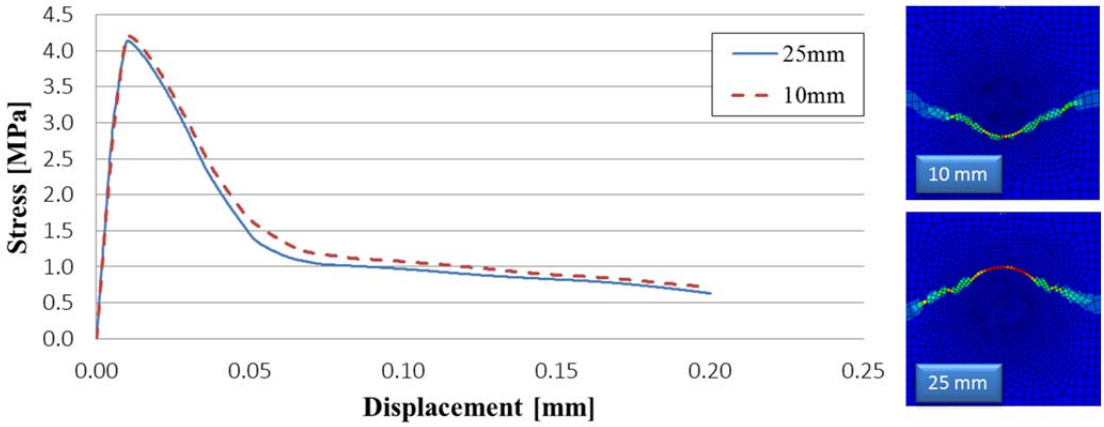

Figure 3.9 *Stress-displacement curves for different sizes of the aggregate to the left and images of the crack propagation to the right.*

3.6.4 Effect of aggregate shape

In order to see how the shape of the aggregate affected the cracking, tests with the aggregate modelled as a triangle and as a square were performed. The cracks in these models started, like for the original model with a circular aggregate, in the interface and followed the shape of the aggregate before it propagated into the cement paste on either side of the aggregate, see Figure 3.10. The shape of the aggregate did thus not affect the crack propagation that much. If more aggregate particles would have been modelled in the same specimen, the aggregate shape would probably have affected the cracking pattern more than it did for a single aggregate specimen.

Since there was not a big difference in the cracking pattern for a single aggregate specimen when using a quadratic or triangular aggregate than a circular, a circle was chosen to simulate the aggregate in the model due to simplicity.

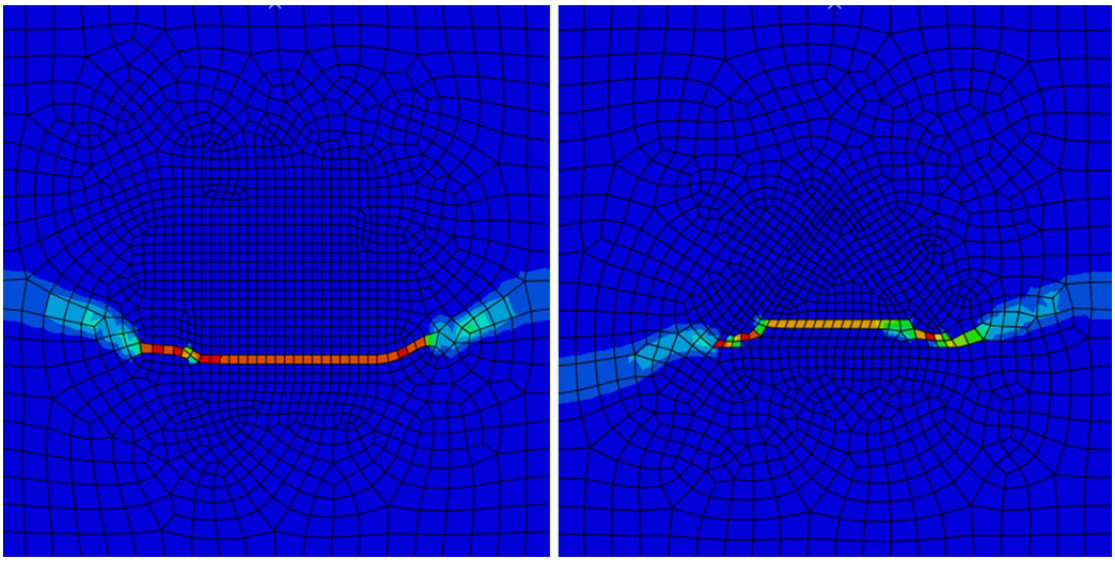

Figure 3.10 *The aggregate modelled as a square and as a triangle.*

3.6.5 Influence from strength of the interface zone

A test about the effect of the interface strength was carried out to see how it affected the crack propagation. By decreasing the strength of the interface the crack followed the transition zone between the aggregate and the cement paste, i.e. the interface, further on each side before it propagated into the cement paste. When the interface was stronger the crack propagated earlier into the cement paste instead of continuing around the aggregate in the interface. See Figure 3.11 for the propagation appearance of the crack due to interface strength.

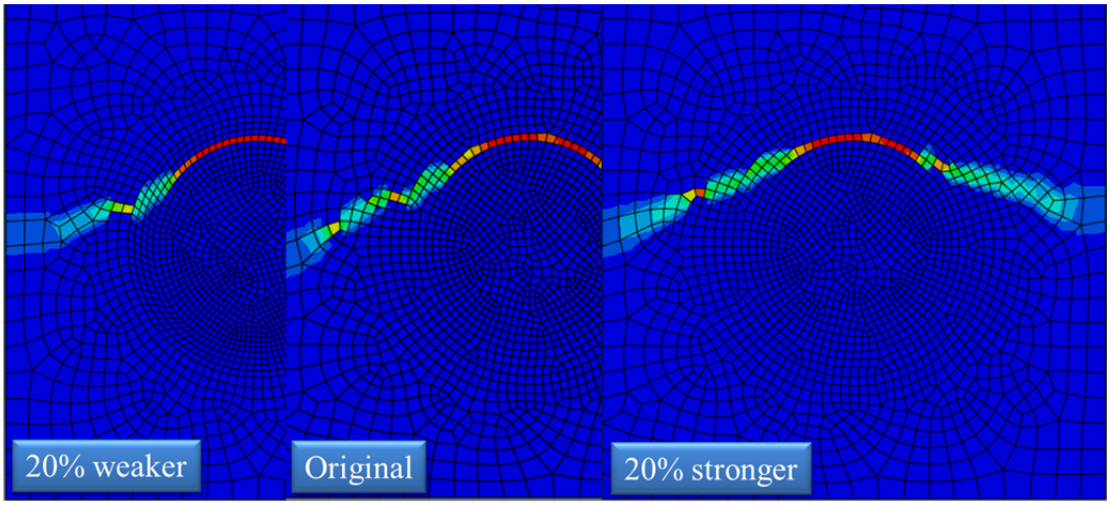

Figure 3.11 *Visualisation of crack propagation for the specimen with 20% weaker interface, with original interface strength and with 20% stronger interface.*

The strength of the interface did not only affect the propagation of the crack but also the maximum tensile stress for the modelled specimen. Figure 3.12 shows the development of the crack depending on the strength of the interface. The graph shows that the concrete had a higher value for maximum stress when the interface was stronger, and the opposite when the interface was weaker, than the original model. When the interface was weaker it also gave less fracture energy, while a stronger interface gave larger fracture energy. Table 3.3 shows the input data used to make the two FE-models; 20% weaker and 20% stronger interface than the original interface strength.

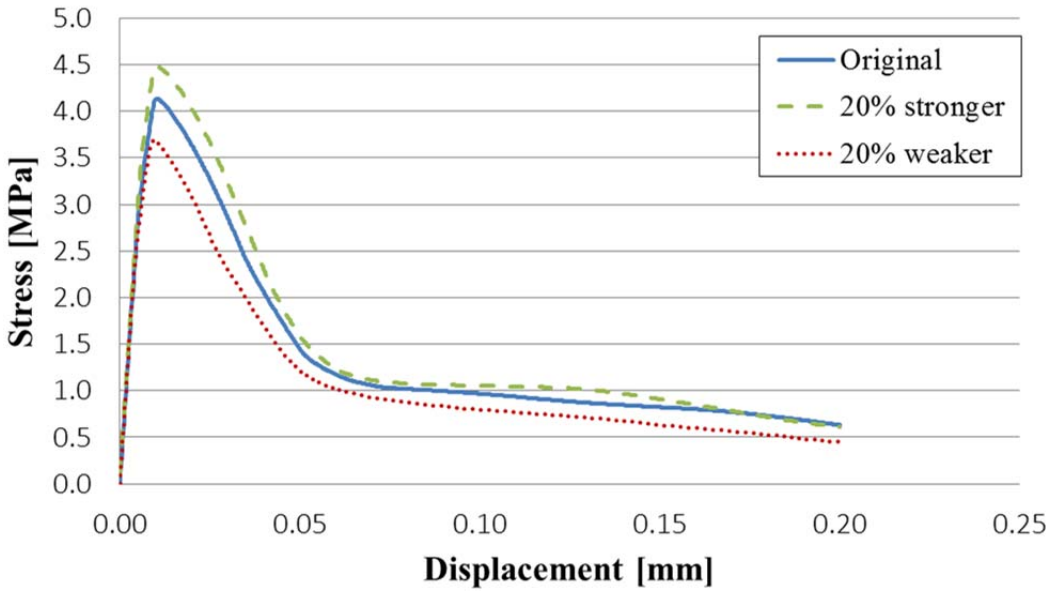

Figure 3.12 Stress-displacement curves for models with different interface strength.

Table 3.3 Input data in the plastic model for models with weakened and strengthened interface.

Test "20% weaker"			
	[1]	[2]	[3]
Stress [MPa]	3.20	0.64	0.00
Displacement [mm]	0.000	0.026	0.200
Test "20% stronger"			
	[1]	[2]	[3]
Stress [MPa]	4.80	0.96	0.00
Displacement [mm]	0.000	0.038	0.200

4 Small-scale Tensile Tests

Direct tensile tests of concrete at meso level were carried out on small-scale test specimens using a tensile stage with the same methodology assessed by (Nilsson & Pagrotsky 2012). The crack formations in the test specimens were monitored and studied with the use of the DIC-system Aramis. The results were thereafter evaluated to improve the input data in the FE-model and to verify the chosen material models.

4.1 Description of the test specimens

Six small-scale concrete specimens, each with one coarse aggregate, were tested in the tensile stage. The coarse aggregate was placed approximately in the centre of each specimen, and had a circular shape with a diameter of 25 mm. The final dimensions of each concrete specimen were approximately 65x65x10 mm^3.

The specimens were cut out from concrete blocks, which were casted in rectangular boxes with a cylindrical core of rock material placed in the middle; see Figure 4.1 and Figure 4.2. Plane parallel top and bottom edges were desired in order to minimize misalignment of the specimens when placed in the testing device. This was achieved by face-grounding of these edges to the final dimensions of the specimens.

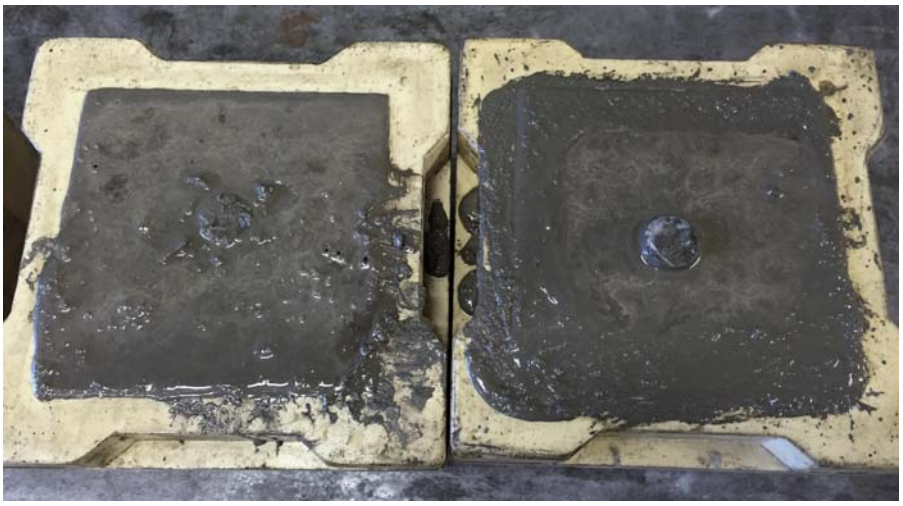

Figure 4.1 Casting of concrete blocks with a cylinder of rock material placed in the middle.

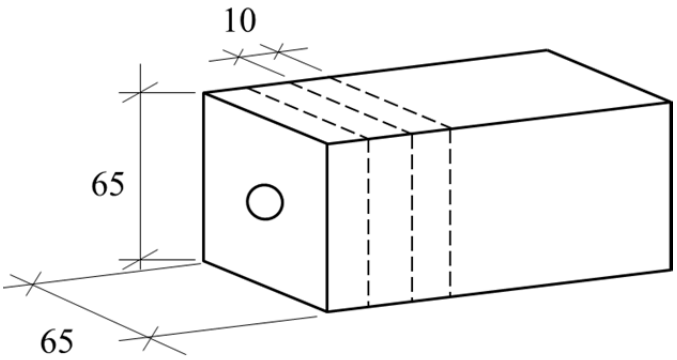

Figure 4.2 Small-scale concrete specimens cut out from rectangular concrete blocks.

Besides the coarse aggregate, finer aggregates were added to the concrete mix. The specimens were therefore divided into two groups; one group of three specimens with fine cement mortar surrounding the main aggregate and one group of three specimens with coarse cement mortar, see Figure 4.3. The specimens with the fine cement mortar had a similar appearance as the FE-model, but were most likely to have a strong brittle failure. The specimens with the coarse cement mortar were therefore made in order to avoid brittle failure when tensile testing, and were most likely to give more accurate concrete behaviour.

The surfaces of each specimen were ground in an Abramin grinding machine in order to make the meso structure details of the specimens noticeable also at the surfaces. This step is necessary since the images taken of the specimens during testing need to be of clear detail in order for the DIC-system to perform correct correlations.

All preparations of the test specimens before testing were performed by SP.

Figure 4.3 The two different types of concrete specimens; one with coarse cement mortar and one with fine cement mortar.

4.2 Description of the test setup and performance

The tensile stage test system is divided into different subsystems; the tensile stage, a control system for the engine of the tensile stage, the data acquisition system and the DIC-system. This is visualised in Figure 4.4.

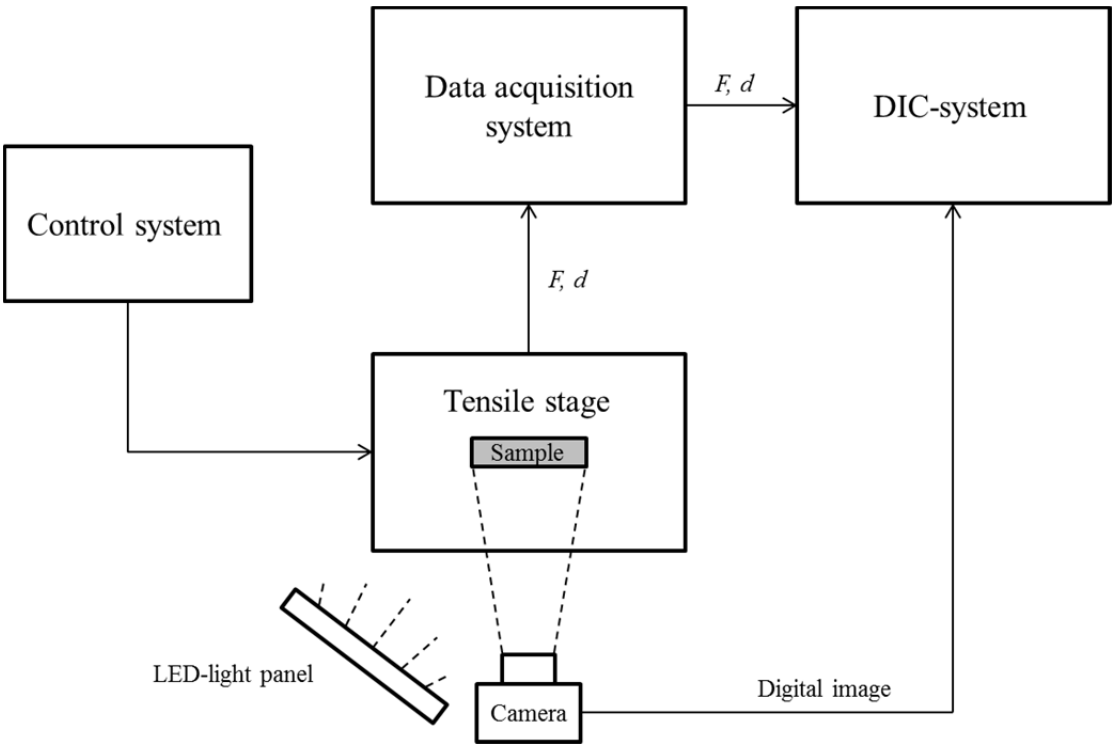

Figure 4.4 Visualisation of the tensile stage test setup.

4.2.1 The tensile stage device

The tensile stage device is a mechanical testing machine intended for small-scale specimens, see Figure 4.5. It has two cross beams which are connected with two roller screws. The screws are both right- and left-handed to achieve symmetrical movement, up and down, of the cross beams when the screws rotate. This symmetrical movement allows the centre of the specimen to remain in the same position throughout the testing and thus remain in the centre of the digital image. The screws are rotated by an engine and they move according to applied rotational speed and is operated by a control system. The test specimen is placed between the platens and during testing the displacement is registered with a displacement transducer and the force with a load cell.

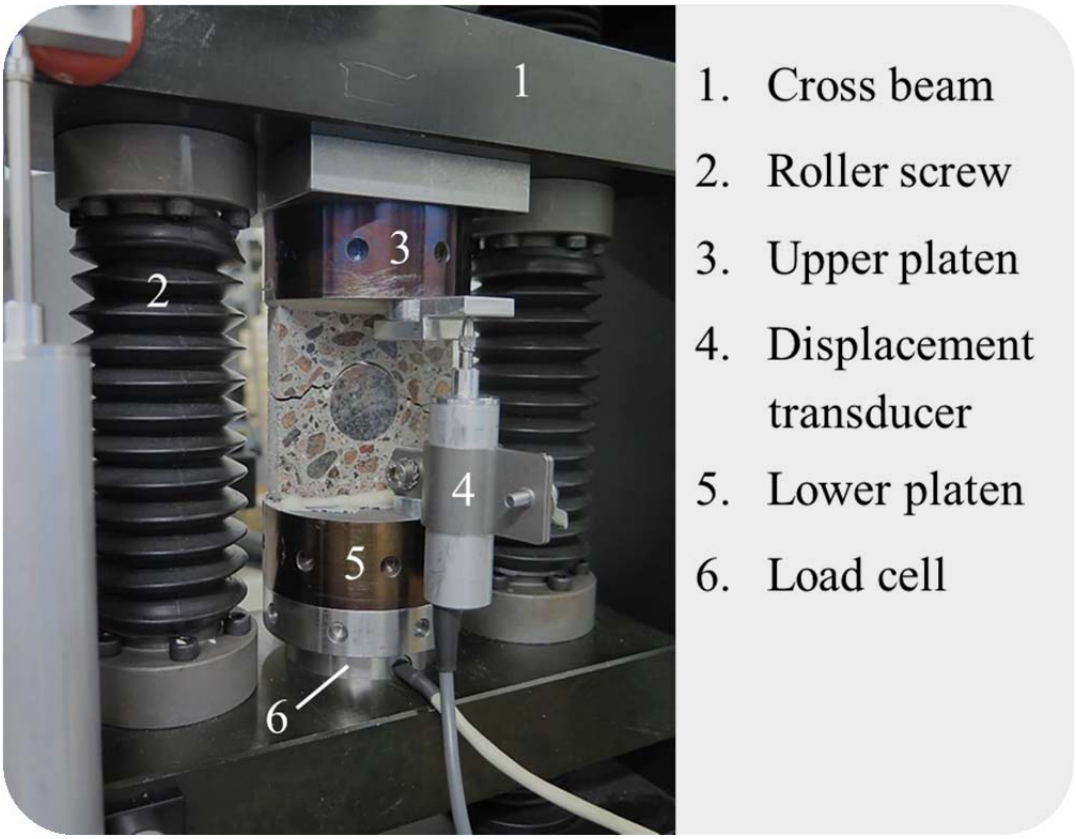

Figure 4.5 The tensile stage device and its components.

4.2.2 DIC

During the tensile testing a Digital Image Correlation (DIC) system was used to study the deformations and cracks at the surface of the 2D test specimens. The idea of DIC has been used since year 1980 and it has been developed until it became the very cost-effective and thorough system which it is today. With the advanced cameras used today, DIC can describe the strain distribution across a specimen with high precision (McCormick & Lord 2010).

DIC is a system that takes images to track the deformation of a tested specimen. The tracked deformation can be translated into images and graphs of strain distribution as well as crack propagation of the specimen. The images of the test specimen are divided into small sub-regions, i.e. facets, which can be seen in Figure 4.6. By matching the coordinates in the facets of correlating images, DIC together with dedicated software post-processes the data to get the results. The size of the facets depends on the size of the test specimen and it is of importance that these facets are not too small. This is because the interaction between the correlating facets, i.e. the overlapping, has to be big enough for the tracking ability of the DIC-system (Hellström & Olander 2012).

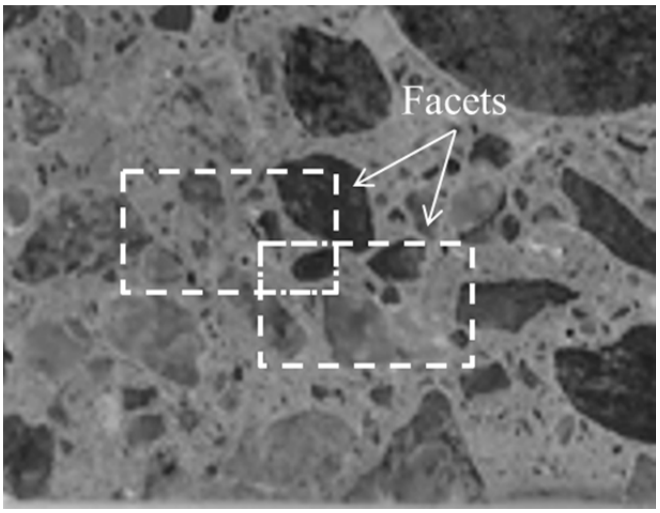

Figure 4.6 Two facets placed with overlapping in a DIC-image.

4.2.3 Testing

The top and bottom edges of the specimen were glued with epoxy adhesive to the platens of the tensile stage to achieve fixed ends. The adhesive also minimized any misalignments of the specimen edges.

At first, one edge was glued to the upper platen with the help of a gluing fixture, see Figure 4.7. Both the specimen and the platens were before gluing cleaned with abrasive paper and acetone in order to achieve proper adhesion between specimen edge and platen. The gluing fixture was used in order to get the specimen on the right place on the platen; the centre of the specimen should be matched with the centre of the platen, and the surface of the platen and centre line of the specimen should be perpendicular.

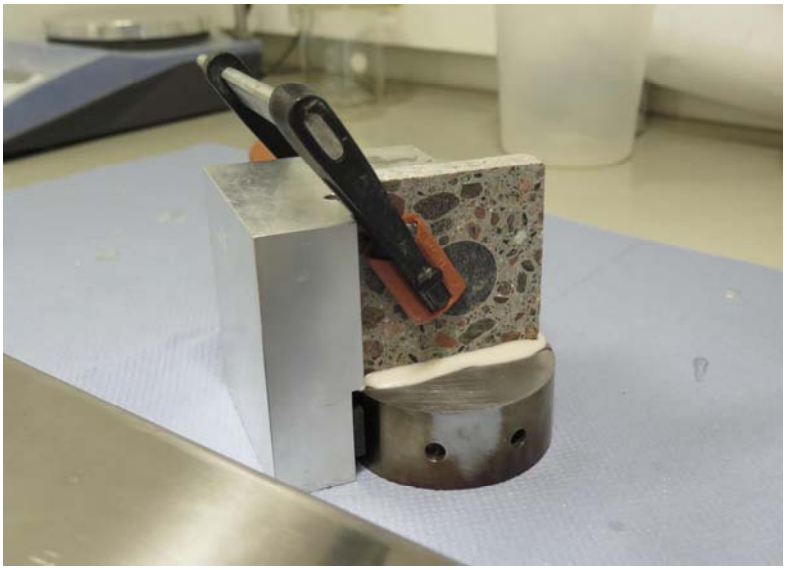

Figure 4.7 The specimen was glued to the upper platen with the help of a gluing fixture.

The upper platen and specimen were thereafter fastened to the testing machine. The last step was to glue the opposite free edge of the specimen to the lower platen directly in the testing machine. The testing was started approximately 20 minutes after the gluing was finished in order to achieve proper strength of the adhesive. When the adhesive dried, tensile stresses were applied to the specimen due to the contraction of the glue, and this extra load had to be decreased manually throughout the drying period of the glue.

During the tests, images were taken on one side of the specimen using a CCD-camera and sent to the DIC-system, see Figure 4.8. The camera had a resolution of 4 megapixels, a 50 mm lens and the images were taken with the frequency of 6 images per second. Before the testing, the camera together with the testing equipment was calibrated in order to give clear DIC-images for the whole specimen surface and to give accurate measurements. In order to get images with sufficient detailing it was necessary to have evenly spread light on the specimens without reflections. This was obtained with the use of a LED-light panel.

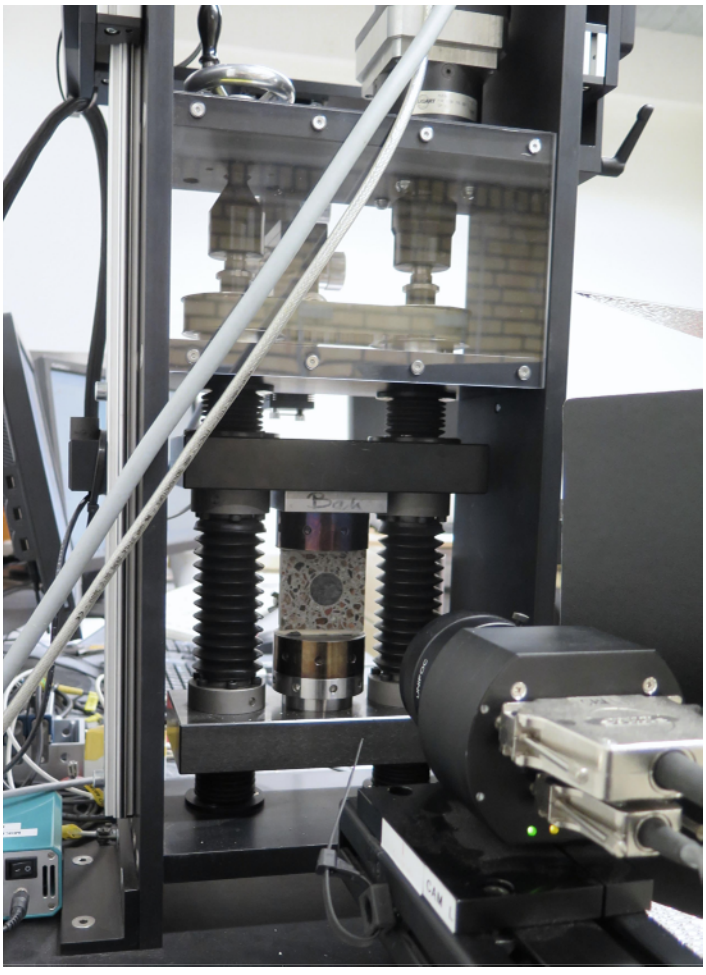

Figure 4.8 The tensile stage with specimen fastened and camera in place.

At the same time as the images were captured and sent to the DIC-system, the force *F* and displacement *d* on the specimen were recorded with a load cell and displacement transducer respectively, see Figure 4.5. The load cell had a maximum capacity of 10

kN and recorded with an accuracy within 1 %. A LVDT displacement transducer was used to measure the relative displacement between the platens, and thus the displacement of the specimen. The relative error of measured displacement was less than 1 %. Both the load and the deformation were recorded with a frequency of 10 Hz. The registered load and displacement were sent to a data acquisition system and thereafter onwards to the DIC-system.

The registered images, load and displacement were linked together in the DIC-system in order to show crack initiation and propagation on the tested specimen during tensile loading until the specimen was fully cracked.

The size used for the facets in the DIC-system was 20x20 pixels. The facets had an overlap of 10 pixels on each side. See Figure 4.6 for the placement organisation of two facets. When using the DIC-system, the whole image of the specimen surface is filled with overlapping facets instead of only two as displayed in the figure. Before the testing started, two images were taken to see if they were clear enough and gave enough information from the facets. Measuring of the coordinates of the facets in the specimen was done with an accuracy of about 1.3 μm.

4.2.4 Possible measurement errors

Possible measurement errors during the tensile testing and in the results could have occurred due to:

- mistakes when gluing the specimen to the platens which could lead to misalignments
- rotations in the platens and fixed ends during testing
- disturbances such as vibrations recorded with the measurement equipment
- elastic deformations in the testing equipment during the tests
- too fast load increase on the specimen after its maximum stress, which could lead to a limitation in measurement points and therefore give results not showing the right cracking behaviour after maximum stress

4.3 Test results

The tensile tests were performed, as described in Section 4.1, on six different specimens. All specimens had one aggregate with the same size in the middle, but the cement mortar around it differed. The specimens were divided into two groups; one group of three specimens with fine cement mortar and one group of three specimens with coarse cement mortar.

To be able to simulate the crack propagation for just one aggregate surrounded by cement paste, as in the FE-model, the cement mortar had to be as fine as possible. Therefore the three specimens with fine cement mortar were casted. A problem with too brittle crack development could though occur if the cement mortar was too fine, and such behaviour could be difficult to capture with the testing equipment since it happens very quickly. The three test specimens with more coarse cement mortar were therefore done with the reason to be able to catch the whole crack propagation.

One specimen with fine cement mortar and one specimen with coarse cement mortar are visualised in Figure 4.9. The three specimens with fine cement mortar were labelled BE1-3 and the three specimens with coarse cement mortar were labelled EB1-3.

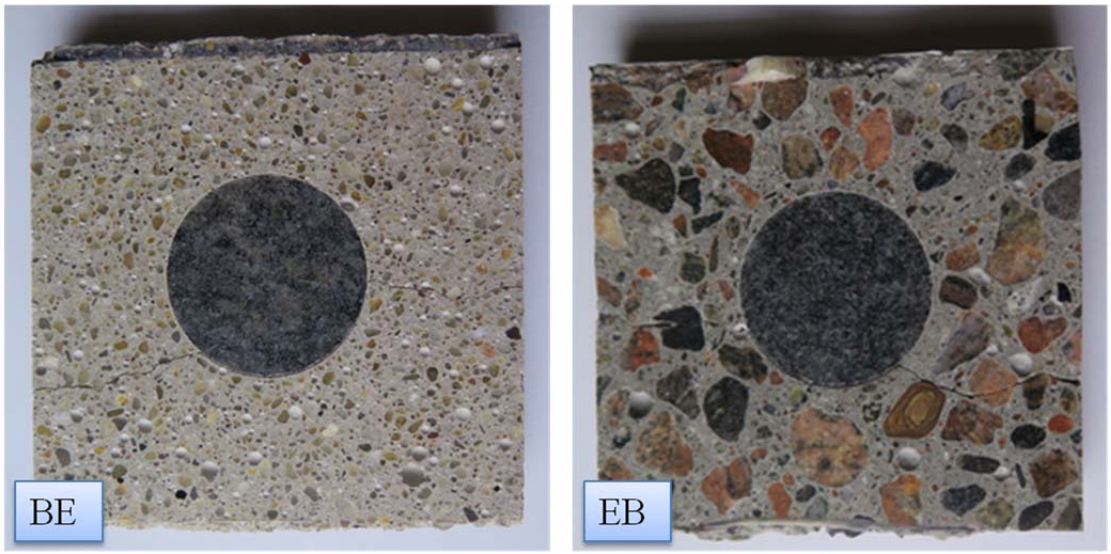

Figure 4.9 *Specimen with fine cement mortar to the left (BE) and specimen with coarse cement mortar to the right (EB).*

Results which were of interest to collect from the tests, and later on to compare with the FE-model, were stress-displacement curves together with images of the crack initiation and propagation. The force *F* on the specimens during the tests was, as explained in Section 4.2.3, recorded with a load cell and thereafter recalculated to stress by dividing by the nominal area (10x65mm^2). The displacement *d* was on the other hand recorded with a transducer, but due to its high sensitivity it also collected disturbances such as vibrations during the tests. In order to get more accurate values, the displacements for each specimen were instead obtained directly from the DIC-images.

Displacements were collected both as global for the whole specimen and locally around the initiating position of the crack. The global displacement, labelled *Global* in the graphs, was obtained by choosing one reference point at the top of the specimen and one at the bottom. Displacements of the specimen throughout the testing were thereafter calculated by the DIC-system as the changed distance between the two reference points. The local displacement, called *Crack,* was obtained in the same way except for the positioning of the reference points. They were instead placed above and below the initiating position of the crack in each specimen.

Four individual points; A, B, C and D, which were of extra interest for each specific specimen have been marked on the stress-displacement curves presented below.

When analysing the crack initiation and propagation in the images obtained from the testing, the strains over the whole specimen were observed. Localised strain concentrations and their development across the specimen represented where a crack initiated and propagated in the specimen.

BE specimens – fine cement mortar

The stress-displacement curves for test BE1 can be seen in Figure 4.10 alongside an image of the fully developed crack represented by strains in the specimen. In the first point (stage A), there was a tendency to high strains in the interface below the aggregate. Approximately in stage B there were high strains on the right edge of the cement paste and maximum stress was reached in stage C. In stage D, a crack appeared above the aggregate and separated the concrete into two pieces. The crack started in the cement paste, on the right side, and propagated further in the direction of the aggregate. The crack followed the interface and propagated into the cement paste on the left side.

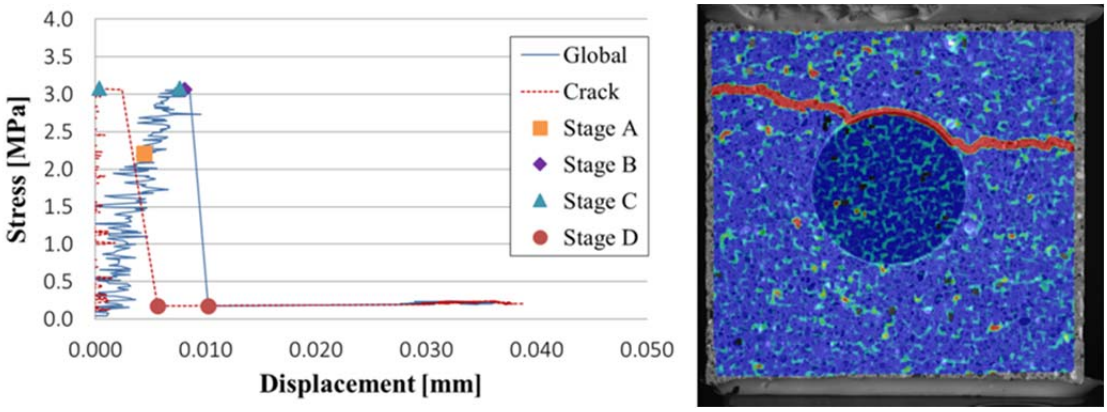

Figure 4.10 BE1: Stress-displacement curves to the left and the fully cracked specimen to the right with strains representing the crack.

Figure 4.11 shows the stress-displacement curves and the fully cracked concrete specimen for test BE2. Roughly around stage A there were high strains, representing the crack, in the cement paste on the right edge. The value of the strains grew larger, but the distribution remained the same. After this, the crack propagated from the cement paste on the right edge towards the interface, and the maximum stress was reached in stage B. The crack propagated successively around the lower part of the aggregate. In stage C the crack started to grow from the interface to the left side of the cement paste and it was fully developed in stage D.

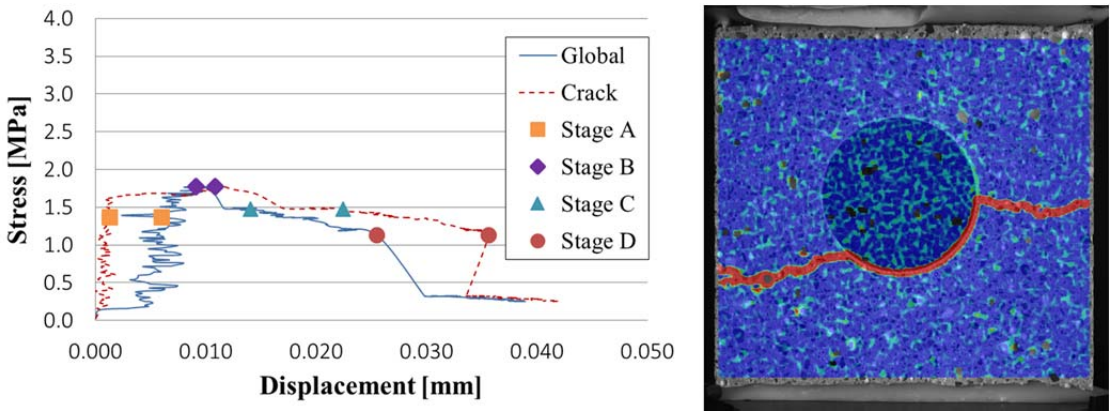

Figure 4.11 BE2: Stress-displacement curves to the left and the fully cracked specimen to the right with strains representing the crack.

Figure 4.12 shows the stress-displacement curves and an image of the crack, represented by strains, for the last specimen with finer cement mortar, BE3. The highest stress in the graph was reached in stage A and the highest strain in the image was situated in the cement paste on the right edge. It continued to grow further towards the interface around the aggregate. In stage B, the crack reached the interface and started to grow along the interface above the aggregate. The crack continued to grow through the interface around the aggregate and into the cement paste on the left side at stage C and the crack was fully developed in stage D.

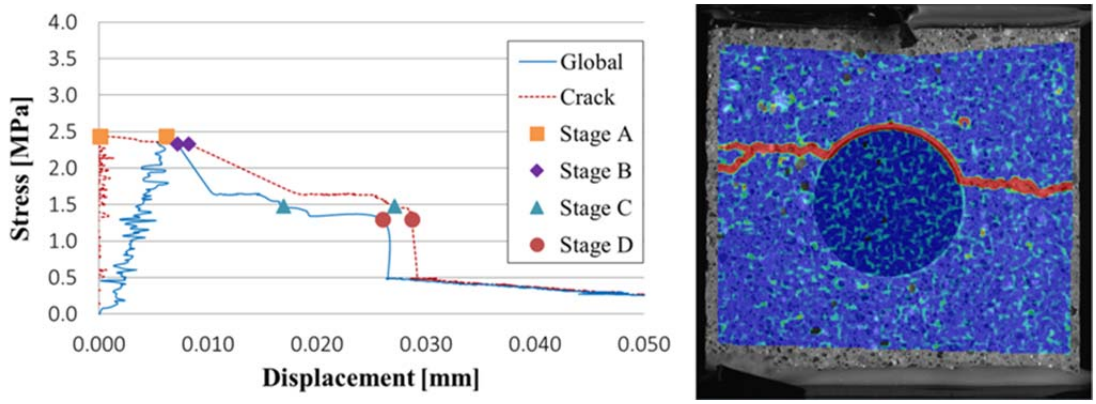

Figure 4.12 BE3: Stress-displacement curves to the left and the fully cracked specimen to the right with strains representing the crack.

EB specimens – coarse cement mortar

The next three presented test results are for the specimens containing the coarse cement mortar. To the left in Figure 4.13, the stress-displacement curves can be seen for test EB1. Strains were beginning to localize around stage A in the interface above the aggregate and in stage B, the strains were starting to localize also in the interface below the aggregate. The maximum stress in the curve was reached in stage C. The localized strains above the aggregate and in the cement paste near the interface were connected and created a crack. The image to the right in Figure 4.13 shows stage D where the crack for the tensile test specimen was fully developed, represented by strains.

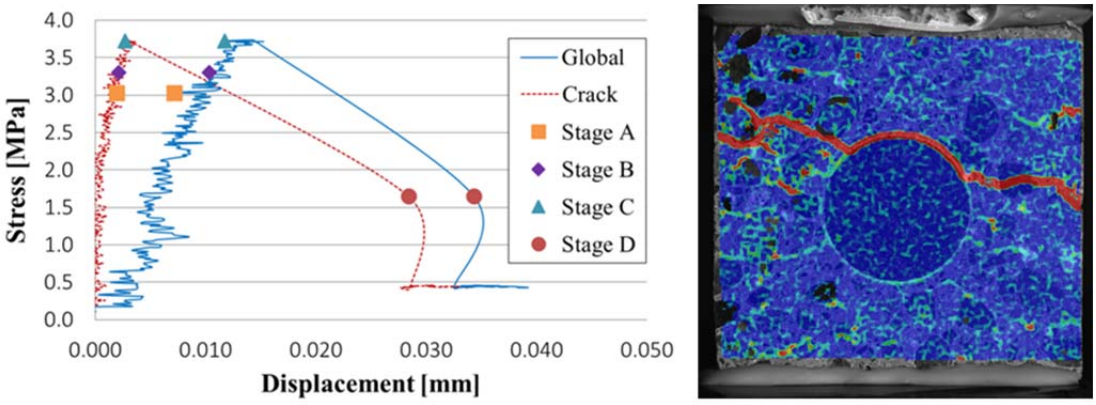

Figure 4.13 EB1: Stress-displacement curves to the left and the fully cracked specimen to the right with strains representing the crack.

Specimen EB2 with an image of its fully developed crack, represented by strains, and its stress-displacement curves can be seen in Figure 4.14. In stage A, there was a tendency to high strains in the interface below the aggregate. Around stage B, the strain propagated from below the aggregate towards the right edge of the cement paste and maximum stress in the diagram was reached in stage C. It looked like the interface under the aggregate was going to separate the concrete specimen, but in the next step the crack appeared in the interface above the aggregate. The crack grew until it was fully developed in stage D.

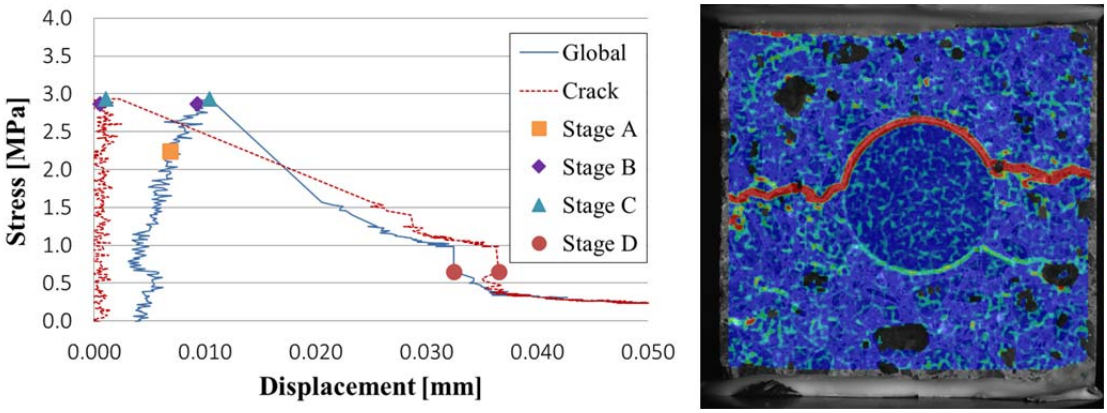

Figure 4.14 EB2: Stress-displacement curves to the left and the fully cracked specimen to the right with strains representing the crack.

Test results for the last specimen, EB3, can be seen in Figure 4.15 with its corresponding stress-displacement curves and an image of the fully developed crack represented by strains. The strains were gathering in different areas in the interface; both over and under the aggregate, as well as in the cement paste in the beginning of the testing. In stage A, the strains were starting to gather in the interface around the aggregate. It looked like the crack would start in the interface below the aggregate in stage B. The localized strains in the cement paste were slowly connected with the localized strains in the interface. In the last stage, stage D, the crack of the concrete specimen was fully developed and was located below the aggregate.

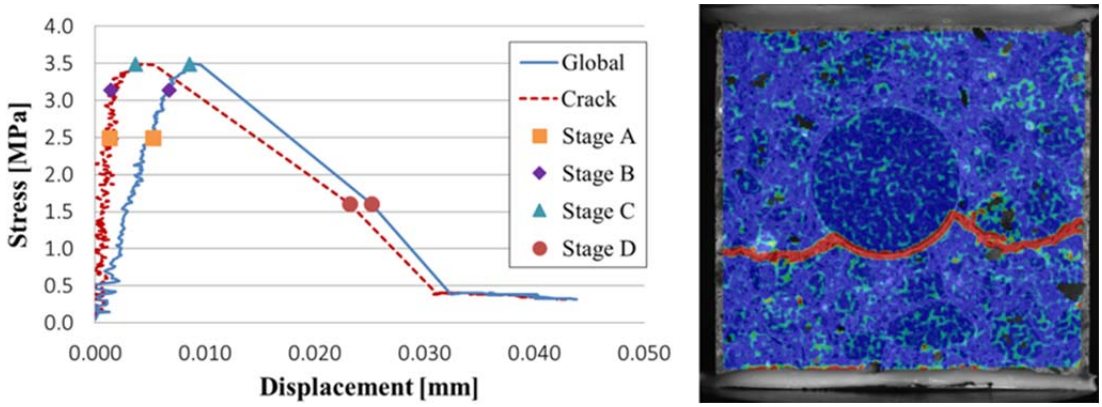

Figure 4.15 EB3: Stress-displacement curves to the left and the fully cracked specimen to the right with strains representing the crack.

More detailed results in form of images and graphs for each test can be seen in Appendix C.

All the test results gave almost the same shape of the curves and looked similar to the theoretical curve, with some differences in the descending branch after the maximum stress. The crack initiation and propagation seen in the images also looked similar to what expected from theory, except for the BE-specimens which had a crack initiation at the edges instead of in the interface. Reasons for this could be that there was a non-intentional rotation of the specimen during the tensile testing, that the EB-tests might have had a better adhesion between the aggregate and the cement paste than the EB-tests or that the cement mortar for the BE-tests had weaker properties than the cement mortar in the EB-tests. The most likely reason was probably due to the non-intentional rotation, either by itself or in combination with one of the other stated reasons.

One of the specimens was chosen to be focused on and thus used as verification and more realistic input data in the FE-model. The choice was based on how the crack initiation and propagation as well as the shape of the stress-displacement curve are explained in theory.

The first three tests, BE1-3, had a very brittle crack development which made it difficult for the DIC-system to catch the descending branch of the curve after maximum stress. Although these first specimens had a more similar appearance as the FE-model, the insecurities regarding the declining part of the curve could give incorrect results. The last three tests, EB1-3, captured the last part of the curve better, this because of the coarse cement mortar preventing a too brittle crack. The EB-tests also had a better accordance with theory regarding crack initiation and propagation seen in the images; the crack initiated in the interface and propagated into the cement mortar instead of starting in the edge of the specimen, propagating towards the interface and thereafter continuing through the cement paste to the edge on the other side of the specimen.

It was chosen to focus on EB3 for verification and improvement of the FE-model. This specimen was chosen because it had a stress-displacement curve which was most similar to the theoretical curve, especially after maximum stress. To be able to compare the results from the tensile test with the FE-model, the stress-displacement curve for the global displacement for EB3 was used, since the results from the FE-model showed the global displacement for the specimen.

4.4 Fluorescence microscopy images of the crack pattern

After the tensile testing, the specimens were treated with epoxy containing fluorescent dye to get clear images of the crack pattern. Two images of each specimen were taken during the fluorescence microscopy; one with regular lights on and one with UV-lights on. The results of this for test EB3 can be seen in Figure 4.16, where the image to the left is taken with regular lights, the image to the right with UV-lights and the image in the middle is a combination of the two images. All the specimens with their corresponding images can be found in Appendix D. Without the UV-lights, only the main crack that separated the concrete specimen into two pieces could be seen. The main crack and also tendency to initiation of other cracks could be seen clearly with the fluorescent light. It can in the figure be seen that there are initiations of cracks

besides the main crack in the interface surrounding the main aggregate, and also in the interfaces around the smaller aggregates in the cement paste.

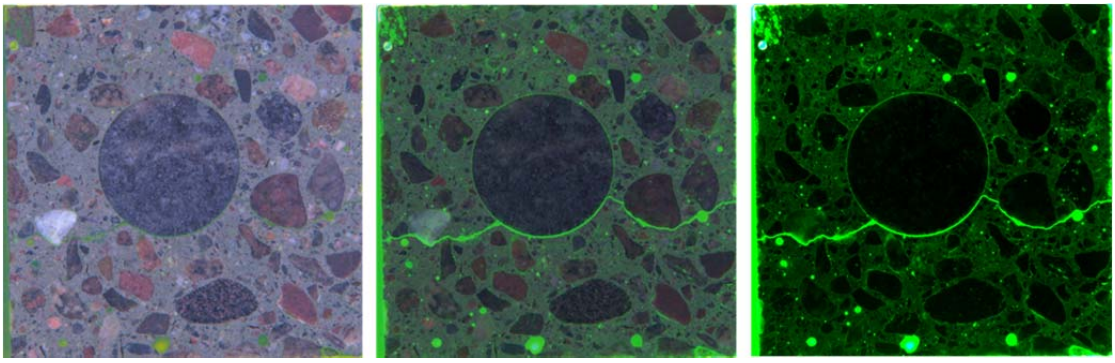

Figure 4.16 Fluorescence images for test EB3. To the left: image taken with regular lights, to the right: image taken with fluorescent light and in the middle: a combination of the other two images.

5 FE-model Verification and Improvement

The simple FE-model, described in Chapter 3, was compared with the results from the tensile testing in order to improve and also verify the model. It was chosen to focus on the tensile test specimen EB3 for the improvement of the FE-model. The stress-displacement curve together with images of the crack initiation and propagation for the tensile tested specimen were compared with the ones for the modelled specimen. With this comparison, correct input data for the modelled specimen could be determined, mainly considering the input data for the cement paste and the interface zone. Especially stresses for when cracking initiated in the interface and the cement paste respectively were used to adjust the material properties of these components in the FE-model.

Also, the geometry of the modelled specimen was corrected to match the geometry of the tested specimen.

5.1 Modified geometry

The aggregate was not centred in the tensile test specimen, and it was therefore moved in the FE-model to get a matching geometry. A matching geometry was desired in order to get as well comparable results of the cracking behaviour and appearance as possible. The new geometry for the modelled specimen and the cracking appearance can be seen in Figure 5.1.

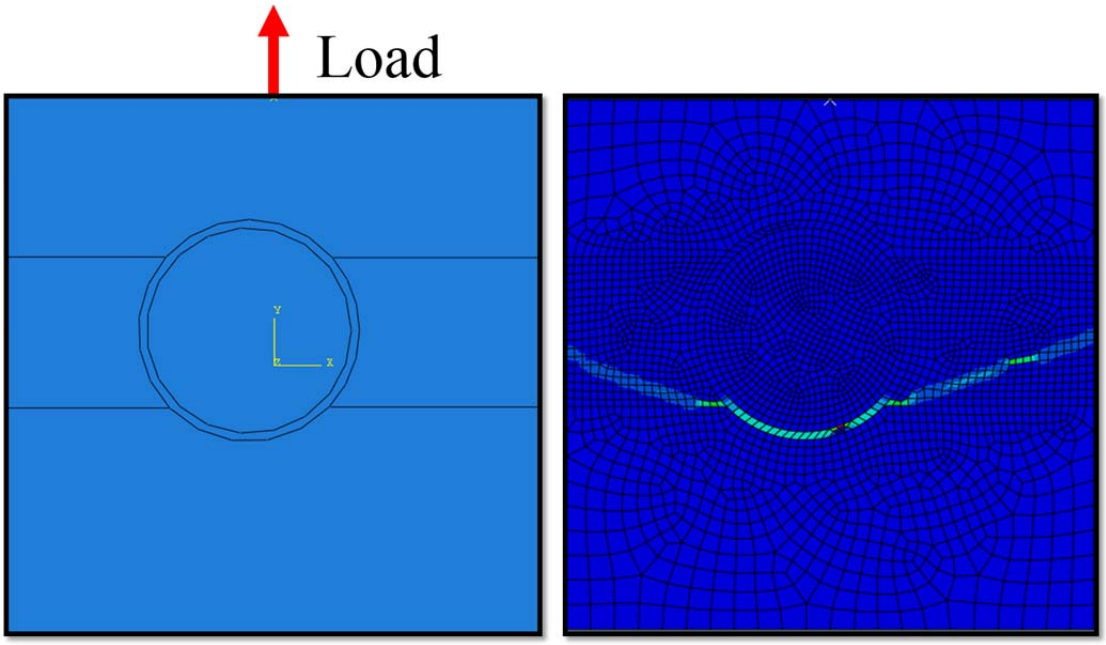

Figure 5.1 *To the left: modified geometry with moved aggregate and load applied. To the right: Results from the analysis.*

5.2 Modified input data

When first compared, the stress-displacement curves for the specimen in the simple FE-model and the tensile tested specimen were not similar. Neither the stress values for crack initiation in the interface and the cement paste, respectively, were similar for the FE-model and the tensile test results. See Figure 5.2 for the comparison of stress-displacement curves and also the points for crack initiation in the interface and in the cement paste respectively for the modelled and tensile tested specimen.

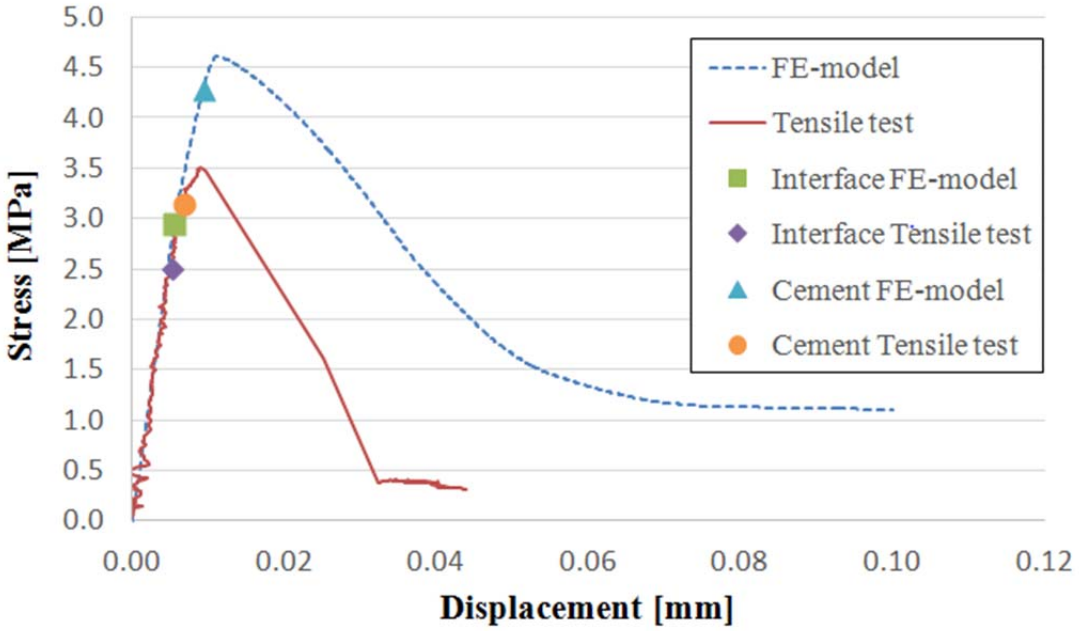

Figure 5.2 *Stress-displacement curves for the simple FE-model and the tensile tested specimen with points showing when cracking initiated in the interface and the cement paste respectively.*

5.2.1 Crack initiation in the interface zone and the cement paste

To get reasonable values for the crack initiation in the interface and in the cement paste in the FE-model, a test was done in a linear elastic version of the FE-model. The nominal force on the tensile tested specimen which initiated cracking in the interface zone was put into the linear elastic model as a load in the reference point, which can be seen in Figure 5.1. The highest stress located in the interface at the applied load was taken out from the results in the linear elastic model. This value was used as a new value for the tensile strength for the interface in the improved simple FE-model. The same procedure was done in order to get the tensile strength for the cement paste. These values were thus inserted in the improved simple FE-model as the stress levels, where crack initiation started in the interface and the cement paste respectively. These values were only used as start values in order to get an improved model giving similar results as the tensile test. The load inserted in the linear elastic model for the interface and the cement paste can be seen in Table 5.1.

Table 5.1 Load inserted in the linear elastic FE-model.

Load taken from tensile test at crack initiation in	
interface zone [kN]	**cement paste [kN]**
1.89	2.37

5.2.2 Influence from the elastic modulus of the components

The elastic modulus of the different components (aggregate, cement paste, interface zone) were changed as shown in Table 5.2 to find out how much of an influence the elastic modulus had on the stress-displacement curve and also on the stress distribution over the modelled specimen. This was done at the same time as the start values for tensile strength of the interface and cement paste were evaluated, see Section 5.2.1.

Table 5.2 Models with different E-modulus for the three components

Model	**E-modulus [GPa]**			**Stress [MPa]**	
	Aggregate	**Interface**	**Cement**	**Interface**	**Cement**
A	48	30	30	3.40	3.43
B	40	30	30	3.24	3.52
C	30	30	30	2.95	3.68
			Average:	**3.20**	**3.54**

Three models were done with different elastic modulus for the aggregate, but with the same values for the cement paste and the interface. The new values for the elastic modulus of the components were chosen based on the different references stated in this thesis. Much lower values for the aggregate than the original model was evaluated since a lower value was likely to give a more even stress distribution over the cross-section. An elastic modulus which was the same for the interface and the cement paste was evaluated since it was more reasonable to have a difference in strength between the cement paste and interface but not for the elasticity.

The values for the maximum stress obtained for the cement paste and the interface when modelling with different elastic modulus can be seen in Table 5.2. The stress values for the interface for the different models were obtained when a load of 1.89 kN was applied, as explained in Section 5.2.1. The stress distribution over the specimen for the different models at this specific applied load can be seen in the upper part of Figure 5.3. In which element the maximum stress in the interface was collected from, can be seen in the same figure. For the cement paste, the stress values for the different models were obtained when instead a load of 2.37 kN was applied. The stress distribution for this applied load and which element the maximum stress values for the cement paste were collected from can be seen in the lower part of Figure 5.3.

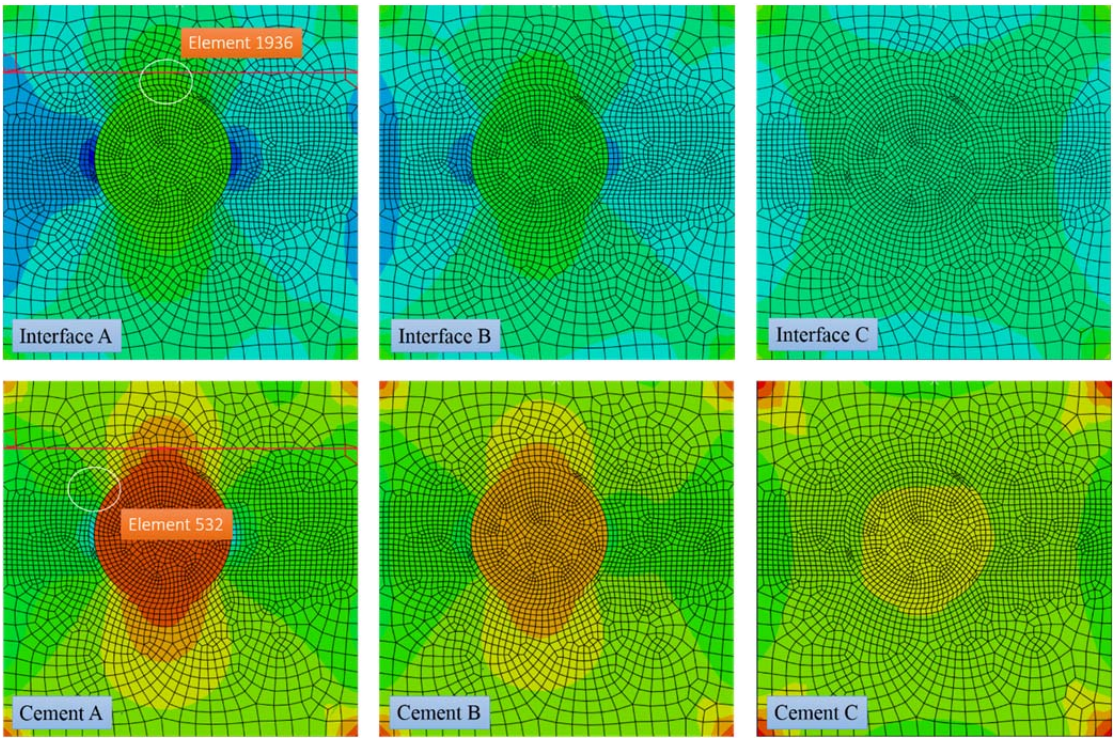

Figure 5.3 *Stress distribution for model A, B and C when a load of 1.89 kN (upper images) and 2.37 kN (lower images) was applied. Used to get average stress value for the interface and the cement paste. The circles show where the stresses were collected from.*

The stress distributions for model A, B and C along the specimen when a load of 1.89 kN and 2.37 kN was applied can be seen in Figure 5.4 and Figure 5.5. The lines in the two left images in Figure 5.3 represents were the stress distributions seen in Figure 5.4 and Figure 5.5 are collected from.

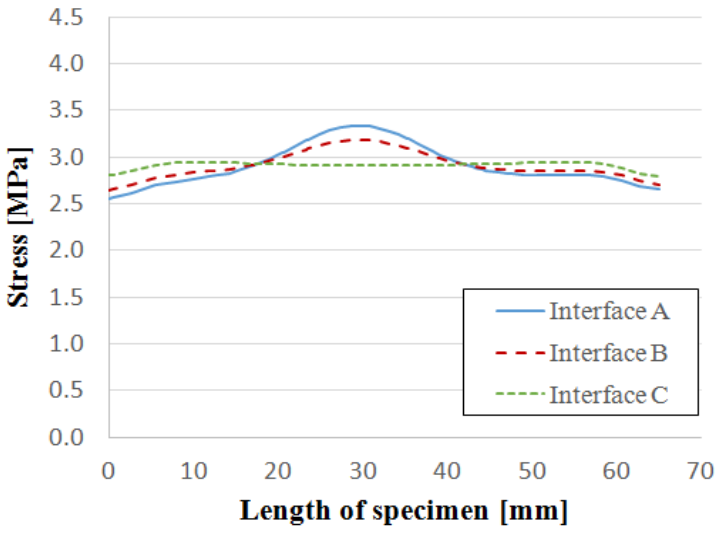

Figure 5.4 *Stress distribution along the line showed in the upper left image in Figure 5.3 for model A, B and C when a load of 1.89 kN was applied.*

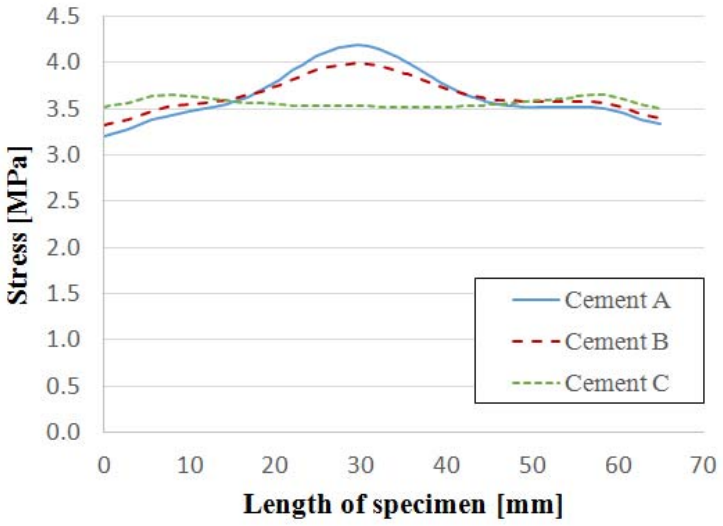

Figure 5.5 *Stress distribution along the line showed in the lower left image in Figure 5.3 for model A, B and C when a load of 2.37 kN was applied.*

The stress values obtained from the different models for the interface and the cement paste, seen in Table 5.2, varied depending on the value of the elastic modulus. It did though not have so much influence on the shape of the stress-displacement curve in the FE-model, but had some influence on which stress level crack initiation started in the interface and the cement paste respectively. Because of the little influence of the elastic modulus on the shape of the stress-displacement curve, and the fact that the aggregate in reality is stronger and stiffer than the cement paste and the interface, the values for elastic modulus in model A were chosen to proceed with.

5.2.3 Modified stress values for interface zone and cement paste

An average value for the maximum stress of the cement paste and the interface, see Table 5.2, was chosen and was used as tensile strength input in the FE-model. The stress-displacement curve obtained for this model can be seen in Figure 5.6 together with the curve from the tensile testing.

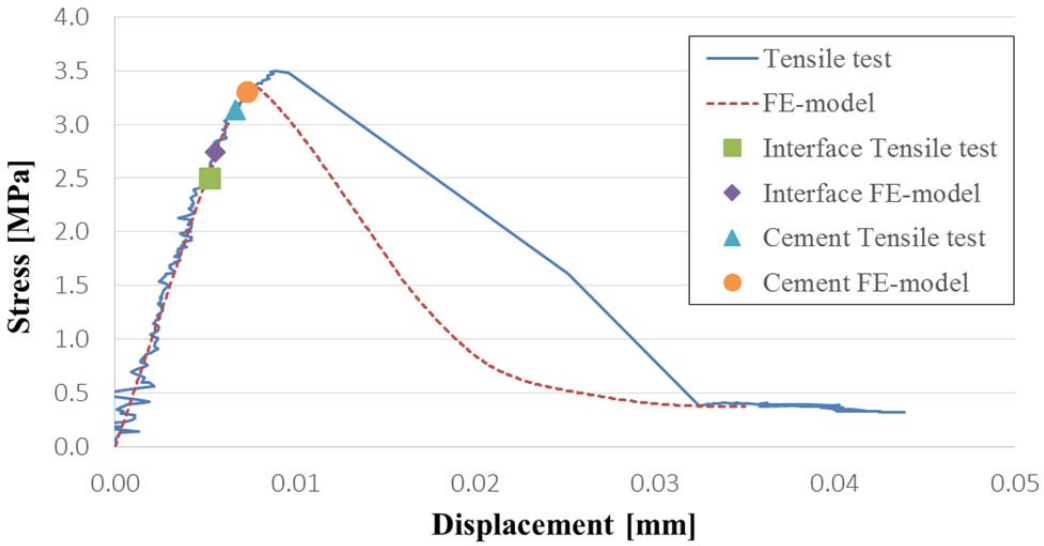

Figure 5.6 *Stress-displacement curves for the tensile test and the FE-model with the average stress values from Table 5.2 used as input values.*

The curves were quite similar, but there was a difference regarding the global maximum stress, which confirms that one of the components probably was modelled too weak. The crack initiation in the cement paste and the interface did also not begin at the same stress levels in the FE-model and the tensile test; see the points in Figure 5.6. Due to these differences in the two curves, both the stress value for the interface and the cement paste in the plastic model had to be revised.

Firstly, the crack initiation point for the interface was revised. This point was the break-point for linear and non-linear behaviour of the curve, and occurred on the ascending branch of the curve before the global maximum stress was reached. If the tensile strength for the interface was revised to a much lower value than the average value, this break-point occurred too early in the FE-model compared to the results from the tensile test. If the tensile strength instead was revised to a too high value, the break-point occurred too late. When changing the stress value for the interface in the plastic model, also the global maximum stress was affected. See Figure 5.7 for the influence of the interface strength on the global stress-displacement curve. A tensile strength which was lower than the average stress value was chosen for the interface as new input value in the plastic model.

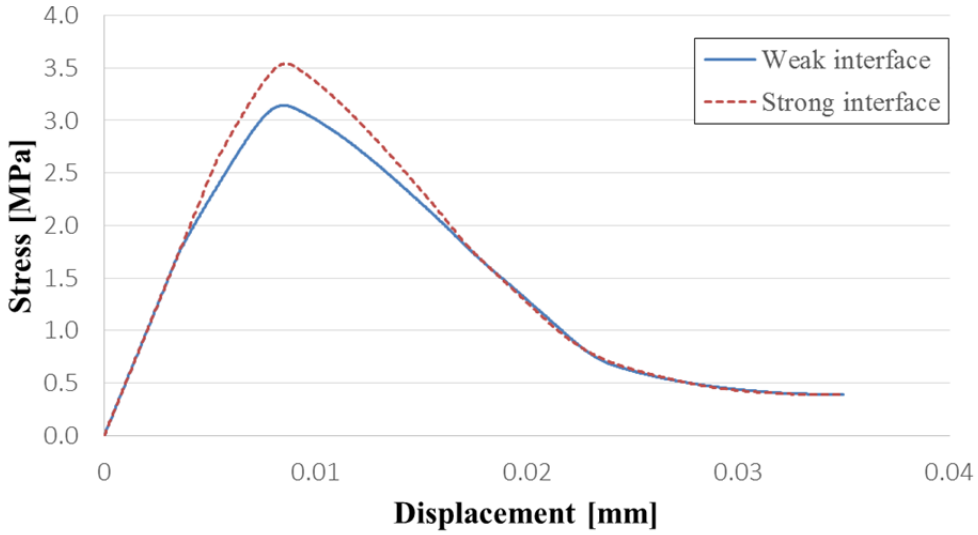

Figure 5.7 *The effect of interface strength on the stress-displacement curve. Here modelled with a difference of 33 %.*

When the crack initiation point for the interface was similar in the curve for the FE-model and the tensile test, the tensile strength for the cement paste had to be changed.

In order to keep equilibrium for the stress distribution, the summation of the average stress values, see Table 5.2, for the cement paste and the interface had to be held around the same value when changing the tensile strength in the plastic model for each component. Since the tensile strength for the interface had been decreased, the tensile strength for the cement paste therefore had to be increased. When increasing the tensile strength for the cement paste, the global maximum stress value in the curve for the FE-model reached a value closer to the maximum stress value in the curve for the tensile test. If the tensile strength for the cement paste was increased too little, the curve did not reach a similar global maximum stress value. If it was increased too much, it went above the global maximum stress value. Also the point for crack initiation in the cement paste got closer to the one in the tensile test curve when increasing the tensile strength of the cement paste.

The second point for the stress values for both the cement paste and the interface in the plastic model were chosen to be the same as for the end-point of the tensile testing curve, i.e. when the graph flattened out. In the simple FE-model, three points for stress and displacement were used in the plastic model; see Figure 3.2 and Table 3.2. In the improved simple model, the plastic model only contained two points, since three points gave numerical problems.

5.2.4 Final improved FE-model

The final stress values for the interface and the cement paste inserted in the improved simple FE-model can be seen in Table 5.3 together with an explaining graph in Figure 5.8. The final global stress-displacement curve for the improved FE-model and also the curve for the tensile test can be seen in Figure 5.9.

Table 5.3 Input data for the cement paste and interface zone in the plastic model.

Input data for cement paste (FE-model)	
Crack opening [mm]	**Stress [MPa]**
0.000	4.00
0.019	0.23
Input data for interface zone (FE-model)	
Crack opening [mm]	**Stress [MPa]**
0.000	2.90
0.014	0.23

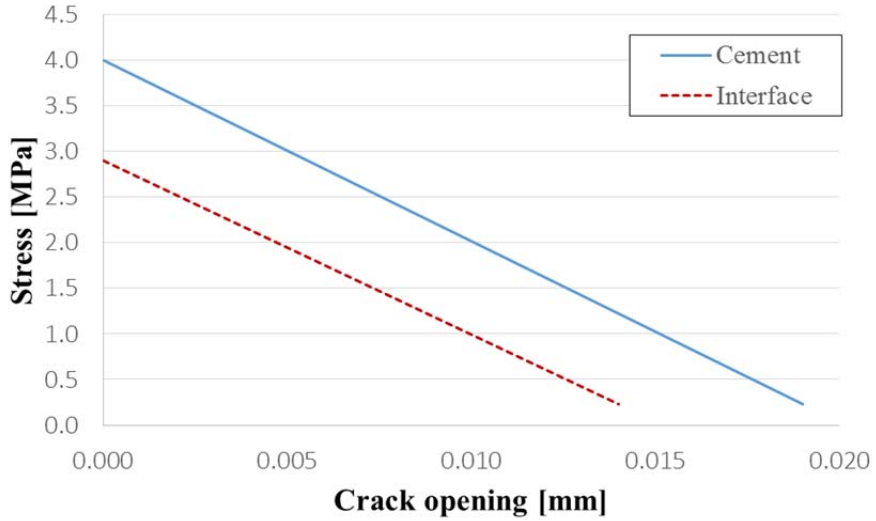

Figure 5.8 Input data for the cement paste and the interface zone in the plastic model.

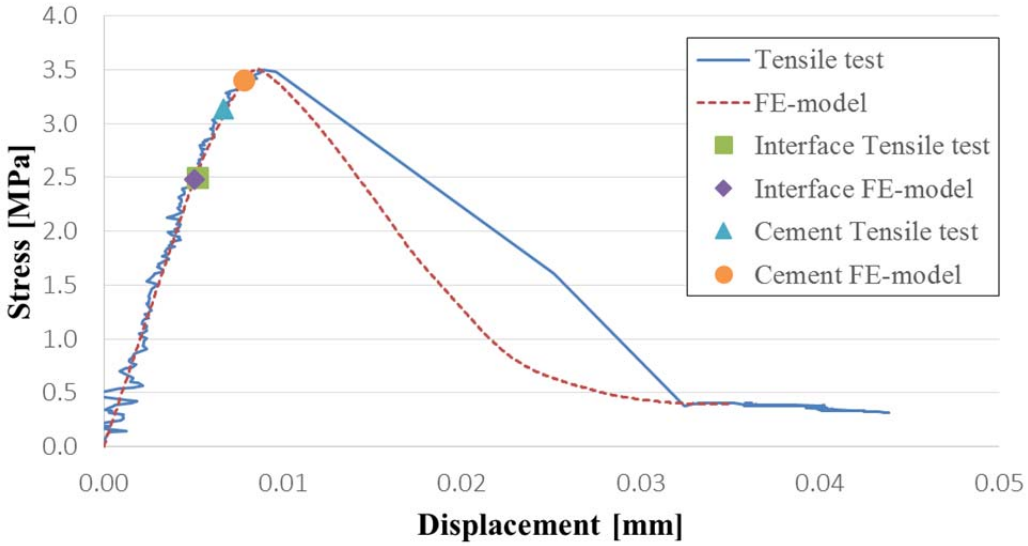

Figure 5.9 Stress-displacement curves for the final improved FE-model and the tensile test (EB3).

The curves had the same linear behaviour and the same maximum stress, but there were some differences in the shape of the curve after the maximum stress. Despite this, both the FE-curve and the tensile test curve were descending down to the same value. The values gathered from the tensile test gave a curve with a notch on the descending branch, which can be explained by the brittle cracking which occurred. Therefore too few measurement points for the descending part of the tensile test curve were obtained, resulting in an inaccurate stress-displacement curve after maximum stress. The stress-displacement curve obtained from the FE-model was more similar to how the curve looks in theory.

After correcting the tensile strength for the cement paste and the interface, the crack initiation for the interface occurred nearly at the same stress level in the stress-displacement curve for the FE-model and the tensile test. This can be seen in Figure 5.9. It can also be seen in Figure 5.9 that the crack initiation in the cement paste occurred before the global maximum stress, which was reasonable.

There was a deviation in the stress values for crack initiation in the cement paste for the FE-model and the tensile test, which could have different reasons. One of the reasons could be that it was hard to see in the tensile test results at which stress level the crack propagated out from the interface into the cement paste, and thus gave crack initiation in the cement paste. The deviation was however of acceptable value. Figure 5.10 and Figure 5.11 show how the tensile test specimen and the modelled specimen looked like when the crack initiated in the interface and the cement paste respectively.

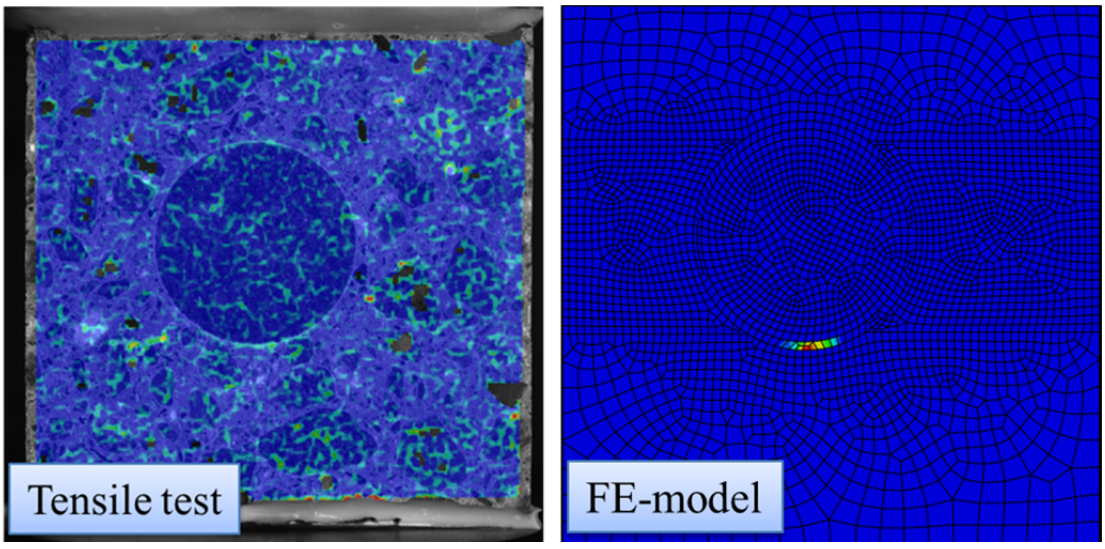

Figure 5.10 The first strains, and thus crack initiation, for the interface in the tensile tested specimen and in the FE-model.

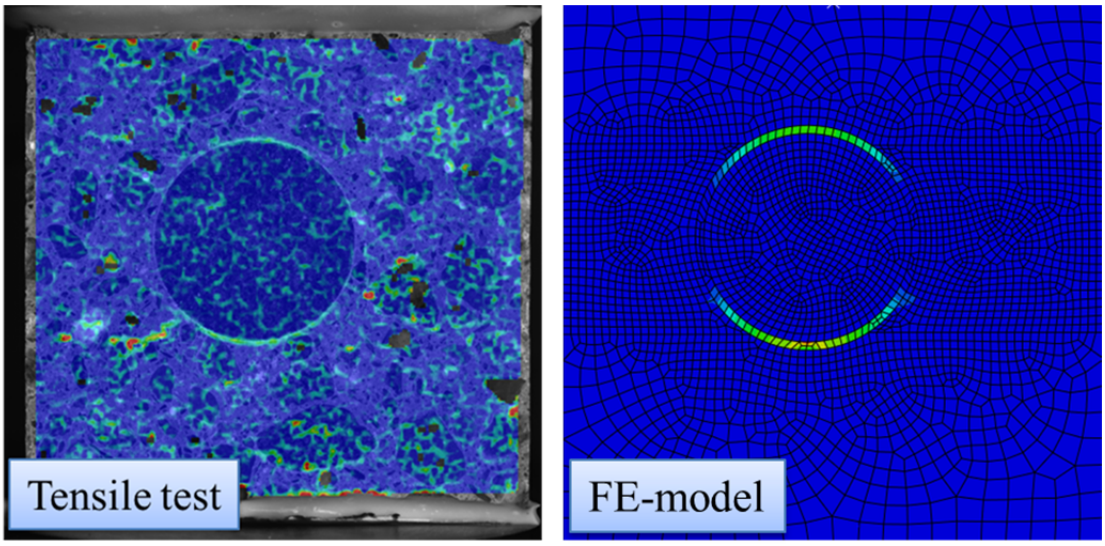

Figure 5.11 *The first strains, and thus crack initiation, for the cement paste in the tensile tested specimen and in the FE-model.*

6 FE-model with more Complex Structure

Two models with more complex structure were also modelled to verify if the improved simple FE-model could be extended to also simulate more realistic concrete specimens. The complex models had larger amount of aggregate particles and larger dimensions, but the same material properties as for the components in the improved simple FE-model. The displacement was at first set to be the same as previous stated, 0.035 mm, to see if the more complex models would react the same way as the improved simple model. Thereafter, the displacement was changed to 0.06 mm for the more complex models to be able to simulate more of the crack propagation.

In Figure 6.1, the two different complex models are visualised. The two images at the top represent one model, and the two images at the bottom of the figure represent another model. The aggregates were modelled in different sizes and the distribution of the aggregates varied for the two models to see how this influenced the results. It can be seen in the two images to the left in the figure that the crack initiation, represented by strains, appeared in almost all the interface zones for the two models. The two images to the right in the figure show how the final crack had propagated when the whole applied displacement was reached.

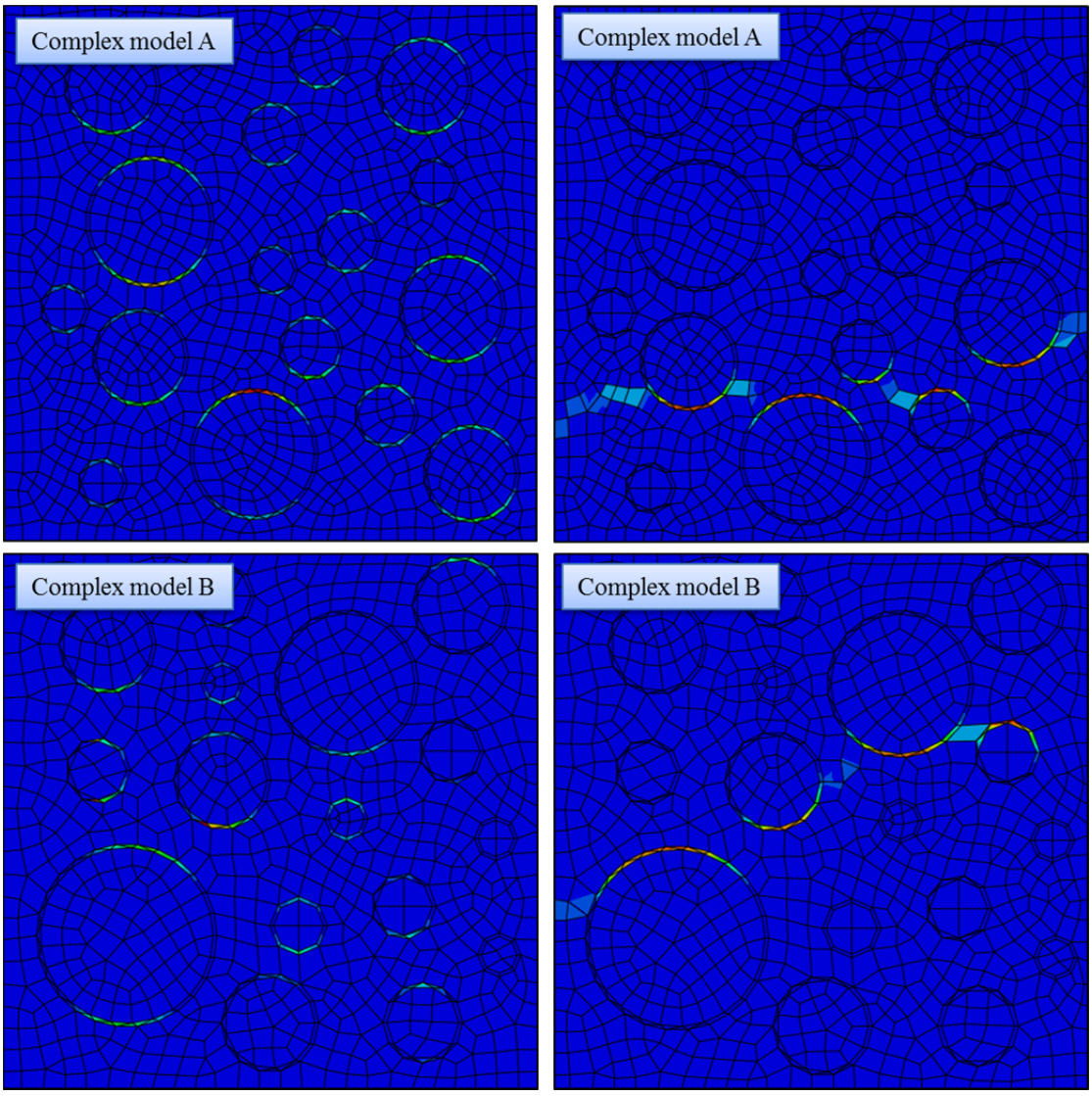

Figure 6.1 *Strains, representing cracks, in the two complex models. The images to the left show crack initiation in almost all interface zones for the two models. The images to the right show crack propagation for the two models after the whole applied displacement.*

The crack initiation started in the interface zones and propagated into the cement paste, like in the improved simple FE-model. It can be concluded that the crack initiation started in almost all the interface zones when more aggregate particles were present in the specimen. The strains, representing the crack initiation, increased in the interfaces of the larger aggregates positioned close to each other, and propagated into the cement paste between these larger aggregates. The size of the aggregate particles thus had an influence of where the crack propagated. Note that the scales are different for the images to the left and the images to the right in Figure 6.1. This is one reason of why the strains in the left images, representing the crack initiation in the interface zones, are not visible around all aggregate particles in the right images. Another reason is that these strains also were smaller at the final stage than before since they were unloaded when the final crack developed.

Figure 6.2 shows the stress-displacement curves for the two complex models with an applied displacement of 0.06 mm. The ascending part of the curves, before the global maximum stress, rose linearly in the beginning with the same slope since the material properties were the same in the two models. Thereafter the curves differed, but both showed a non-linear behaviour starting at the break-point for when crack initiation started in the interface zones. After the global maximum stress, the crack began to propagate into the cement paste for the two models. The fracture energy, described in Section 2.2.2, varied for the two models, which is logic since the amount of aggregate particles in volume and therefore also the amount of interface zones varied between the models.

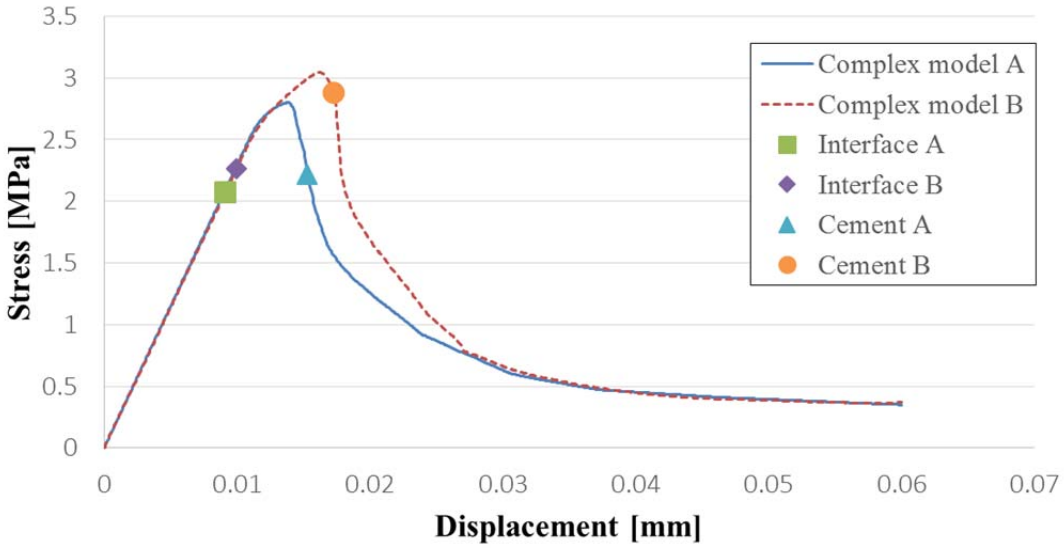

Figure 6.2 Stress-displacement curves for the more complex models.

Larger displacement was also applied to the models in order to catch the whole crack propagation until fracture, but larger displacement gave numerical problems. This could though maybe be solved if the function *constraint with tie* was used when modelling the geometry instead of using *partitions,* see Section 3.2. When using *constraint with tie* the mesh could have been modelled differently than in this project, which might have solved the problem.

7 Discussion

Different steps were done to achieve the improved simple FE-model, described in Chapter 5. A simple FE-model was first achieved based on the theory of concrete fracture mechanics. After this tensile stage tests were performed to obtain the information needed to create an improved simple FE-model. By the help of the improved model, two complex models with larger dimensions and with more aggregates were created.

In both the simple FE-model and in the chosen tensile stage test, EB3, the crack started in the interface and propagated into the cement paste. For the other EB-tests, with coarse cement mortar, the crack also started in the interface. This was not the case for the BE-tests, i.e. the tests with fine cement mortar. In these tests, the crack started in the cement paste at the edge of the specimens and propagated to the interface surrounding the aggregate. A reason for crack initiation at the edge instead of in the interface for the BE-tests could be that there was a non-intentional rotation during the tensile testing. Other reasons could be that the cement mortar was weaker in these specimens or that they had a better adhesion between the aggregate and the cement mortar than the EB-tests. This might cause some insecurity regarding the results obtained for the BE-tests. The fact that the interface was modelled with larger dimensions than in reality might have influenced the results in the model.

It was chosen to proceed with one of the EB-tests, since the BE-tests had such a brittle fracture. This was because the EB-tests with coarse cement mortar were better at catching the crack propagation. In reality, the BE-tests had a more similar appearance as the specimen in the FE-model since it was modelled only with one aggregate, disregarding the small aggregates surrounding the main aggregate. Even if this influenced the results, it may not have had such a big impact. In both the tensile testing and the modelling there was registered weakness in the interface which had an impact on the crack initiation and propagation.

The stress-displacement curves obtained from the FE-model and the DIC-system looked very similar after the FE-model was adjusted according to the tensile test results, see Figure 5.9. It can be seen in the diagram that the crack initiated in the interface below the aggregate at the same stress level before the maximum stress for both the modelled specimen and the tested specimen. The point where the crack propagated into the cement paste differed however in the two different curves. This was probably because of the fact that it was difficult to see in the visualisation from the DIC-system where the crack initiated in the cement paste. In the fluorescence image (Figure 4.16) it can be seen that there were many small cracks in the specimen which could not be seen with the naked eye. This confirms the difficulty in seeing the cracks and this could probably have had an effect on the crack propagation in the cement paste.

As mentioned above, the EB-test had a course cement mortar surrounding the main aggregate, which means that the cement paste contained many small aggregates. This probably affected the crack propagation since these small aggregates also were surrounded by an interface. It might have begun to crack too early in the interface because there was another aggregate near the main aggregate which weakened the main interface even more. It is also possible that these extra interfaces might have had

an impact on the cement paste, resulting in too early crack propagation into the cement paste. See the left part of Figure 7.1 for a visualisation of this phenomenon. As seen in the right part of Figure 7.1, smaller aggregates can also affect the path of the crack propagation.

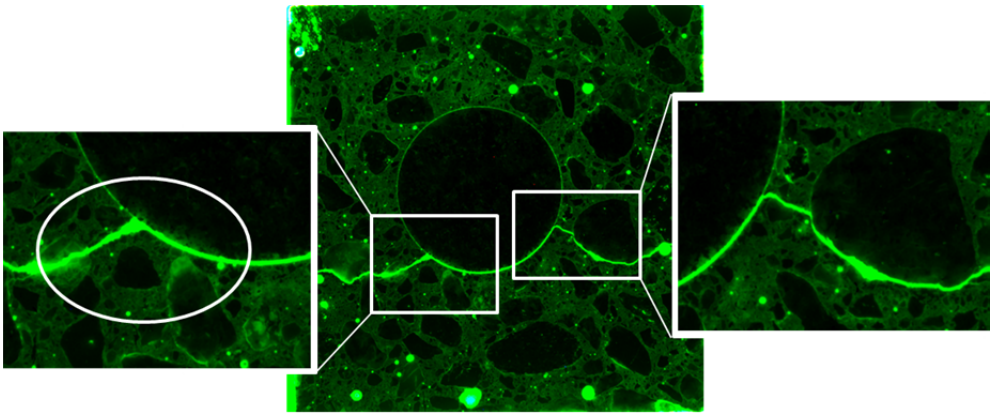

Figure 7.1 *To the left: Smaller aggregates near the main aggregate. To the right: A smaller aggregate affecting the path of the crack propagation.*

The descending part of the curve after maximum stress in the stress-displacement curve obtained from the tensile test had a strange shape compared to the one in the FE-model. Most likely this shape came from the fast crack propagation for the EB3 test. The DIC-system might have had limited measurement points that caused some insecurities resulting in the strange shape.

With the help of the improved simple FE-model, two up-scaled complex models were done with plural aggregates. The models were done with the same material properties for the components as in the improved simple FE-model, but the applied displacement was increased. This gave results which only obtained the crack initiation in the interface surrounding the aggregates and propagation into some parts of the cement paste. The whole crack propagation for the two models was not achieved, but it was possible to see where the fracture would occur, which can be seen in Figure 6.1 in Chapter 6.

Another way of performing the thesis project could have been to start with the tensile testing instead of the establishment of the simple FE-model. After that, a FE-model of real concrete crack initiation and propagation could be established using the test results as input data right away. If using this methodology, the two processes: the establishment of the simple FE-model and the verification and improvement of the model, could have been merged into one process. This could have decreased the time used for modelling, improvement and verification. It could though also have made no difference at all or even increased the time used, since two processes would be performed simultaneously.

The test results were accurate due to the used measurement equipment, except for the descending branch of the stress-displacement curve since the testing equipment had elastic deformations during the tests. The number of specimens tested was assumed to be enough for this project, but if this was increased also the significance of the test results might have increased.

8 Conclusion

A realistic model of concrete crack initiation and propagation at meso level was accomplished with the help of four different objectives, which can be seen below. The first objective was to establish a simple FE-model with only one aggregate. After this, tensile stage tests were done to catch the behaviour of real concrete specimens. An improved simple FE-model was done with the combination of the simple FE-model and the tensile stage tests. The last objective was to use these previous objectives to create an up-scaled model with plural aggregates.

1. Establish a FE-model of simple fictitious concrete specimen with one single aggregate. A finite element model in 2D was established of a single fictitious concrete specimen with only one aggregate. This was done with the help of previous studies as well as manuals. The concrete specimen was studied at meso level, and therefore consisted of cement paste, interface zone and aggregate. One part of the modelling was to find rough values as input data for the material properties, modelling techniques for the different components, which boundary conditions that should be used and also which material models were most appropriate to use. This was done and it resulted in a model that could represent the concrete at meso level based on the theory regarding cracking of concrete. The stress-displacement curve consisted of a linear part and a non-linear part which was expected and desired. Illustrations of the crack propagation confirmed the theory regarding crack initiation in the interface and that it propagated into the cement paste, which again confirmed the model.

2. Carry out tensile stage tests on real small-scale concrete specimens similar to the modelled specimen. The next step was to carry out tensile stage tests on real small-scale concrete specimens. In total six different tests were executed which were separated into specimens with fine and coarse cement mortar. The first three tests had a very brittle crack, so it was decided that it was better to use one of the tests with coarse cement mortar as verification and improvement of the FE-model. All the tests gave stress-displacement curves that were believable and the one with the clearest graph was chosen. The results that were taken out from the DIC-system were similar to the result that was achieved with the FE-model. This confirmed that it was possible to model the concrete specimen in the FE-program. The similarities between the images of the strains in the tensile test and the FE-model also confirmed the model.

3. Create improved simple FE-model after comparison with results from the tensile stage tests of the real concrete specimens. The tensile stage tests gave results that were used to improve the simple FE-model. By adjusting the FE-model using the stress-displacement curve as well as the resulting images from the testing, a new model was established. Loads from the tensile testing were used in the FE-model to find the right input data for the different material components. The right material data was found after some studies and updates of the FE-model. It gave the same shape of the global stress-displacement curve as the one obtained from the tensile testing. Crack initiation happened first, and also at the same stress level, in the interface for both the tensile tested specimen and the modelled specimen. The crack propagation was similar, starting in the interface and propagated into the cement paste. Therefore it can be concluded that it was possible to accomplish a realistic model of crack

initiation and propagation in concrete at meso level by using FE-modelling combined with tensile stage testing.

To simulate real concrete in the FE-model different inputs were considered. Right ***material properties*** were achieved by using the results from the tensile testing to get the same stress-displacement curve and crack initiation and propagation. The ***material models*** were achieved by simulating a stress-displacement graph containing a linear and a non-linear part with the *Concrete damaged plasticity model*. When combining the simple FE-model and the tensile test the ***boundary conditions*** had to be modelled in a proper way in the improved simple FE-model. This was done by fastening the lower boundary condition in all directions and by putting a displacement in the reference point in the upper boundary. The ***interface zone*** between the cement paste and the aggregate was modelled weaker than the cement paste and the aggregate and with a thickness of 1 mm, i.e. the thickness of an element in the model. Tensile testing showed that ***cracking*** was most likely to start in the interface and propagate into the cement paste.

4. Develop the FE-model in order to reflect actual concrete structure with more aggregate particles. When the improved simple model for a specimen with one single aggregate was achieved, two up-scaled complex models were done with more aggregates with different sizes. This was done with the same material properties for the components as in the improved simple model, but with different applied displacement. The up-scaled FE-models showed where the cracks started in the interface zones, how they propagated into the cement paste and interacted with the aggregates. However, the final fracture was not possible to capture.

The final conclusion is that it was possible to establish a 2D finite element model which simulated real concrete cracking behaviour at meso level. This model can contribute to the research of developing and designing new environmental friendly types of concrete mixes, since it gives a better understanding of concrete cracking at meso level.

8.1 Further investigations

There is a need for further investigation regarding the established FE-model. The concrete has been modelled with one single aggregate, as stated earlier, but there were some difficulties when scaling up the model with plural aggregates. With further investigation in the FE-program, a model which could be used for concrete specimens with larger dimensions and more aggregate particles could be achieved.

OOF2 is a program for finite element analysis of microstructure and can be used in combination with the FE-model. It could be an easier way to convert a concrete pattern at meso level including the mesh directly into the FE-model. With this method it could be possible to convert a picture of the concrete structure into the FE-model, instead of manually model the whole geometry of the cement paste containing aggregates. As a result this would simplify the work considerably.

9 References

Burström, P.G., 2010. *Byggnadsmaterial - Uppbyggnad, tillverkning och egenskaper* 2:5 ed., Lund: Studentlitteratur AB.

CBI Betonginstitutet, 2008. Crushed rock as aggregate in concrete. Available at: http://www.cbi.se/viewNavMenu.do?menuID=317&oid=645 [Accessed March 17, 2015].

Cementa, Byggcement. Available at: http://www.cementa.se/en/node/4288 [Accessed February 16, 2015].

Dassault Systèmes, 2012a. Abaqus 6.12 Online Documentation. Available at: http://www.maths.cam.ac.uk/computing/software/abaqus_docs/docs/v6.12/ [Accessed May 28, 2015].

Dassault Systèmes, 2012b. Abaqus 6.12: Abaqus Analysis User's Manual: Concrete. Available at: http://www.maths.cam.ac.uk/computing/software/abaqus_docs/docs/v6.12/books/usb/default.htm?startat=pt05ch23s06abm39.html#usb-mat-cconcretedamaged [Accessed May 28, 2015].

Dassault Systèmes, 2012c. Abaqus 6.12: Abaqus Theory Manual: Other inelastic models. Available at: http://www.maths.cam.ac.uk/computing/software/abaqus_docs/docs/v6.12/books/stm/default.htm?startat=ch04s05ath120.html#stm-mat-concretedamaged [Accessed May 28, 2015].

Dassault Systèmes, 2012d. Abaqus 6.12: Abaqus/CAE User's Manual - pdf. Available at: http://www.maths.cam.ac.uk/computing/software/abaqus_docs/docs/v6.12/pdf_books/CAE.pdf [Accessed May 28, 2015].

Dassault Systèmes, 2012e. Abaqus 6.12: Analysis User's Manual Volume III: Materials. , pp.23.1.1–4. Available at: http://www.maths.cam.ac.uk/computing/software/abaqus_docs/docs/v6.12/pdf_books/ANALYSIS_3.pdf [Accessed May 28, 2015].

Domone, P. & Illston, J. eds., 2010. *Construction Materials - Their Nature and Behaviour* 4th ed., Abingdon: Spon Press.

Du, X., Jin, L. & Ma, G., 2014. Numerical modeling tensile failure behavior of concrete at mesoscale using extended finite element method. *International Journal of Damage Mechanics*, 23(7), pp.872–898.

Engström, B., 2014. *Restraint cracking of reinforced concrete structures*. Göteborg: Department of Civil and Environmental Engineering, Chalmers University of Technology, Report 2007:10.

European Commission, 2014. Progress Towards Achieving the Kyoto and EU 2020 Objectives. Available at: http://ec.europa.eu/clima/policies/g-gas/docs/kyoto_progress_2014_en.pdf [Accessed March 17, 2015].

Flansbjer, M. & Lindqvist, J.E., 2013. *Mesomechanical study of concrete material*, SP Technical Research Institute of Sweden, SP Working Report 2013:06, Borås.

Grassl, P. & Jirásek, M., 2010. Meso-scale approach to modelling the fracture process zone of concrete subjected to uniaxial tension. *International Journal of Solids and Structures*, 47(7-8), pp.957–968.

Grassl, P. & Rempling, R., 2008. A damage-plasticity interface approach to the meso-scale modelling of concrete subjected to cyclic compressive loading. *Engineering Fracture Mechanics*, 75(16), pp.4804–4818.

Hellström, P. & Olander, K., 2012. *Analysis and modeling of properties of Compacted Graphite Iron on a microstructural level*. Department of Applied Mechanics, Chalmers University of Technology, Master's Thesis 2012:08, Göteborg.

Kim, S.-M. & Al-Rub, R.K.A., 2011. Meso-scale computational modeling of the plastic-damage response of cementitious composites. *Cement and Concrete Research*, 41(3), pp.339–358.

Lee, J. & Fenves, G.L., 1998. Plastic-Damage Model for Cyclic Loading of Concrete Structures. *Journal of Engineering Mechanics*, 124(8), pp.892–900.

Lindgren, P. & Östergren, A., 2010. *Konstruktion av dragsteg*. Department of Applied Mechanics, Chalmers University of Technology, Bachelor's Thesis 2010:05, Göteborg.

López, C.M., Carol, I. & Aguado, A., 2008. Meso-structural study of concrete fracture using interface elements. I: numerical model and tensile behavior. *Materials and Structures*, 41(3), pp.583–599.

Lubliner, J. et al., 1989. A Plastic-Damage Model for Concrete. *International Journal of Solids and Structures*, 25(3), pp.229–326.

McCormick, N.J. & Lord, J.D., 2010. Practical In Situ Applications of DIC for Large Structures. *Applied Mechanics and Materials*, 24-25, pp.161–166.

Van Mier, J.G.M., 2013. *Concrete Fracture - A Multiscale Approach*, Boca Raton: CRC Press.

Van Mier, J.G.M., 1995. Fracture mechanics of concrete: will applications start to emerge? *Heron*, 40(2), pp.147–162.

Nilsson, H. & Pagrotsky, O., 2012. *Metodik för optisk mätning av sprickbildning i dragen betong på mesonivå*. Department of Civil and Environmental Engineering, Chalmers University of Technology, Bachelor's Thesis 2012:114, Göteborg.

Pais, M., 2015. Matthew Pais. Available at: http://www.matthewpais.com/research [Accessed May 27, 2015].

PBL Netherlands Environmental Assessment Agency, 2014. Trends in Global CO2 Emissions: 2014 Report. Available at: http://www.pbl.nl/sites/default/files/cms/publicaties/PBL_2014_Trends_in_global_CO2_emisions_2014_1490_0.pdf [Accessed March 17, 2015].

Plos, M., 2000. *Finite element analyses of reinforced concrete structures*. Department of Structural Engineering, Chalmers University of Technology, Compendium 96:14, Göteborg.

Skoček, J., 2010. *Fracture propagation in cementitious materials - Multi-scale approach: measurements and modeling*. Ph.D. Thesis, Department of Civil Engineering, Technical University of Denmark, Kgs. Lyngby.

Wang, X.F. et al., 2015. Monte Carlo simulations of mesoscale fracture modelling of concrete with random aggregates and pores. *Construction and Building Materials*, 75, pp.35–45.

Appendix A

Concrete Damaged Plasticity

Element sizes:

$l_{element.1} := 65mm$

Size of increments

$\Delta L = \varepsilon \times L$

E-modulus:

Cement: $E_c := 30GPa$ $E_c = 3 \times 10^4 \cdot \frac{N}{mm^2}$

Aggregate: $E_a := 120GPa$ $E_a = 1.2 \times 10^5 \cdot \frac{N}{mm^2}$

Poisson's Ratio:

Cement: $\nu_c := 0.2$

Aggregate: $\nu_a := 0.25$

Interface: $\nu_i := 0.25$

Compressive behaviour:

The compressive behaviour is not in use. To not have an effect on the results, the compressive values are set to a bigger value than the tensile values.

Yield stress: $f_{t.com} := 15MPa$ $f_{t.com} = 15 \cdot \frac{N}{mm^2}$

Inelastic strain: $\varepsilon_{com} := 0$

Displacement

Yield stress:

Value 1:	Value 2:	Value 3:
$f_{t.d.1} := 5MPa$	$f_{t.d.2} := 1MPa$	$f_{t.d.3} := 0$

Displacement:

Value 1:	Value 2:	Value 3:
$d_1 := 0mm$	$d_2 := 0.04mm$	$d_3 := 0.2mm$

Strain

Yield stress:

Value 1: $f_{t.s.1} := f_{t.d.1} = 5 \cdot MPa$

Value 2: $f_{t.s.2} := f_{t.d.2} = 1 \cdot MPa$

Value 3: $f_{t.s.3} := f_{t.d.3} = 0$

Cracking strain:

Value 1: $\varepsilon_{s.1} := \frac{d_1}{l_{element.1}} = 0$

Value 2: $\varepsilon_{s.2} := \frac{d_2}{l_{element.1}} = 6.154 \times 10^{-4}$

Value 3: $\varepsilon_{s.3} := \frac{d_3}{l_{element.1}} = 3.077 \times 10^{-3}$

GFI

Yield stress:

Value 1: $f_{t.GFI.1} := f_{t.d.1} = 5 \cdot MPa$

Value 2: $f_{t.GFI.2} := f_{t.d.2} = 1 \cdot MPa$

Value 3: $f_{t.GFI.3} := f_{t.d.3} = 0$

Fracture energy:

$$G_f := 173 \frac{N \cdot m}{m^2}$$

$$G_{f.tot} := \frac{\left(f_{t.GFI.1} - f_{t.GFI.2}\right) \cdot d_2}{2} + f_{t.GFI.2} \cdot d_2 + \frac{f_{t.GFI.2} \cdot \left(d_3 - d_2\right)}{2} = 0.2 \cdot N \cdot \frac{mm}{mm^2}$$

$$G_{f.12} := \frac{\left(f_{t.GFI.1} - f_{t.GFI.2}\right) \cdot d_2}{2} + f_{t.GFI.2} \cdot d_2 = 0.12 \cdot N \cdot \frac{mm}{mm^2}$$

$$G_{f.3} := \frac{f_{t.GFI.2} \cdot \left(d_3 - d_2\right)}{2} = 0.08 \cdot N \cdot \frac{mm}{mm^2}$$

Results - hand calculation

To verify the Abaqus model some values are compared to hand calculations.

Cracking strain - linear behaviour:

$$\varepsilon_{c.h.1} := \frac{f_{t.d.1}}{E_c} = 1.667 \times 10^{-4}$$

Appendix B

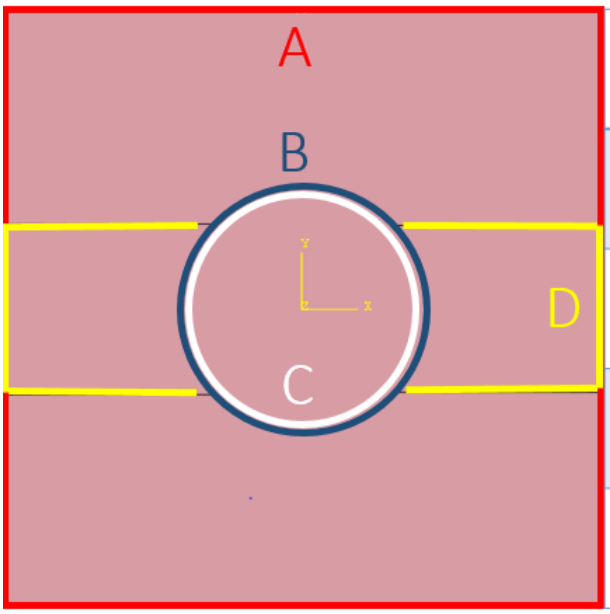

Convergence data	
6353 elements	2 mm at boarder A and 0.5mm at boarder B and C.
8401 elements	1 mm at boarder A and 0.4 mm at boarder B and C.
8789 elements	1 mm at boarder A and 0.3 mm at boarder B and C.
16857 elements	1 mm at boarder A and 0.2 mm at boarder B and C.

Figure B.1 Convergence data.

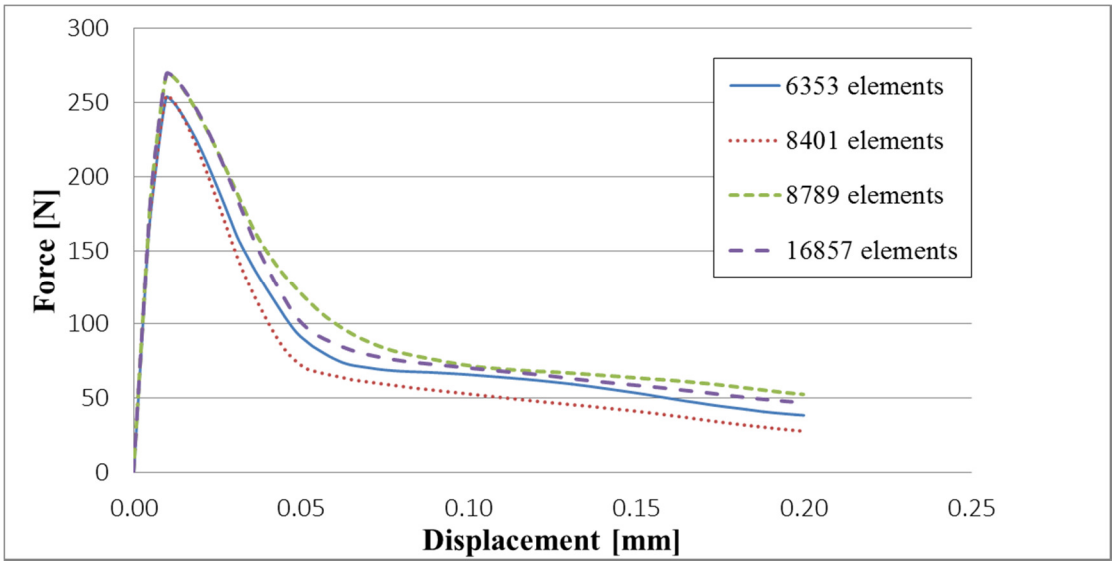

Figure B.2 Convergence study with force-displacement curves.

Appendix C

Test - BE1

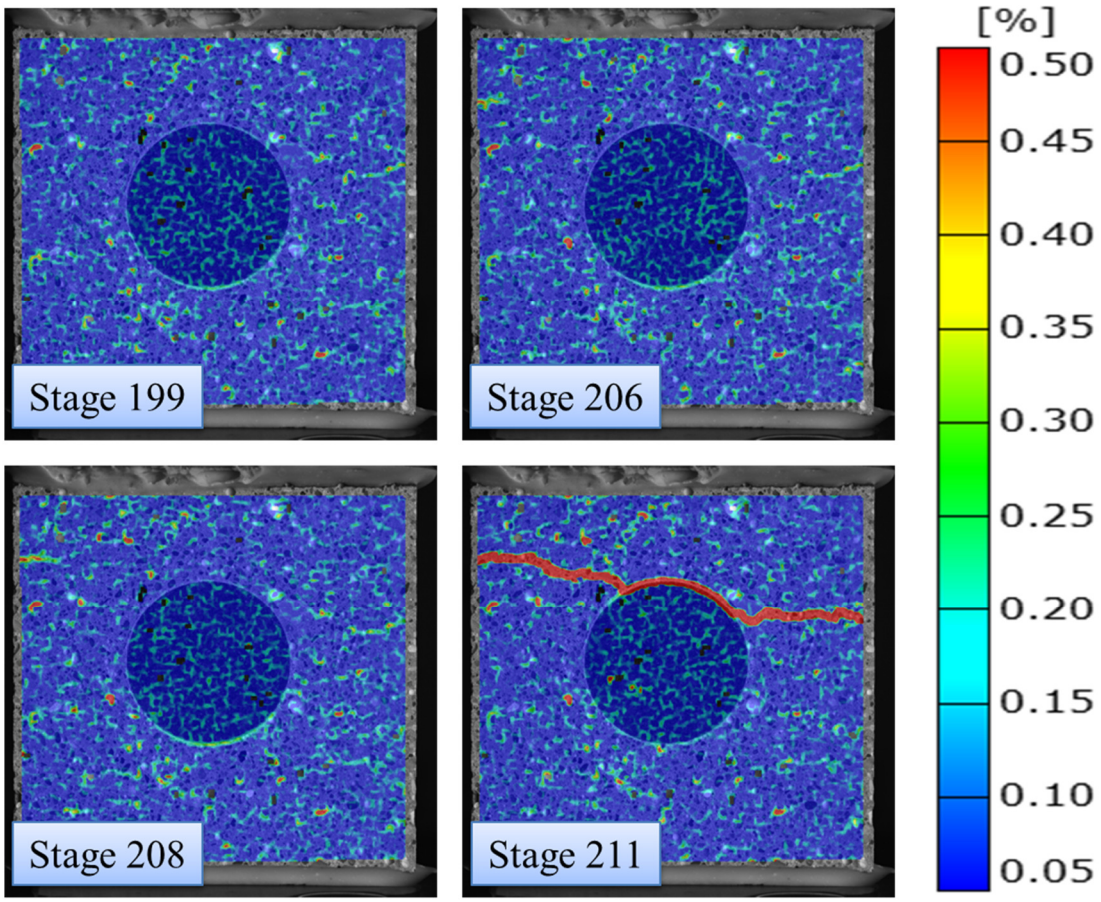

Figure C.1 Different stages of strains in test BE1.

Table C-1 Values and description of test BE1.

Stage	Stress [MPa]	Description
150-199	2.20636	In stage 150 to 199 there was tendency to high strains in the interface below the aggregate. Figure C.1, shows how the strains developed in stage 199.
206	3.06257	Approximately from stage 206 there were high strains on the right edge of the cement paste, see Figure C.1.
208	3.08233	Maximum stress was in stage 208, see Figure C.1.
211	0.177826	In stage 211 a crack, represented by strains, appeared and separated the specimen into two parts. It started on the edge in the cement paste and propagated further in the direction of the aggregate. Figure C.1, shows how the crack followed the weaker part of the concrete, i.e. the interface. The crack was located above the aggregate.

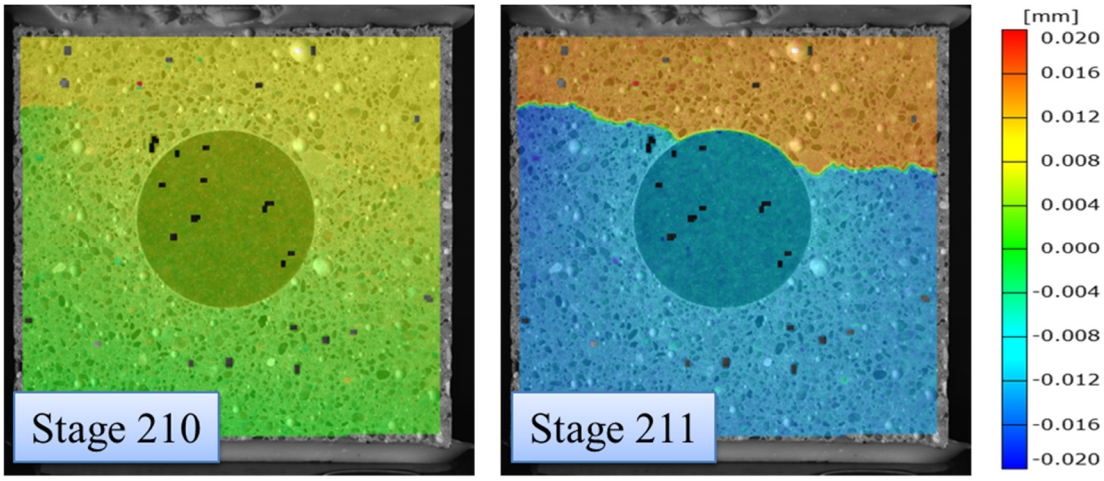

Figure C.2 Displacement before and after cracking for test BE1.

Test - BE2

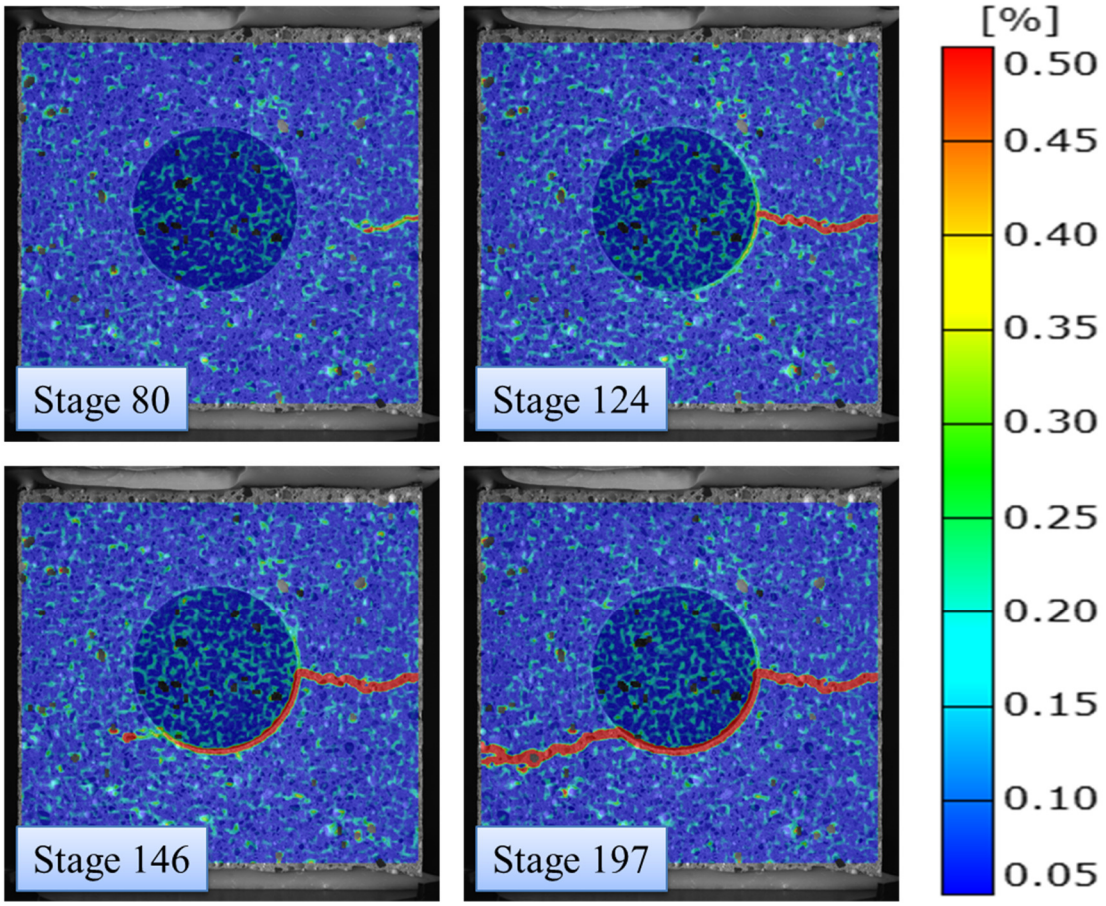

Figure C.3 Different stages of strains for test BE2.

Table C-2 Values and description of test BE2.

Stage	Stress [MPa]	Description
50-80	1.37258696	In stage 50 to 80 there were high strains on the right edge of the cement paste, which grew larger in strain values but not in size, see Figure C.3.
124	1.77706911	The crack propagated from the right edge of the cement paste towards the interface. Maximum stress was in stage 124, see Figure C.3.
146	1.47868064	The crack propagated successively around the lower part of the aggregate as the stress decreased. In stage 146 the crack started to propagate from the area around the aggregate to the left side of the cement, see Figure C.3.
197	1.13387619	The crack grew slowly until it was fully developed in stage 197, see Figure C.3.

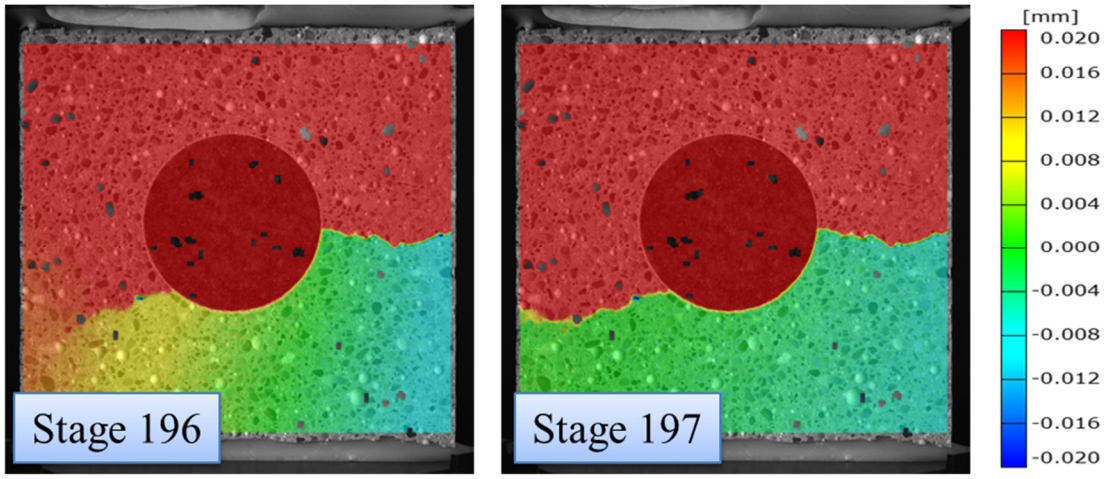

Figure C.4 Displacement before and after cracking for test BE2.

Test - BE3

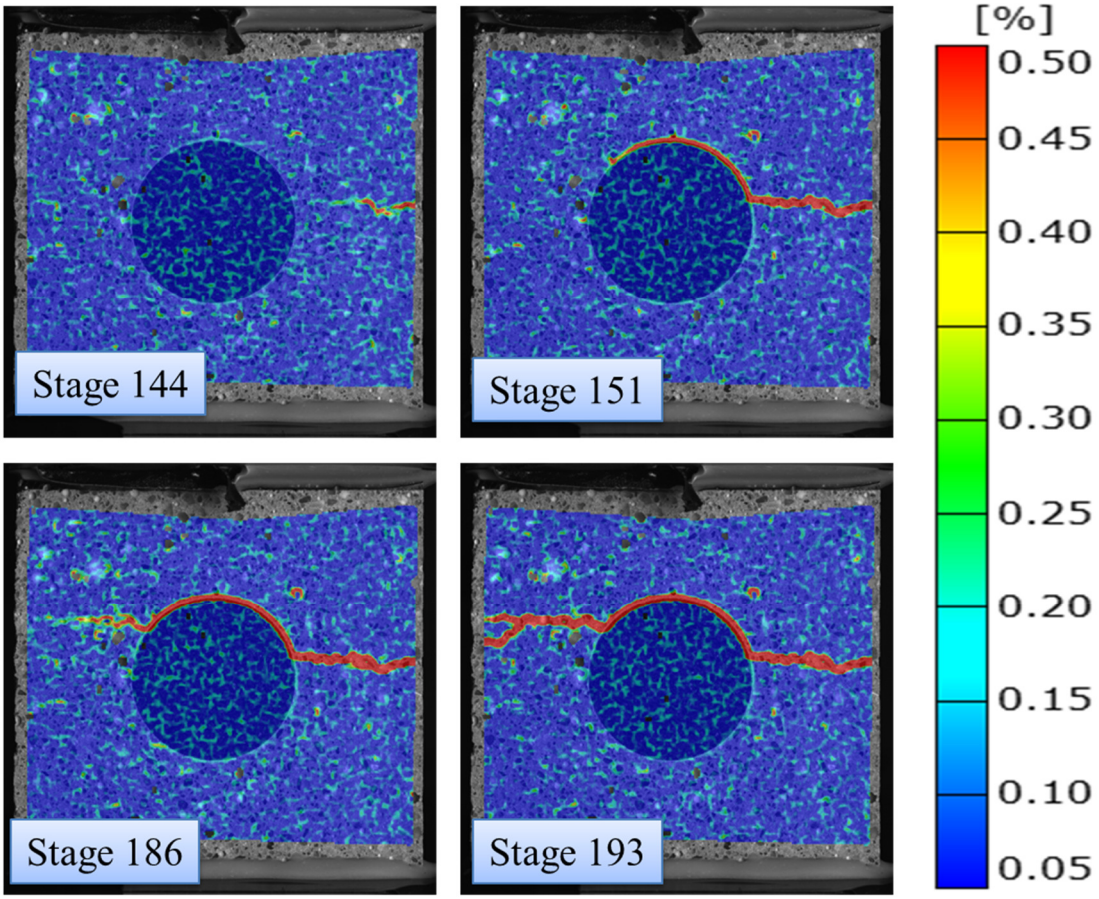

Figure C.5 Different stages of strains for test BE3.

Table C-3 Values and description of test BE3.

Stage	Strain [MPa]	Description
144	2.43155498	Highest stress in stage 144, see Figure C.5.
151	2.33190108	High strains were situated in the cement paste on the right edge. It continued to grow further in towards the interface around the aggregate. In stage 151 the crack reached the interface and started to grow along the interface on the upper side of the aggregate, see Figure C.5.
186	1.47487761	In stage 186 the crack propagated away from the interface and into the cement paste on the left side of the aggregate, see Figure C.5.
193	1.2955006	The concrete specimen was fully cracked in stage 193, see Figure C.5.

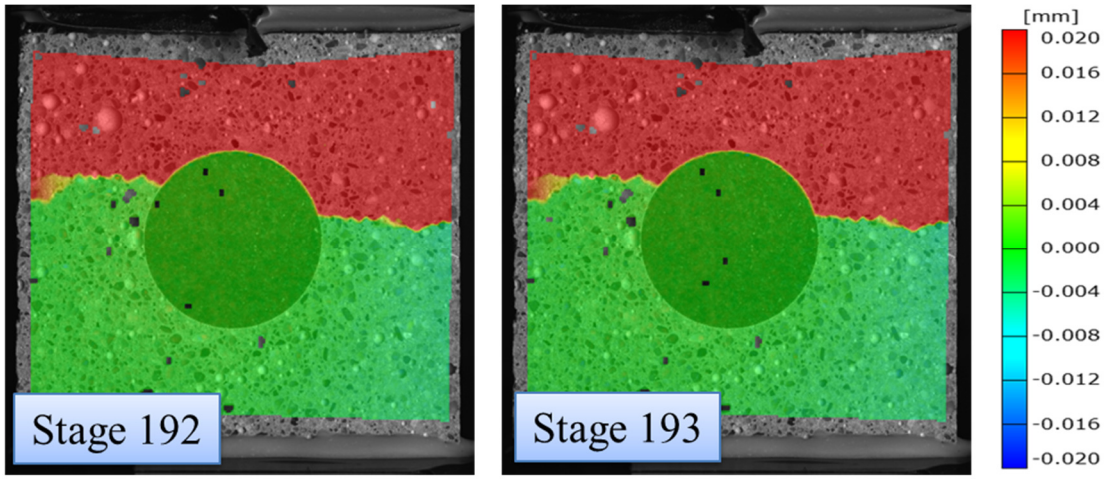

Figure C.6 Displacement before and after cracking for test BE3.

Test - EB1

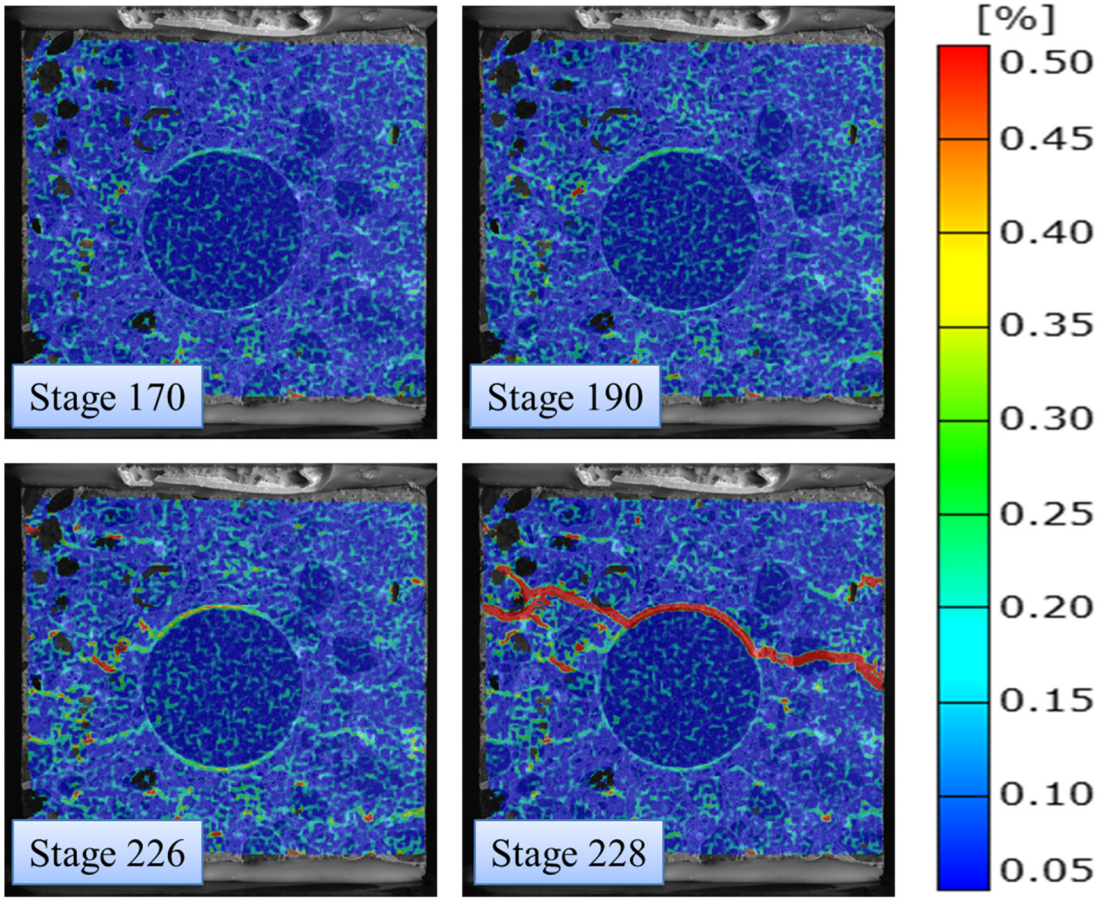

Figure C.7 Different stages of strains for test EB1.

Table C-4 Values and description of test EB1.

Stage	Strain [MPa]	Description
160-170	3.03094321	Strains were beginning to localise in stage 160 to 170 in the interface above the aggregate. Figure C.7 shows how the stresses were distributed in stage 170.
190	3.298794	In stage 190 the strains started to localise in the interface below the aggregate, see Figure C.7.
226	3.72171631	Maximum stress appeared in stage 226, see Figure C.7.
229	1.64939699	The test was fully cracked in stage 229, see Figure C.7.

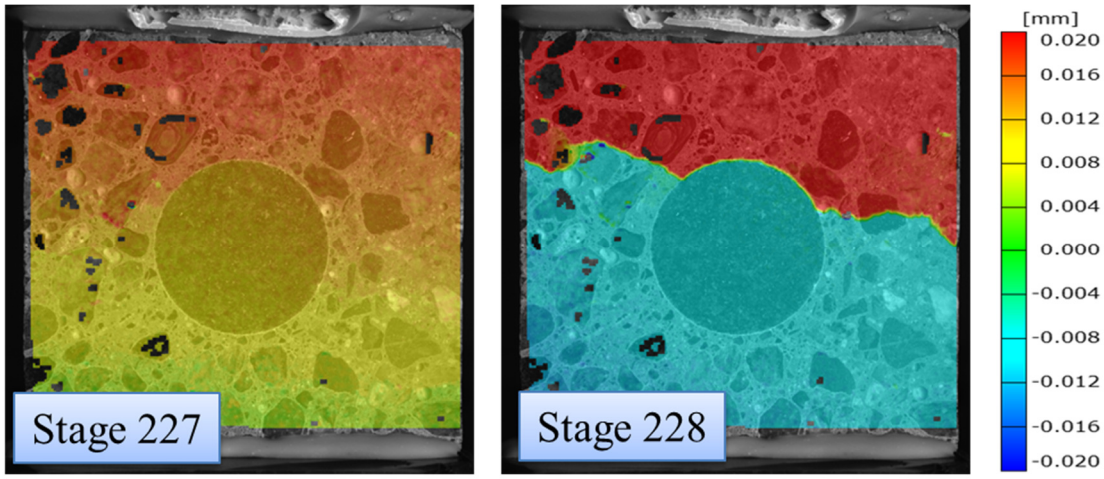

Figure C.8 Displacement before and after cracking for test EB1.

Test - EB2

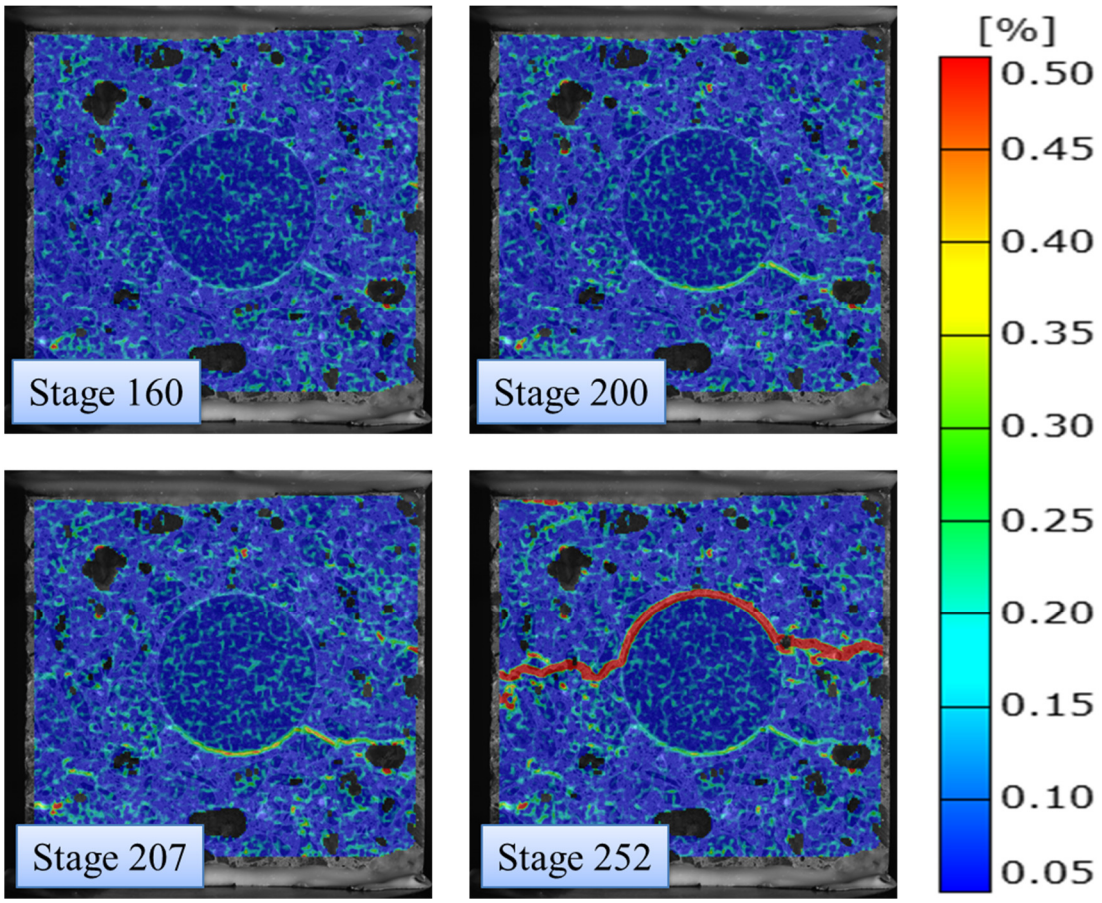

Figure C.9 Different stages of strains for test EB2.

Table C-5 Values and description of test EB2.

Stage	Strain [MPa]	Description
160	2.24404	In stage 160 there was a tendency to high strains in the interface below the aggregate, see Figure C.9.
200	2.86966	Around stage 200 the strains propagated from below the aggregate towards the right edge of the cement paste, se Figure C.9.
207	2.93085	Maximum stress was in stage 207, see Figure C.9. It looked like a crack in the interface under the aggregate was going to separate the concrete specimen, but in the next step the crack appeared in the interface above the aggregate instead.
252	0.652812	The crack grew until it was fully developed in stage 252, see Figure C.9.

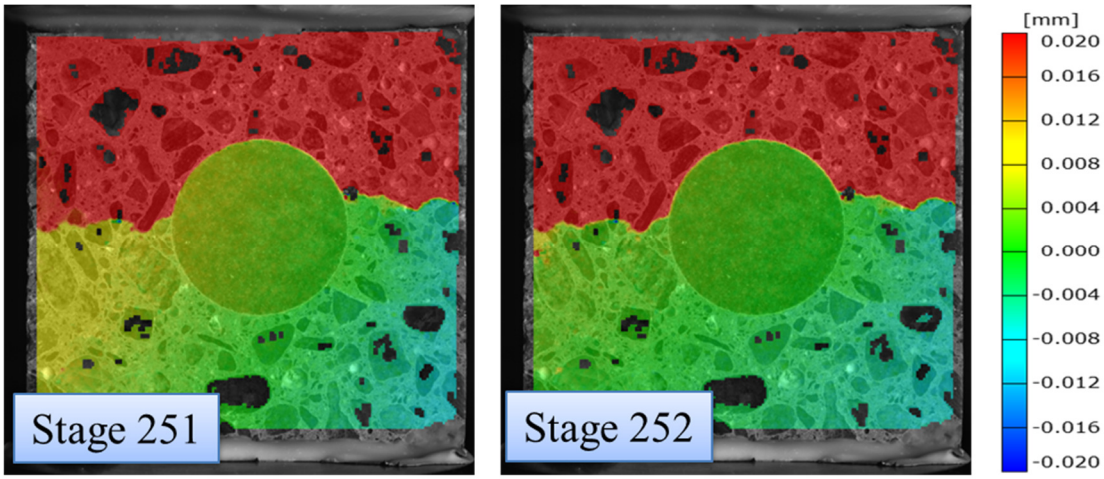

Figure C.10 Displacement before and after cracking for test EB2.

Test - EB3

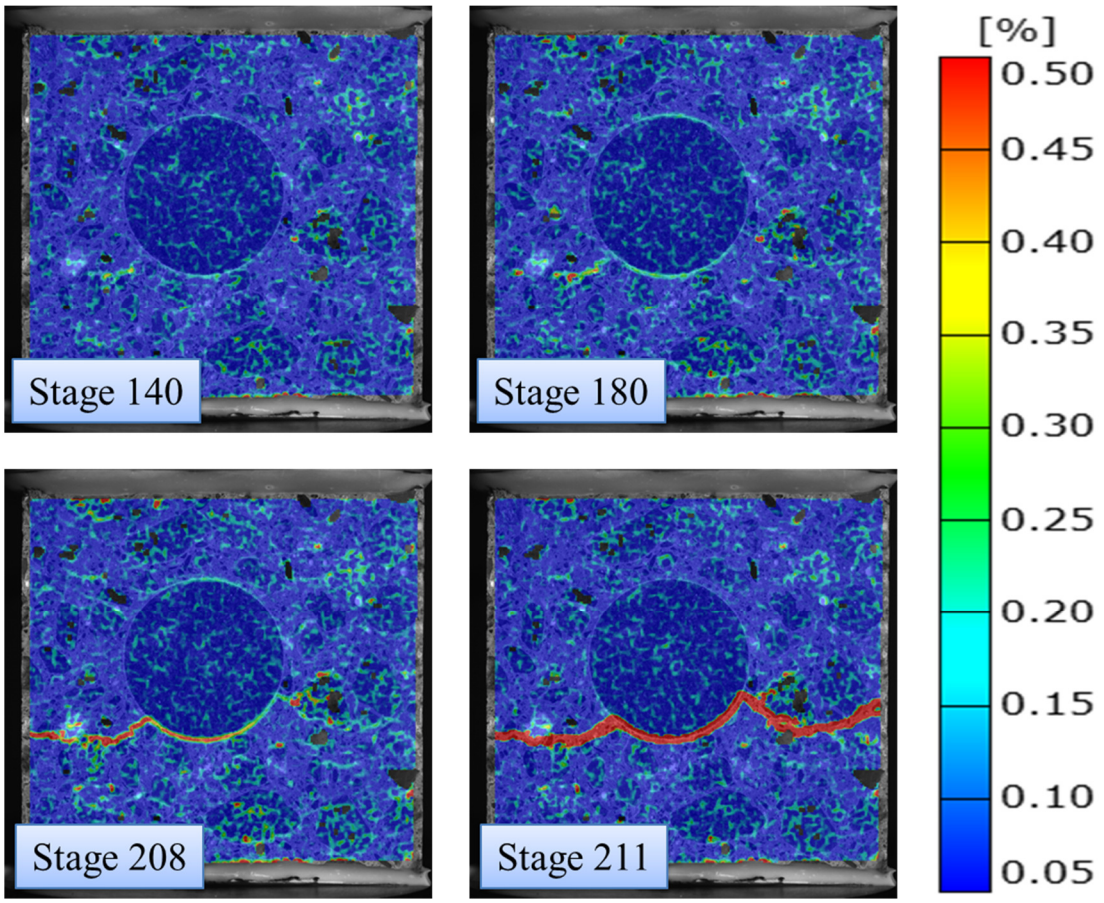

Figure C.11 Different stages of strains for test EB3.

Table C-6 Values and description of test EB3.

Stage	Strain [MPa]	Description
140	2.4986696	Strains were gathering in different areas in the interface both over and under the aggregate as well as the cement paste. In stage 140 the strains started to gather around the aggregate, see Figure C.11.
180	3.13786416	In stage 180 it looked like the crack would start in the interface below the aggregate. Slowly, small cracks located in the cement paste, were connected with the cracks in the interface, see Figure C.11.
208	3.48651572	Maximum stress in stage 208, see Figure C.11.
211	1.60767114	The crack in concrete specimen was fully developed in stage 211, with the crack located under the aggregate, see Figure C.11.

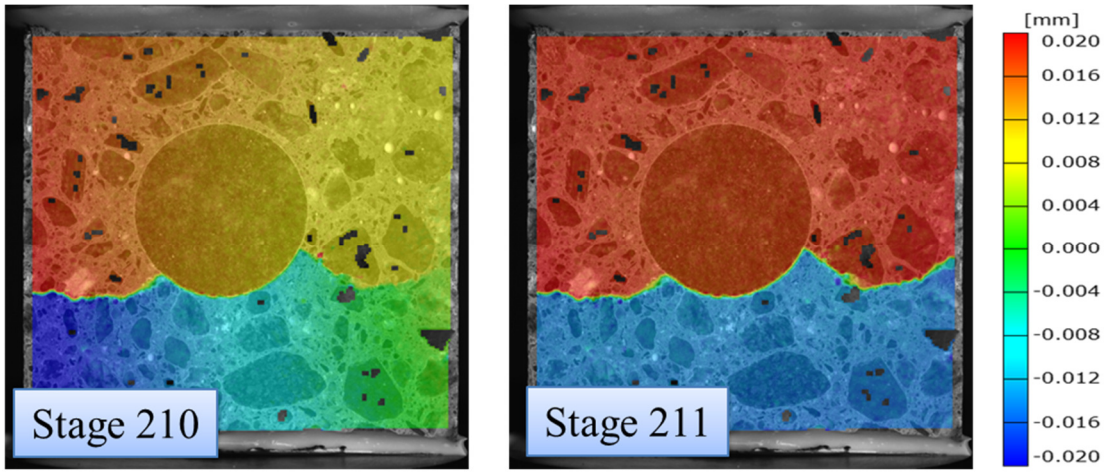

Figure C.12 Displacement before and after cracking for test EB3.

Appendix D

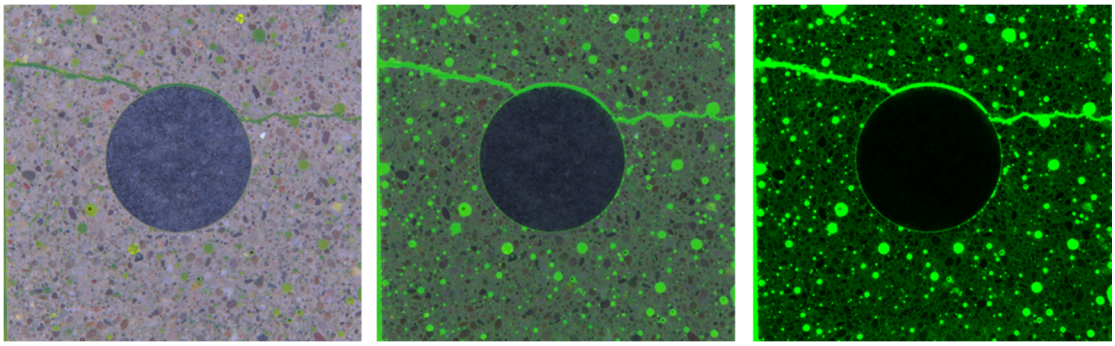

Figure D.1 *Fluorescence images for test BE1. To the left: image taken with regular lights, to the right: image taken with fluorescent light and in the middle: a combination of the other two images.*

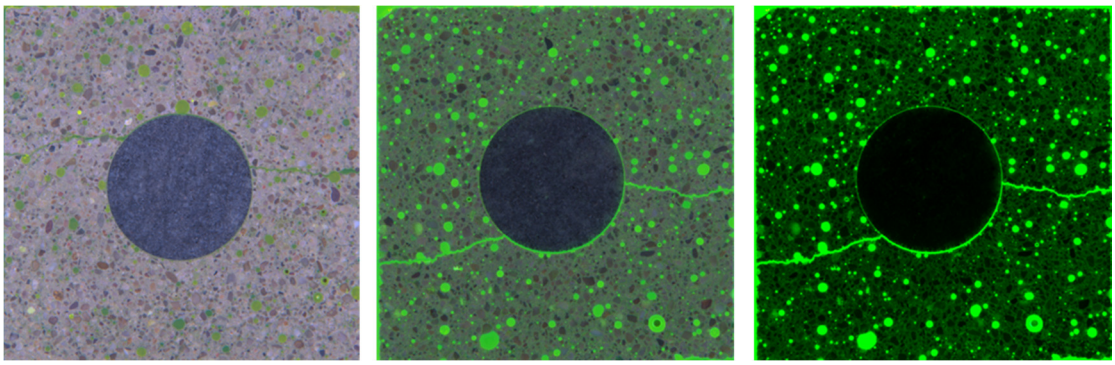

Figure D.2 *Fluorescence images for test BE2. To the left: image taken with regular lights, to the right: image taken with fluorescent light and in the middle: a combination of the other two images.*

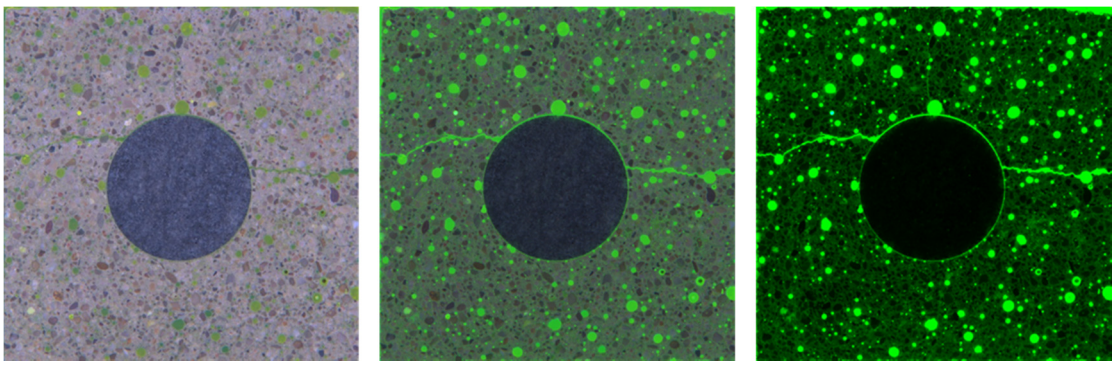

Figure D.3 *Fluorescence images for test BE3. To the left: image taken with regular lights, to the right: image taken with fluorescent light and in the middle: a combination of the other two images.*

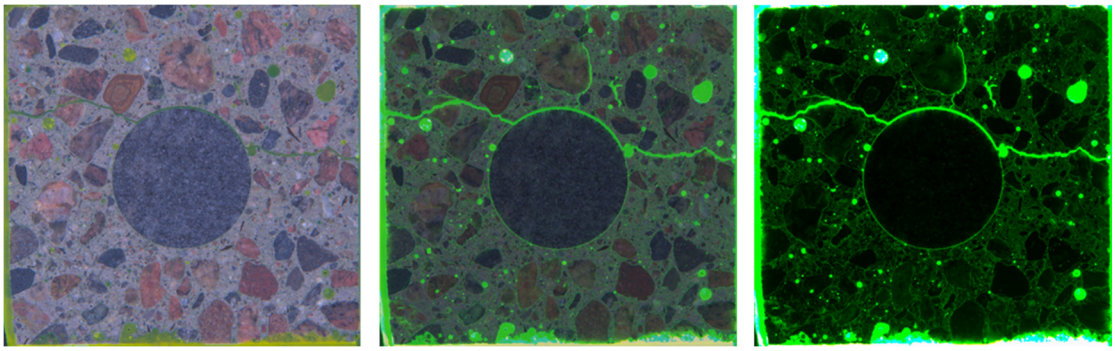

Figure D.4 *Fluorescence images for test EB1. To the left: image taken with regular lights, to the right: image taken with fluorescent light and in the middle: a combination of the other two images.*

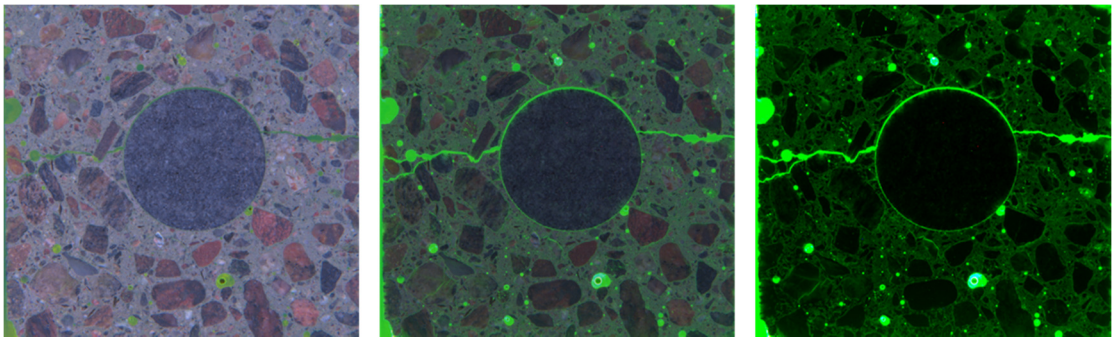

Figure D.5 *Fluorescence images for test EB2. To the left: image taken with regular lights, to the right: image taken with fluorescent light and in the middle: a combination of the other two images.*

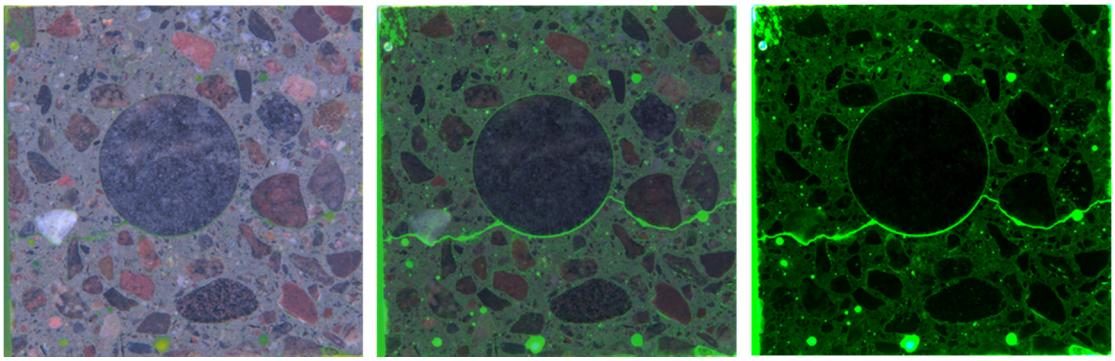

Figure D.6 *Fluorescence images for test EB3. To the left: image taken with regular lights, to the right: image taken with fluorescent light and in the middle: a combination of the other two images.*